Alexander Troiss, BSc

Vacuum Compression Molding as a Versatile Tool for Pharmaceutical Material Characterization

Master Thesis

submitted in fulfilment of the requirements for the degree

Diplom-Ingenieur

Master's Programme Chemical and Process Engineering

submitted to

Graz University of Technology

Supervisor:

Univ.-Prof. Dipl.-Ing. Dr.techn. Johannes Khinast

Institute of Process and Particle Engineering

Graz, March 2017

Affidavit

I declare that I have authored this thesis independently, that I have not used other than the declared sources/resources, and that I have explicitly marked all material which has been quoted either literally or by content from the used sources. The text document which has been uploaded to TUGRAZonline is identical to the present master thesis.

Graz, _____ _____

Date Signature

Eidesstattliche Erklärung

Ich erkläre an Eides statt, dass ich die vorliegende Arbeit selbstständig verfasst, andere als die angegebenen Quellen/Hilfsmittel nicht benutzt, und die den benutzten Quellen wörtlich und inhaltlich entnommenen Stellen als solche kenntlich gemacht habe. Das in TUGRAZonline hochgeladene Textdokument ist mit der vorliegenden Masterarbeit identisch.

Graz, am _____ _____

Datum Unterschrift

Acknowledgment

First of all I want to express my gratitude to Professor Johannes Khinast for granting me the opportunity to conduct my master's thesis at Research Center Pharmaceutical Engineering GmbH.

Moreover, I want to thank to all people who have supported me during this work. Especially I want to acknowledge Dr. Daniel Treffer for his outstanding support and for his guidance. Special thanks go to Dr. Amrit Paudel for many fruitful discussions.

Many parts of this work would not have been possible without the help of Johann Grubbauer, who manufactured many prototype parts. Philipp Pernitsch is acknowledged for his assistance with the DSC measurements.

Special thanks go to Anton Paar GmbH for giving me the possibility to use their high-end rheological equipment for my experiments.

Financial support of this thesis of the Austrian Research Promotion Agency (FFG) is gratefully acknowledged.

Abstract

For the development of pharmaceutical formulations, as well as the design and the simulation of production equipment, the processed materials have to be extensively characterized. In the early stages, a large number of different formulations are tested. However, often only low quantities of very expensive, active pharmaceutical ingredients (APIs) are available. The production of appropriate test specimens using conventional methods not only requires costly large-scale equipment, it is also time consuming and has a large material expenditure. Thus, specimen preparation currently represents a bottleneck in the work-flow of pharmaceutical research and development.

A novel approach to resolve this problem is the so-called vacuum-compression molding process (VCM), which enables the rapid production of homogeneous specimens with minimal material expenditure. The VCM approach, which was originally developed for the production of specimens intended for use in shear-rheological analyses, has set a new benchmark in terms of measurement accuracy and reproducibility of pharmaceutical polymers.

In the work at hand, the VCM method was adapted to enable its application to further important material characterization methods, including differential scanning calorimetry (DSC), dynamic mechanical analysis (DMTA) and extensional rheometry.

For DSC analyses, small specimens with a diameter of 5 mm are required. An appropriate VCM tool was designed and manufactured. Subsequently, homogeneous specimens of various pharmaceutical polymers were prepared and subjected to DSC measurements. The results show that in many cases the measurement sensitivity can be improved by homogeneous VCM specimens. The sensitivity in particular is enhanced, due to improved heat transfer between DSC pan and specimen material. This allows to detect glass transitions and weak thermal effects more easily.

By using modulated DSC, the homogeneous VCM specimens allow for the first time a reliable measurement of thermal conductivity of pharmaceutical formulations. The accurate knowledge of this physical quantity is essential, especially for simulation purposes. There is hardly any data to be found in literature on thermal conductivity of pharmaceutical polymers and the influence of API addition is unexplored. Hence, a large number of thermal conductivity measurements was carried out to evaluate the reproducibility of the method. The results show that the thermal conductivity of most pharmaceutical polymers is very low. HPMC Affinisol® 100 LV conducts heat considerable better than the other investigated polymers. The API addition to a polymer showed little influence on its thermal conductivity for the investigated mixtures.

For DMTA, rectangular bars (e.g. 10x40x1mm) are required as specimen geometry. Using a new VCM tool, which was developed in course of this work, it is possible to produce such specimens with a high degree of quality. The subsequently conducted DMTA measurements, using the VCM specimens, showed excellent reproducibility.

With these results, glass transitions can be determined reliably, and knowledge about the thermo-mechanical behavior of pharmaceutical polymers in solid state can be obtained.

Shear-rheological measurements show that polymers are plasticized by addition of API and their flow behavior, especially the shear-thinning behavior, is influenced in a complex manner. Extensional-rheological characterization of Soluplus® revealed its non-linear behavior in extension, which is characteristic for a branched polymer.

In this work, the VCM Process for specimen production was successfully transferred to further material characterization methods, where it provides advantages in the investigated fields concerning the reproducibility and accuracy by providing homogeneous, degradation free specimens.

Kurzfassung

Für die Entwicklung von pharmazeutischen Formulierungen sowie für die Auslegung und Simulation von deren Produktionsprozessen müssen die eingesetzten Materialien umfangreich charakterisiert werden. In frühen Phasen werden eine große Anzahl an verschiedenen Formulierungen untersucht, jedoch stehen oft nur sehr geringe Mengen an Wirkstoff zur Verfügung. Die Herstellung der Probekörper für die Charakterisierung mit konventionellen Methoden ist oft kosten-, zeit- und materialintensiv und stellt somit gemeinhin einen Engpass im Arbeitsablauf der Entwicklung dar.

Ein neuer Ansatz zur Lösung dieses Problems ist das sogenannte Vakuum-Kompressionsform Verfahren (engl. Vacuum Compression Molding, VCM), welches die schnelle Herstellung von homogenen Probekörpern mit geringem Materialaufwand ermöglicht. Das Verfahren wurde für die Probenherstellung für rheologische Untersuchungen entwickelt und hat in diesem Bereich neue Maßstäbe hinsichtlich der Messgenauigkeit und Reproduzierbarkeit von pharmazeutischen Materialien gesetzt.

In der vorliegenden Arbeit wurde das VCM Verfahren für die Anwendung in weiteren Charakterisierungsmethoden (dynamische Differenzkalorimetrie (DSC), dynamisch mechanische Thermoanalyse (DMTA) und Dehnrheometrie) angepasst und evaluiert. Für DSC Untersuchungen werden Proben mit einem Durchmesser von 5 mm benötigt. Ein entsprechendes VCM Tool wurde entwickelt, gefertigt und damit homogene Proben aus pharmazeutischen Polymeren hergestellt. Die DSC-Messungen von VCM Proben wurden mit traditionell vorbereiteten Proben verglichen. Die Ergebnisse zeigen, dass die Sensitivität der Messung durch den Einsatz von VCM Probekörpern anstatt von Pulver in vielen Fällen verbessert werden kann. Die Sensitivität wird durch den besseren Wärmeübergang zwischen DSC Tiegel und Probe gesteigert. Dadurch können Glasübergänge und andere thermische Ereignisse leichter detektiert werden. Die homogenen VCM Proben ermöglichen erstmals die zuverlässige Messung der Wärmeleitfähigkeit von pharmazeutischen Formulierungen durch spezielle modulierte DSC-Methoden. Die Kenntnis dieser Größe ist fundamental, z.B. für Simulationszwecke. Literaturdaten sind rar bzw. nicht existent und der Einfluss von Wirkstoffbeladung auf die Wärmeleitfähigkeit von Polymeren ist gänzlich unerforscht. Daher wurden zahlreiche Wärmeleitfähigkeitsmessungen durchgeführt und die Reproduzierbarkeit evaluiert. Die Resultate zeigen, dass die meisten pharmazeutischen Polymere sehr schlechte Wärmeleiter sind. Einzig HPMC Affinisol® 100 LV zeigte eine deutlich höhere Wärmeleitfähigkeit als die übrigen untersuchten Polymere. Der Einfluss von Wirkstoffzugabe auf die Wärmeleitfähigkeit ist nicht von signifikantem Ausmaß.

Für DMTA werden quaderförmige (z.B. 10x40x1mm) Probenkörper benötigt. Durch das entwickelte VCM Werkzeug können solche Probenkörper mit hoher Qualität hergestellt werden. Die Machbarkeit von DMTA Messungen mit den neuartigen Probenkörpern wurde untersucht und die Wiederholbarkeit der Messungen evaluiert. Die DMTA Messungen zeigten eine gute Wiederholbarkeit, was die Eignung der VCM Probenkörper für

dieses Messverfahren bestätigt. Mit diesen Ergebnissen konnten Glasübergangstemperaturen gut bestimmt werden, sowie Erkenntnisse über das thermo-mechanische Verhalten von pharmazeutischen Polymeren im festen Zustand gewonnen werden.

Aus scher-rheologischen Untersuchungen geht hervor, dass die Polymere durch Wirkstoffbeladung plastifiziert werden und dass das Fließverhalten, insbesondere das scherverdünnende Verhalten, in einer komplexen Art beeinflusst wird. Die dehnrheologische Charakterisierung von Soluplus® zeigt dessen nichtlineares Verhalten bei höheren Dehnraten, was dem Verhalten eines verzweigten Polymers entspricht.

Das VCM Verfahren zur Probenkörperherstellung wurde im Zuge dieser Arbeit erfolgreich auf weitere Materialcharakterisierungsmethoden übertragen und eröffnet nun in den untersuchten Bereichen Vorteile hinsichtlich Reproduzierbarkeit und Genauigkeit durch homogene, degradationsfreie Probenkörper.

Table of Contents

1 Introduction

Modern active pharmaceutical ingredients (APIs) are often almost insoluble in water, and therefore the bio-availability of the drug in the human body is poor. To enhance bio-availability, such APIs are dispersed in a polymer, which acts as solubilizer. Such polymeric formulations can be processed via hot-melt extrusion or injection molding, for example. The characterization of the thermal, rheological and mechanical behavior of polymeric formulations is crucial, for example to assess processability or the stability of the formulation against recrystallization during storage. Important analytical tools to test formulation properties include rheometry, differential scanning calorimetry (DSC) and dynamic mechanical analysis (DMTA). In development of new formulations many times only very little quantities of API in form of powder is available (in the order of a few grams). APIs are usually expensive, especially before mass production has started. Thus, because of the high material expense, production or pilot-scale processing equipment cannot be used for specimen production.

Furthermore, often many different formulation compositions have to be tested. This so-called screening of polymeric formulations via high-throughput experimentation establishes the need to test (1) a high number of polymeric specimens with (2) very limited amount of material in (3) a short period of time.

Proper preparation of test specimens starting powders can be a restrictive task, especially if sensitive or expensive materials are used. State of the art methods are often time-consuming and do not yield satisfactory specimen quality. This is the case because pharmaceutical polymers and APIs can be highly sensitive to mechanical or thermal stresses. Thermal degradation therefore is a common problem, especially due to the often narrow temperature-window between glass-transition temperature and onset of degradation. Furthermore, pronounced hygroscopicity of the polymers can lead to formation of water vapor filled bubbles during softening of the material. Hence, data obtained using conventionally prepared specimens often yields either irreproducible data or, in worst case, may lead to false conclusions regarding the materials thermal or rheological behavior. This sample preparation problem can slow down the development process considerably.

In a recent publication, the potential of a novel benchtop-scale vacuum-compression molding (VCM) device, the so-called VCM Tool, for the standardization of specimen preparation of pharmaceutical polymers was demonstrated [1]. The principle of the VCM Tool is, at first glance, quite similar to traditional compression molding. It allows to produce homogeneous solid specimens of thermoplastic powders or pellets by compression-induced fusion in a vacuum environment. Powder or pellets can be fed to the tool, which is subsequently sealed and evacuated. Particles are fused using heat, yielding a solid sample without any inclusions of air, water or any other volatile substances (figure 1). This approach has umerous advantages compared to established

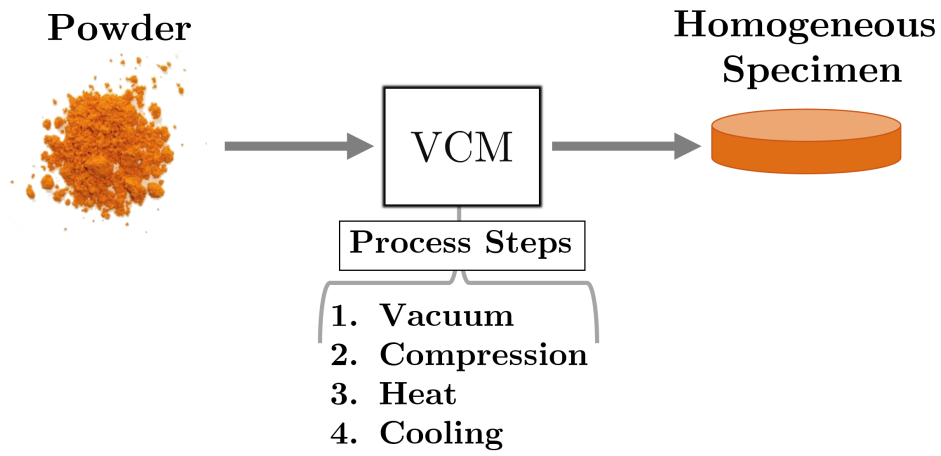

Figure 1 : Vacuum Compression Molding (VCM) allows the transformation of powders into homogeneous specimens directly from powder

techniques. Therefore, this new tool has large potential to facilitate or even enable the characterization of certain materials.

Objective and Outline of this Thesis

This thesis intends to demonstrate the applicability of the VCM process to improve the results of selected material testing methods. In particular, the thermal and mechanical behavior of materials relevant for pharmaceutical applications are characterized. This is carried out to gain a more comprehensive understanding of the material behavior, which is crucial for pharmaceutical product development and equipment design.

As already mentioned, the first field of application which has been scientifically explored is the characterization of the shear rheology of *pure* pharmaceutical polymers used for hot-melt extrusion. In this field the VCM approach was first introduced in 2015[1] and demonstrated compelling potential, which awakened interest in further research. For application in rheometry, a typical specimen prepared using VCM is a disc with a diameter of 25 mm and a height of approx. 1 mm.

A specific objective of this thesis is to broaden the field of applications of the VCM process from its original main field of application, rheometry, to other material characterization methods which are suspected to benefit from the higher sample quality the VCM process can provide. However, different measurement methods require different specimen geometries. Emphasis is put on two new promising fields of application which both require the design of a dedicated VCM tool to be able to produce the required specimen geometries. These are differential scanning calorimetry (DSC) and dynamic mechanical thermal analysis (DMTA).

To that end, VCM devices for both methods are developed, allowing the preparation of rectangular bars which are required for DMTA and of disc specimens with a diameter of 5mm for DSC applications. As mentioned above, using these measurement methods and the developed specialized VCM tools, the thermal and mechanical behavior of materials relevant for pharmaceutical applications are investigated. In particular, the feasibility

to carry out DMTA measurements of pharmaceutical polymers using VCM prepared specimens is evaluated and the repeatability is checked. Via DSC measurements of a multitude of pharmaceutical polymers and two formulations, the new VCM preparation method is compared to the traditional approach of simply heating powder in the DSC pans. A true novelty presented in this thesis is the thermal conductivity measurement of pharmaceutical polymers using modulated differential scanning calorimetry. The developed VCM Tool for DSC enables, for the first time, application of this particular method. Thermal conductivity as a function of temperature is determined for variety of common pharmaceutical polymers and two formulations. Moreover, using the methodology from the first VCM publication[1] the shear rheology of two polymeric formulations, comprising two different polymers and APIs, is investigated in detail and compared to the behavior of the pure polymers.

2 Theoretical Background

2.1 Basics of Polymer Science

Structure of Thermoplastic Polymers

A thermoplastic polymer is a material that shows liquid-like behavior when heated above a specific temperature and solidifies upon cooling. Most polymers of pharmaceutical relevance belong to this class. The polymer chains interact through inter-molecular forces, which are increasingly weakened as temperature is increased, result in a liquid-like polymer melt. Two basic structure types of these polymers can be distinguished (figure 2). Amorphous polymers consist of irregularly entangled polymer chains, while semi-crystalline materials comprise both irregular amorphous regions and lamellar-shaped crystalline structures. The type of structure strongly influences both the mechanical and thermal properties of the material. The ability of polymers to crystallize depends on their molecular structure. Straight chains with regularly spaced side groups favor crystallization. The mechanical properties of semi-crystalline polymers depend strongly on the direction of molecular alignment and are therefore anisotropic.

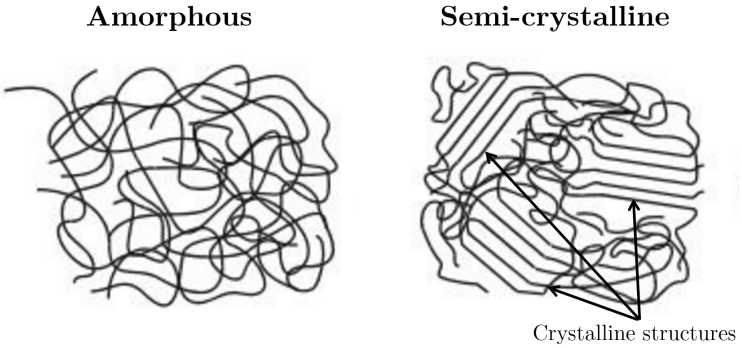

Figure 2 : Schematic structure of amorphous and semi-crystalline polymers

Pharmaceutical polymers are often copolymers, meaning that their chains are composed of more than one type of monomer molecule. Three different basic structures of copolymers can be distinguished (figure 3). In statistical copolymers the sequence of the different monomers is random. Block copolymers comprise several homopolymer units which are linked. Graft copolymers are a type of branched polymer in which the side chains are structurally distinct from the main chain.

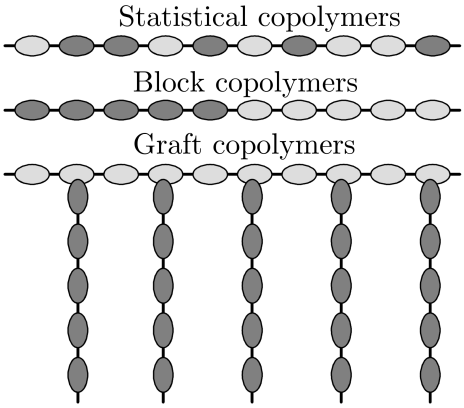

Figure 3 : Schematic structure of different copolymer types. [2].

2.1.1 Glass Transition

Glass transition of major importance for almost all properties of amorphous or semi-crystalline polymers. At low temperature, the molecular motions of amorphous polymers appear to be frozen, however above a critical temperature, denoted as glass-transition temperature T_g, the free volume between the polymer chains increases, allowing the molecules to gain mobility. This causes a discontinuity in many physical properties of the material. For example, at temperatures below T_g a polymer will exhibit brittle behavior, but once the temperature is increased to a value above the glass transition temperature, the material softens, exhibits more flexible and ductile behavior and gradually begins to flow. Polymers with a T_g below room temperature, because of their flexibility, are generally termed *thermoplastic elastomers* while polymers with a T_g above room temperature are called simply *thermoplastics*. Above T_g, the heat capacity suddenly increases due to the increased free volume between the molecules, that allows more degrees of freedom for molecular thermal motion. In semi-crystalline polymers, softening at temperatures above glass-transition is prevented by the relatively strong inter-molecular forces due to the crystalline structures. Liquid-like flow for semi-crystalline polymers is observed not until the crystalline domains melt, at a melting temperature T_m, which generally is significantly higher than T_g.

Glass transition is a kinetic phenomenon, which expresses itself in a dependence of the glass transition temperature on experimental time-scales [3]. For example in calorimetry, different heating- or cooling rates usually influence the value of T_g. Higher values of T_g are observed for fast heating rates. Therefore, when comparing T_g values, the corresponding experimental conditions have to be considered.

The T_g can also be utilized to evaluate miscibility and compositional homogeneity of multi-component systems. This is especially important for pharmaceutical applications, e.g. to investigate drug/polymer interactions. If systems with multiple amorphous components are investigated, occurrence of a single T_g usually means that the components are miscible, and a homogeneous amorphous system was generated. Multiple glass transition temperatures, however, are an indicator of phase separation.

2.1.2 Melting and Crystallization

Melting is an endothermic, i.e. heat consuming, process in which a solid, crystalline material is transformed into amorphous state. Melting of a pure substance occurs at a constant temperature, the so-called melting point T_m, until the material is fully molten. Melting in terms of polymers can only occurs in semi-crystalline polymers and means the heat induced transformation of crystalline domains into amorphous state. Therefore, if so called polymer melts are formed by heating an amorphous thermoplastic polymer, strictly speaking this is no melting process but rather a softening due to relaxation of polymer chains at temperatures above glass transition. Nevertheless, this term is frequently used in professional circles. Crystallization is the opposite process of melting, i.e crystal lattices are formed from a liquid in an exothermic process.

2.1.3 Aging and Enthalpy Recovery

A substance that is present in glassy state experiences a change in its physical properties over time due to relaxation (physical aging). However, many products, e.g. pharmaceutical formulations exist in the glassy state at typical storage conditions. Unwanted changes in physical properties over time can have major impact on product performance. Therefore, it is important to study these effects, in order to make sure that no significant changes of the materials occur during relevant time-scales [4].

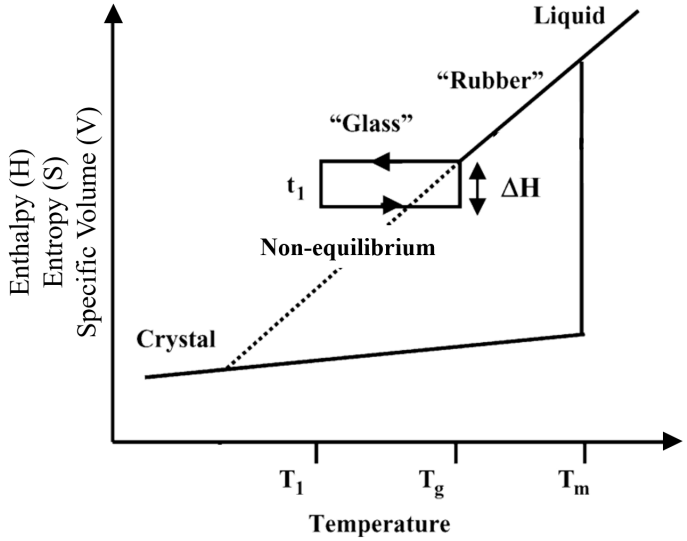

Figure 4 : Schematic representation of the relationship between enthalpy (or specific volume or entropy) and temperature for a liquid undergoing crystallization or glass transition during cooling. Enthalpy recovery (ΔH) after storage at the aging temperature $T1$ for an aging time t_1 below the T_g and its recovery at T_g during heating is shown as well. Adopted from [5].

Enthalpic recovery is a property exhibited by amorphous materials. Due to relaxation, enthalpy is lost over time, which is recovered when heating the material through T_g . This relaxation is also referred to as aging. The process is illustrated in figure 4. When a liquid is cooled it can fail to crystallize, if the molecular motions are not able to keep up with the cooling rate. The liquid then enters the so called rubbery state and subsequently undergoes glass transition and enters a pseudo-equilibrium state.

Compared to the crystalline state, the entropy S and enthalpy H are higher than for the crystal, i.e. there exists an excess enthalpy or -entropy, respectively with respect to the properties of the crystalline state. These excess quantities are frozen in, when cooling below the T_g, with their absolute values depending on the conditions (e.g. sample geometry, cooling rate) while formation of the glass. If a glass is stored for an aging time t_1 at a temperature T_1, close to its glass transition temperature, the frozen-in excess enthalpy is partially lost. due to relaxation. This is accompanied by a decrease of free volume of the material. As mentioned above, the lost excess enthalpy is regained when the aged glass is heated to a temperature above T_g (ΔH). The rate of relaxation is an indicator for molecular mobility, and therefore is directly related to the stability of the amorphous substance. For example, amorphous pharmaceuticals with a slower relaxation rate will have a longer shelf life before crystallization occurs. The rate of relaxation depends on the temperature while aging relative to T_g. As the temperature decreases from T_g the rate of relaxation also decreases. Therefore, generally speaking, the higher the T_g, the higher the stability of amorphous substances at room temperature [4].

2.1.4 Thermal Conductivity

Thermal conductivity (κ) is one of the fundamental properties relevant for heat transfer. It is a proportional factor of the heat flux along a temperature gradient, and is given by Fourier's law:

$$\kappa = \frac{-\vec{q}}{\nabla T} \left[\frac{W}{m\,K} \right] \tag{2.1}$$

where $\vec{q}$ is the heat flux density vector and ∇T is the gradient of the temperature field. The negative sign is due to the second law of thermodynamics, which states that heat can only be transferred from a high to a low temperature level, which means that a negative temperature gradient has to be present for heat conduction.

Thermal energy can be transferred using multiple mechanisms. In thermal insulators, transport of oscillation energy of adjacent atoms is the dominant mechanism of thermal energy transport. This is also referred to as phonon transport. Materials which are good electrical conductors are often good thermal conductors as well, because their free electrons contribute to transport of thermal energy. Because most polymers are electrical insulators, their thermal conductivity is also generally low. However, knowledge of the thermal conductivity of a material is important for almost all operations and processes which comprise heat transfer. The property influences the design of process equipment and dictates the speed of many mixing, extruding and molding operations [6]. This is especially important for polymer processing operations which involve rapid cooling or heating, like e.g. injection molding [7].

There is no theory which allows to estimate the thermal conductivity of polymeric melts or solids with high accuracy [8]. Hence, measurements are inevitable.

2.2 Pharmaceutical Polymer Processing

Amorphous solid dispersions (ASDs) are drug-polymer dispersions, used to stabilize API molecules in their amorphous state, which leads to an improved bioavailability of poorly water soluble APIs. The solubility improvement of the drug is due to its lack of crystal structure in its amorphous form, meaning that there is no need to break up the crystal lattice of the the drug [9]. More specifically, ASD can appear in different forms, namely solid solutions (SS) and solid dispersions (SDs). Solid solutions consist of a polymer in which the API is dispersed on a molecular level. In contrast, in solid dispersions, amorphous clusters of API are embedded in the polymer, i.e. no single molecules are dispersed. ASDs can be used in many routes of drug delivery, including oral, mucosal, subcutaneous, subdermal and transdermal [10].

Important manufacturing methods that are used to process ASDs are, for example, hot-melt extrusion and injection molding.

2.2.1 Hot-Melt Extrusion

Hot-melt extrusion (HME) is a solvent-free continuous process, which enables the production of solid dosage forms containing ASDs of poorly soluble drugs in thermoplastic polymers [11]. In figure 5, the principle of ASD production using pharmaceutical HME is shown. The API (crystalline form) and an amorphous polymer are fed into the extruder, conveyed, molten and sheared inside the extruder and subsequently the melt is discharged and collected for further processing.

The lattice energy of the crystal has to be overcome to transform the API into its amorphous form. Furthermore, the API and the polymer need to be mixed and afterwards co-dispersed. This is accomplished by the extruder by applying shear stresses to the API and to the polymer. Viscous dissipation and heating of the barrel supplies energy in order to overcome the lattice energy of the crystal and to soften the polymer. The extruder screws lead to mixing and dispersion of the material at the same time, which allows to achieve an excellent content uniformity in the finished product [12].

In order to correctly design and simulate a pharmaceutical HME process, the physical properties of the involved materials (i.e. polymer and API) have to be characterized extensively. Relevant quantities include melt viscosity, heat capacity, thermal conductivity, glass transition temperatures as well as melting temperature and melting enthalpy of the API[12].

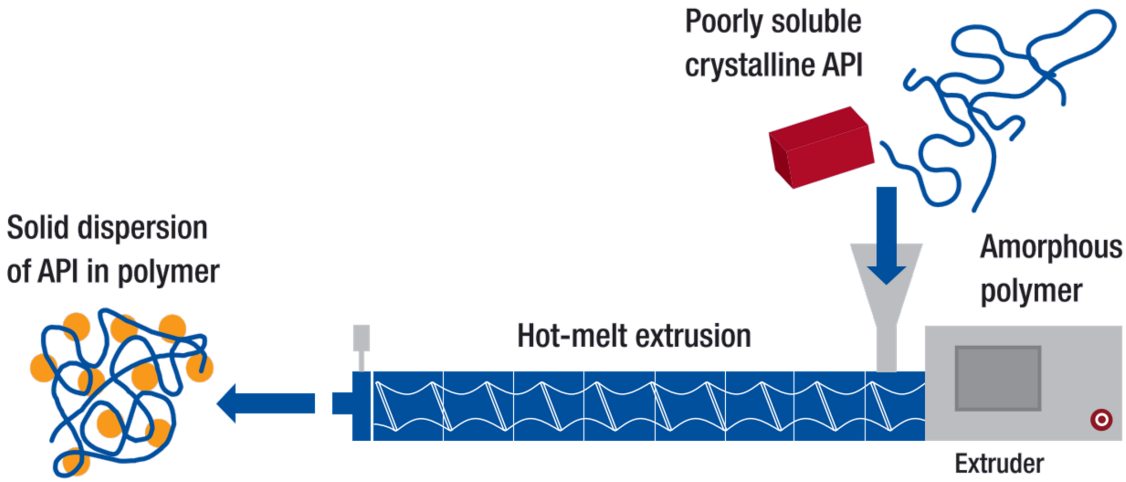

Figure 5 : Schematic illustration of a typical hot-melt extrusion process used for production of solid dispersions[12]

2.2.2 Injection Molding

Injection molding (IM) is a well established process in the plastics industry and an emerging technology in the pharmaceutical field [13]. Injection molding can be used to prepare solid solutions and for shaping of the material into a final dosage form (e.g. a tablets, implants or drug-eluting devices) in a single step. Injection molding is not a technology for production of quickly dissolving products, but dosage forms intended for controlled-release applications. The release pattern can be adjusted by the polymer and additives used as well as by the geometry of the injection molded dosage form [12].

A schematic illustration of the injection molding process is depicted in figure 6. The granular feed is molten and mixed by an upstream screw unit (similar to HME) and the resulting melt is subsequently injected semi-continuously into a cold mold under high pressure (up to several 1000 bars) where it solidifies. The operation pressure depends on the rheological properties of the melt and on the mold geometry. After a sufficiently long cooling time, the product is ejected mechanically from the mold.

The time of one molding cycle depends on material properties of the polymeric formulation. The limiting step in the cycle is usually the cooling time after injection, because the thermal conductivity of polymer melts is usually very low. Thus, this is the thermal conductivity of the polymer or formulation is the determining parameter of the cycle time, and accurate knowledge about its value enables to calculate the minimum required cooling time [7].

For correct simulation and design of IM processes, the same physical properties of the processed materials have to be taken into account, and thus have to be characterized, as for HME (see section above).

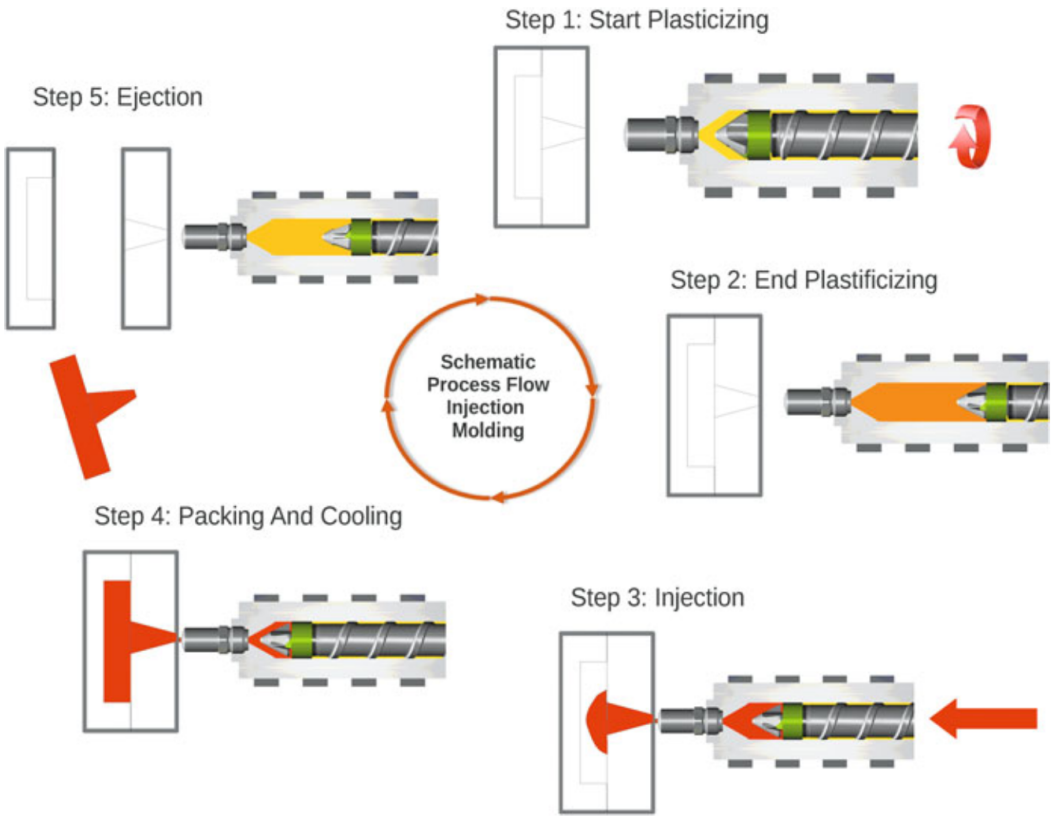

Figure 6 : Illustration of the injection molding process cycle[14]

2.3 Vacuum Compression Molding

The formation of a homogeneous melt in vacuum compression molding can be described as complete fusion of polymer particles, softened by heating while being compacted by a compressive force. This fusion process can be separated into two steps. First, sintering of the powder particles occurs, i.e. the material starts to fuse at the contact points of adjacent particles. Subsequently, after the material is heated above its softening temperature, flow is initiated due to the applied compressive force, which fills up all voids that existed between the particles. Thus, a homogeneous polymer melt is obtained. The phenomena which govern this process are not trivial, therefore to understand how the VCM process works in detail the occurring phenomena are explained in the following sections.

2.3.1 Existing Literature

Little has to be published concerning vacuum-compression molding of thermoplastics. Tung first described an apparatus for molding of polyethylene specimens in a vacuum, which were subjected to rheological analysis [15]. The apparatus design that was used in this study is depicted in figure 7. The design consists of a screw-retained chamber, sealed with O-ring seals in which a piston is enclosed. The enclosed piston is actuated by compressed air, which compacts the powdered raw material. Heat transfer is accomplished by immersing the apparatus in a constant temperature bath.

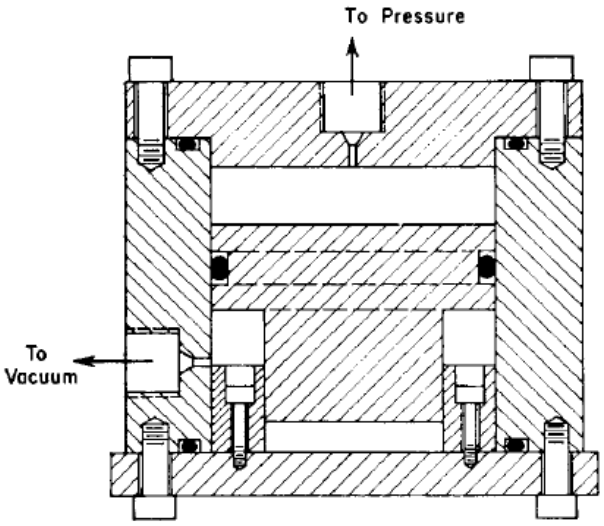

Figure 7 : Vacuum Compression Molding apparatus design (cross-section) published by Tung in 1960 [15]

Another publication compared conventionally compression-molded polypropylene specimens with others molded under vacuum conditions. In mechanical testing, numerous significant differences between the two preparation methods were found, indicating numerous advantages by the usage of a vacuum during molding. Furthermore, it was reported that the usage of vacuum tremendously reduced the necessary pressure to obtain fully fused, void-free polymer specimens compared to traditional compression molding [16].

However, despite the manifold possible interesting applications in the field of polymer material characterization, very little follow-up research has been published until now. Therefore, because of the many potential benefits of the VCM technique, there is definitely a lack of research in this field, which justifies the present study.

2.3.2 Polymer Melt Formation from Powder

The formation of a homogeneous melt in vacuum compression molding can be described as complete fusion of polymer particles, softened by heating while being compacted by a compressive force. This fusion process can be separated into two steps. First, sintering of the powder particles occurs, i.e. the material starts to fuse at the contact points of adjacent particles. Subsequently, after the material is heated above its softening temperature, flow is initiated due to the applied compressive force, which fills up all voids that existed between the particles. This way, a homogeneous polymer melt is obtained.

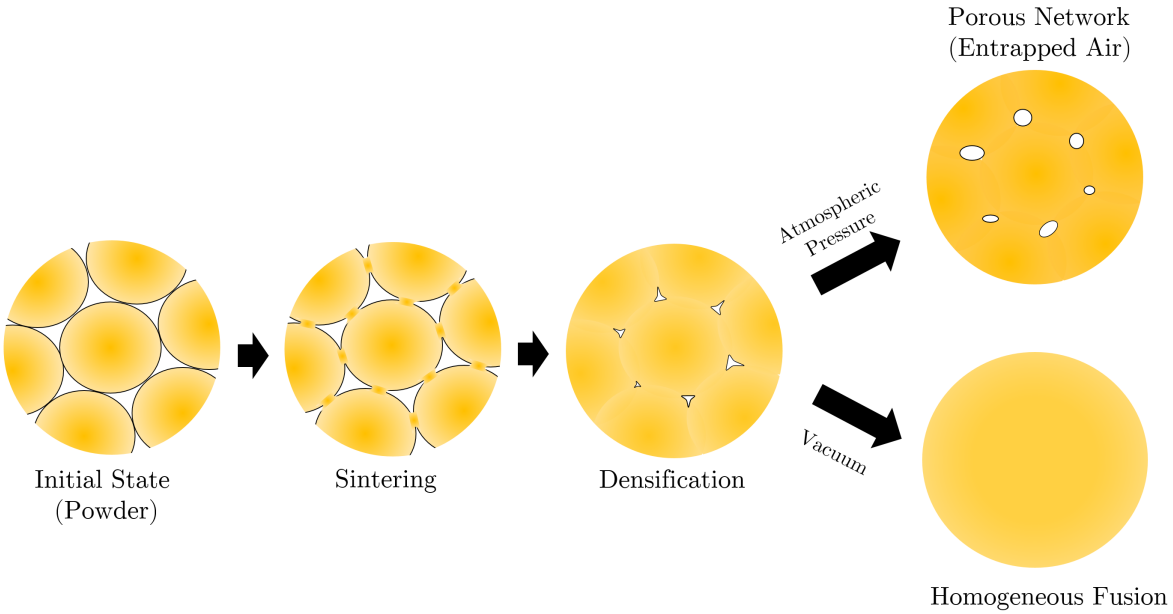

Figure 8 : Stages of formation of a polymer melt from compacted powder

The formation of a polymer melt from powder can be described using the theory of metal sintering and densification. According to Rao and Throne [17], in this process several stages take place, which are illustrated in figure 8. The initial state of the material is solid powder, which possibly has to be compacted to accelerate or even enable to start the fusion process. During the first stage, when heating the powder to a temperature well above the glass transition temperature of the polymer, particles stick or fuse together at their contact points (*sintering*). The void fraction does only slightly change during this phase. In the second stage the fused particles undergo softening and become to liquid-like droplets, which subsequently begin to coalesce with adjacent droplets (*densification*). In this phase, the void fraction markedly decreases. Coalescence of the droplets is caused by diffusion of the polymer chains between the interfaces of the droplets. The interfaces gradually disappear due to this process and mechanical strength at the interface develops. [18]. Sintering of polymers in the solid (glassy) state is therefore not possible, as the restricted molecular mobility impedes diffusion. During densification, air bubbles are entrapped in the voids between the droplets, forming a porous 3D-network. Application of a vacuum, however, allows complete fusion of the particles.

Particularly sintering of semi-crystalline polymers strongly depends on their melting behavior. For this type of polymers, in absence of external stresses, melting does not necessarily cause powder sintering [19], which necessitates the application of an external stress to compress the powder or the fusing material, respectively. Spontaneous densification without application of an external compressive force only occurs if the interfacial tension forces are able to overcome the viscous forces. Therefore, the driving force of spontaneous densification is the natural tendency of surface minimization due to interfacial tension, while viscous forces impede coalescence. Application of an external stress on the one hand accelerates sintering and on the other hand helps to overcome the viscous forces, accelerating coalescence. When sintering takes place in restricted dimensions, e.g. in a mold under pressure, thermal expansion enhances the sintering process [20]. Moreover, viscoelastic forces have an influence on coalescence.

Bellehumeur et al. found that the sintering process is slowed down depending on the degree of elasticity of the used polymer [21].

2.3.3 Influence of Air Inclusions and their Removal

The air bubbles that stay entrapped after densification can cause major alteration of the material properties. The removal of bubbles from viscous melts has been subject of many studies dealing with metal and glass-processing. However, little has been published, concerning bubble removal from polymer melts. The bubble removal process is influenced by parameters like viscosities, interfacial tension and diffusion coefficients of the involved materials. The higher the viscosity in the molten state, the higher is the fraction of air bubbles which are entrapped in the molten mass [19]. If the softening/melting process during densification is sufficiently slow, the entrapped air bubbles are pushed ahead of the coalescing melt front to a free surface, or they remain in the polymer after cooling [22]. Wolff and Münsted found that bubble inclusions within polymeric fluids can lead to significant experimental error in rheological measurements, which could lead to false conclusions drawn from the data [23]. Kelly found that in a polyethylene melt, diffusion of oxygen and nitrogen from entrapped air-bubbles into the polymer melt occurs, which is accompanied by a decreasing bubble diameter. The bubble size continued to decrease until the melt was saturated with oxygen and nitrogen [24]. Air bubbles in polymer test specimens can be a serious problem, because its rheological- and other properties are potentially affected. For example, it was shown that dissolved gases can lower the melt viscosity of polystyrene by up to 20% [25]. Moreover, it is known that at elevated temperatures (lower than typical processing temperatures) oxygen can induce chain scission and crystallization of polyethylene and polypropylene, causing embrittlement of the material [26, 27, 28]. The glass transition temperature T_g and interfacial tension can be influenced as well [29, 30]. Furthermore, the presence of a large number of bubbles makes impossible to optically or visually inspect the pure material due to reflection and diffraction of light occurring at the phase boundaries between the air bubbles and polymer.

Processing polymers in a vacuum environment is of benefit in applications where no inclusions of gasses (e.g. air) can be tolerated. A major advantage is the preservation of the intrinsic properties of the processed materials. This is, for example, due to the elimination of oxygen during the molding cycle, preventing possible oxidation.

The usefulness of vacuum compression molding was demonstrated in an early study by Rogers et al., who used a relatively large press with an evacuated mold to prepare polypropylene specimens for tensile testing [16]. The experimental findings of the authors clearly show that polypropylene exhibits oxidative embrittlement due to air exposure, when conventionally molded (figure 9). Material processed in vacuum exhibited ductile behavior due to the absence of oxygen-induced crystallization.

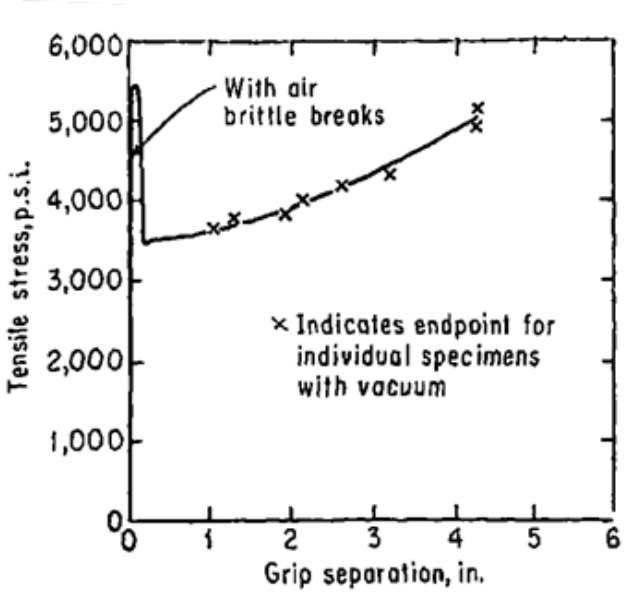

Figure 9 : Tensile-test comparison of atmospheric molded polypropylene specimens and their vacuum-compression molded counterparts, showing the embrittlement due to oxygen, adopted from [16], used with permission

2.4 Conventional Sample Preparation Methods

Many authors use solvent casting, conventional compression molding, powder compaction or injection-molding for the preparation of their specimens. The characteristics, advantages and drawbacks of these conventional methods are explained in this section

2.4.1 Compression Molding

Compression molding in its traditional form is one of the oldest methods of forming polymer powder or pellets into a film of controlled thickness. The material is placed between two heated, flat plates which are pressed together. This causes fusion of the polymer particles to a melt, which is squeezed between the plates, until the desired film thickness is reached. The plates are subsequently cooled and the film is removed. To expel air inclusions in compression molding of polymer melts, values of up to 15 MPa or 150 bars, respectively, are reported in literature [31]. In practice, such high pressures can only be achieved using hydraulic presses.

The squeezing flow in conventional compression molding is comprising shear between the plates as main contribution, distorted by extensional flow due to stretching in radial direction or compression in vertical direction, respectively. This means that the rates of deformation depend on the radial position, which may influence the properties of the resulting specimen by molecular orientation of the polymer chains [32].

The high thermal inertia of conventional platen presses and the strong deformation due to the squeezing flow make these machines an unattractive choice when working with thermally or shear sensitive compounds.

In a conventional compression-molding process, the pressure acting on the polymer melt expels air from between the particles while fusing them together. If vacuum is

utilized, sintering and densification can occur much more easily, allowing polymer particles to fuse freely, without the counter-pressure of entrapped air in voids. This has the consequence that there is no oxygen is present in entrapped bubbles, which could diffuse into the polymer, causing a change of material properties. By application of a compressive force, voids are entirely filled up by the flowing material, without pressure of entrapped gas counteracting. Therefore, when applying a vacuum, only a comparatively low compressive force is necessary, which helps to intensify the contact between the particle interfaces, accelerating coalescence and filling of voids due to flow. Furthermore, in vacuum molding, no squeezing flow is necessary to expel air bubbles, so the mold geometry can be fixed. This effectively eliminates flow-induced orientations, that can occur in conventional compression molding.

2.4.2 Solvent Casting

In solvent casting, the sample material is fully dissolved in a suitable solvent, and subsequently the solution is casted into a mold. Then, the solvent is evaporated to obtain a solid specimen. Some authors also apply a vacuum or heat the solution to increase the rate of evaporation. Nevertheless, even in best conditions, long hours are required until an equilibrium is established. The main disadvantage of this technique is, that solvent is often retained within the material, significantly influencing its thermo-mechanical properties.

Rhim et al. studied the influence of processing method on the mechanical performance of poly-lactic acid (PLA) films. The authors compared solvent casting with conventional compression-molding and found that the solvent cast films retained 13.7% of the solvent chloroform, which acted as a plasticizer. The solvent casted specimens exhibited ductile behavior, compression-molded counterparts were strong and brittle. Furthermore, the compression-molded specimens showed comparatively higher thermal stability [33].

Saldanha and Kyu investigated the influence of solvent casting on the phase morphology of a polymethylmethacrylate (PMMA) and polycarbonate (PC) blend. They found that interaction of solvents with the polymers can induce crystallization and phase separation [34].

Solvent casting is also used by authors to prepare test specimens of pharmaceutical polymers. For example, Lim et al. studied the effect of different plasticizers on the mechanical properties of Soluplus® using solvent-cast film specimens [35]. The authors reported that it was not possible to remove the cast films of the neat polymer (i.e. without added plasticizers) from the casting mold due to brittleness. Moreover, the authors did not specify the residual solvent content after drying the solvent-cast films. Thus, it is questionable whether intrinsic material properties of Soluplus® or rather properties of a Soluplus®/solvent composite were measured in this study.

2.4.3 Injection Molding

Injection molding is the most common manufacturing technique for mass-produced plastics products and also an emerging technology in the pharmaceutical field [13]. It allows to directly produce complex parts with a good surface finish at low costs.

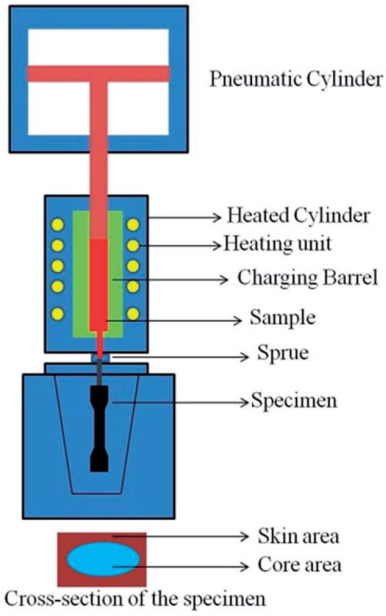

Figure 10 : Schematic sketch of the laboratory injection-molding machine *Minijet* by ThermoScientific[36]

Small-scale injection molding machines are used for production of polymeric test specimens. An example is a injection molding machine commercialized as MiniJet(TM) by ThermoScientific. Unlike traditional injection molding machines, this device is equipped with a piston instead of a screw. A schematic sketch of the device is depicted in figure 10. It consists of a heated cylinder in which the specimen material is plasticized. A pneumatic cylinder subsequently pushes piston down, forcing the hot polymer melt to flow into a cold mold, where it rapidly solidifies. The cross-section of an exemplary specimen is shown at the bottom of the figure. A skin area near the wall and a core area, farther away from the wall can be distinguished. These areas can differ strongly in terms of mechanical properties. Moreover, they strongly differ in crystallinity in the particular case of semi-crystalline polymers are considered, where the skin shows a higher fraction of amorphous phase while the core is more crystalline. This skin-core effect is a commonly observed for injection molded parts. The reason for this is the rapid vitrification of material which directly comes into contact with the cold mold surface. The material which is located more in the center during injection solidifies more slowly. Due to the non-uniform shrinkage of the material, strong residual stresses develop. Residual stresses act internally at room temperature, with effects equivalent to externally applied stresses. Moreover, mechanical behavior of injection-molded parts is influenced by residual stresses. Also the flow itself can be the source of residual stresses evolution. Rapid injection and cooling of the polymer melt during injection, can cause material orientations to freeze in, which leads to flow-induced residual stresses [37]. These material orientations in the solidified specimen are a drawback especially for semi-crystalline polymers, which exhibit a strong anisotropy along the direction of molecular alignment or perpendicular to it, respectively. An example for the flow induced superstructures in injection molded specimens shown in figure 11. The flow field in the mold during injection is approximately parabolic, like it is typical for laminar flow. The strong flow during injection in combination with rapid cooling leads to the parabolic traces on the surface of the specimen, which is a clear sign that material

orientations are present within the specimen.

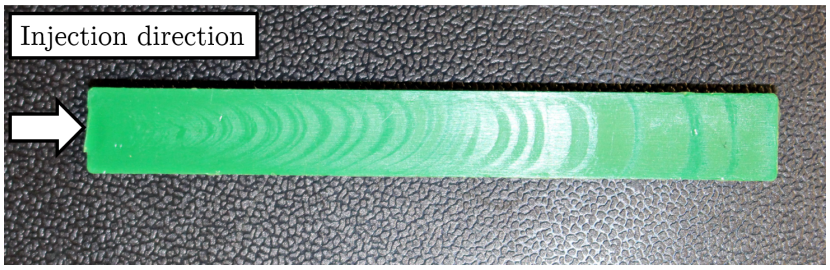

Figure 11 : Flow-induced material orientations in an injection molded rectangular bar of polypropylene

Conclusion

The drawbacks of all these methods lead to the conclusion that there is a need for a more reliable, fast and reproducible method to produce homogeneous test specimens from thermoplastic powder/pellets. A solvent-free method which minimizes degradation, while a homogeneous specimen free of air- or moisture inclusion related phase-boundaries is obtained. Moreover, there should not be any flow induced orientations remaining within the finished sample. One intention of this thesis is to show that vacuum-compression molding (VCM) is a method that satisfies these prerequisites. Therefore, in the following sections, the characteristics of specimens prepared using the VCM approach are introduced, discussed and evaluated

2.5 Differential Scanning Calorimetry (DSC)

Differential scanning calorimetry (DSC) is a thermoanalytical technique to characterize physical and chemical changes of materials via changes in enthalpy or heat capacity, respectively. Nearly all pharmaceutical processes involve such changes, which led to wide application of DSC in this field. The key principle of differential thermal analysis is to measure energy differences between a the sample and a reference material as a function of a pre-determined temperature cycle. From these measured energy differences, information about the response of a sample to thermal stresses can be deducted. Understanding of these responses is a very important part of the development of stable medicinal products [38]. Established pharmaceutical applications of DSC include glass-transition temperature studies, measurement of heat capacity, assessment of compatibility of formulation components, detection of polymorphism, and purity determination [38].

In polymer extrusion and injection molding, the temperature- and velocity fields are strongly coupled due to the strong temperature dependence of viscosity and the high magnitude of shear heating. Therefore, to be able to accurately simulate the flow in these processes, not only the mechanical parameters of the material have to be known (e.g. viscosities), but also the thermal material properties (heat capacity, thermal conductivity) are of great importance. This is especially important because errors in the calculation of the temperature field due to wrong material parameters are fed back to the calculation of the velocity field, introducing an error. Accurately knowing the thermal properties of the processed material as a function of temperature is therefore key to achieve good simulation results, which are in agreement with experiments. However, in openly accessible literature, thermal conductivity data for pharmaceutical polymers is still pretty much lacking. Furthermore, addition of APIs and other excipients like plasticizers to the formulation might have considerable impact on the thermal properties. Thus, in pharmaceutical process development, it is necessary to measure these properties for each individual formulation. Thus, there is the need for a method that allows to measure the thermal conductivity of pharmaceutical formulations. In principle, dedicated equipment designed for this task could be used, for example the line-source method and the laser-flash method. Both methods can be used to determine the thermal conductivity/diffusivity of solid and molten materials. However, the necessary equipment is often not available. Therefore, it would be desirable to be able to measure the thermal conductivity using differential scanning calorimetry (DSC). DSC is an established material characterization method in pharmaceutical research, and a DSC instrument it is available in almost every research laboratory.

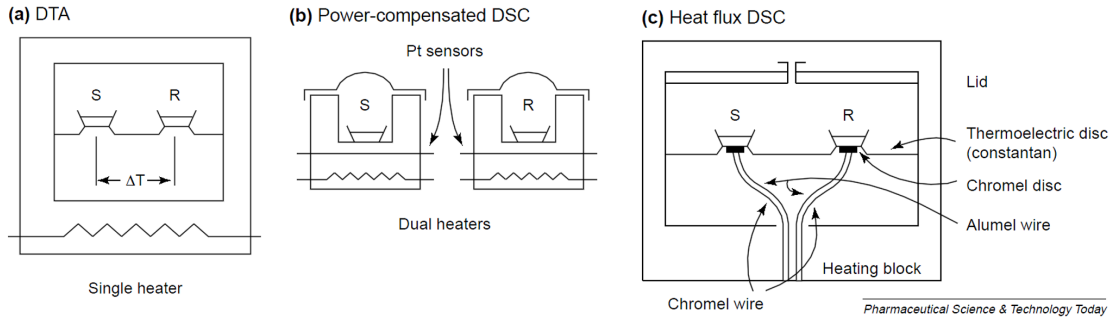

Figure 12 : Schematic diagrams of different differential thermal analysis principles, reproduced with permission from [39]

2.5.1 Modulated Differential Scanning Calorimetry (MDSC)

Modulated temperature differential scanning calorimetry is an extension of DSC, in which the heating program is modulated, e.g., by sinusoidal temperature oscillations.

A modulated DSC temperature program of MDSC is given by:

$$T(t) = T_0 + bt + A_T \sin(\omega t) \tag{2.2}$$

T_0 is the initial temperature, b is the underlying heating rate, A_T is the amplitude of the temperature modulation, and ω is the angular frequency. In figure 13, the temperature program of modulated DSC is compared to the linear ramp used in conventional DSC.

The measured total heat flow (HF) is analyzed mathematically to split up the heat-flow into a heat-capacity related component (reversing heat flow) and a component due to kinetically hindered thermal events (non-reversing heat-flow)[40]. The modulated DSC heat-flow equation is generally expressed as:

$$\underbrace{\frac{dQ}{dt}}_{=HF} = \underbrace{C_p \frac{dT}{dt}}_{\text{Reversing heat-flow}} + \underbrace{f\,(t,T)}_{\text{Non-reversing heat-flow}} \tag{2.3}$$

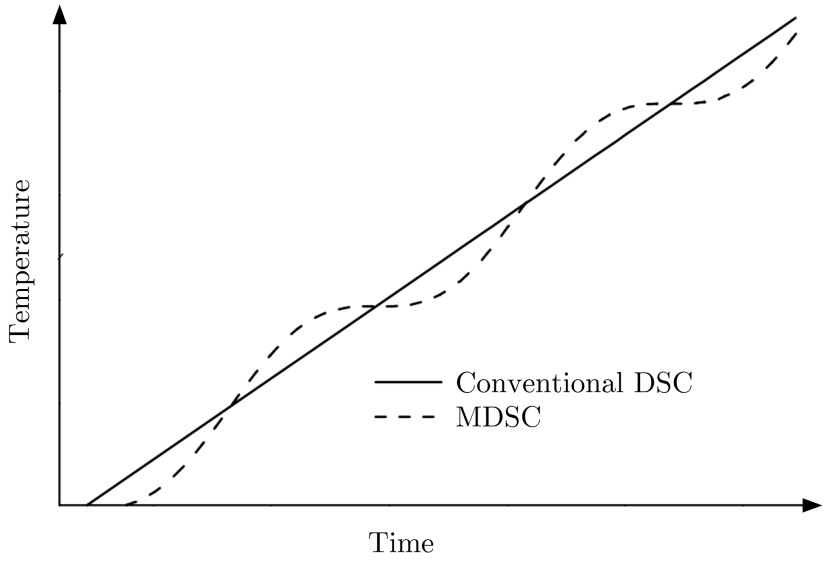

Figure 13 : Comparison of the heating programs of modulated DSC (MDSC) and conventional DSC [41]

The separation of the heat-flow into reversing and non-reversing signals allows to decompose complex, overlapping thermal processes [38]. The reversing heat flow is heat capacity related, hence arises due to the molecular motion of the sample. A reversing quantity means, that at any given time there is a heat flow contribution that is proportional to the heating rate, i.e. a fast response occurs within the time scale of the measurements. Therefore, this heat flow contribution is reversible. Examples include glass transition and melting. Contrarily, the non-reversing heat flow contribution $f\,(t, T)$ arises as consequence of processes that are either irreversible within the time of the measurement or reversible processes which are kinetically hindered. There are many different forms of $\mathrm{f}(t, T)$. Examples include, for example, enthalpic recovery, evaporation, crystallization, decomposition, and curing [42].

A typical MDSC thermograms of a material with amorphous and crystalline fractions is depicted in figure 14. In the top part of the figure, the raw data of the applied modulated heating rate and the measured modulated heat flow are shown, which are deconvoluted and averaged to obtain the non-reversing an reversing components of the total heat flow. For details concerning the deconvolution procedure, it is referred to reference [41]. Glass transition and melting are heat-capacity related thermal events and therefore can be seen in the reversing heat flow curve. Enthalpic recovery, cold crystallization and crystal perfection however are kinetically hindered processes and therefore appear in the non-reversing heat flow. Amorphous materials mostly only exhibit glass transition in the reversing heat flow and enthalpic recovery in the non-reversing heat flow. This is a major benefit of this method, compared to traditional DSC, which does not allow to separate the signal into component responses.

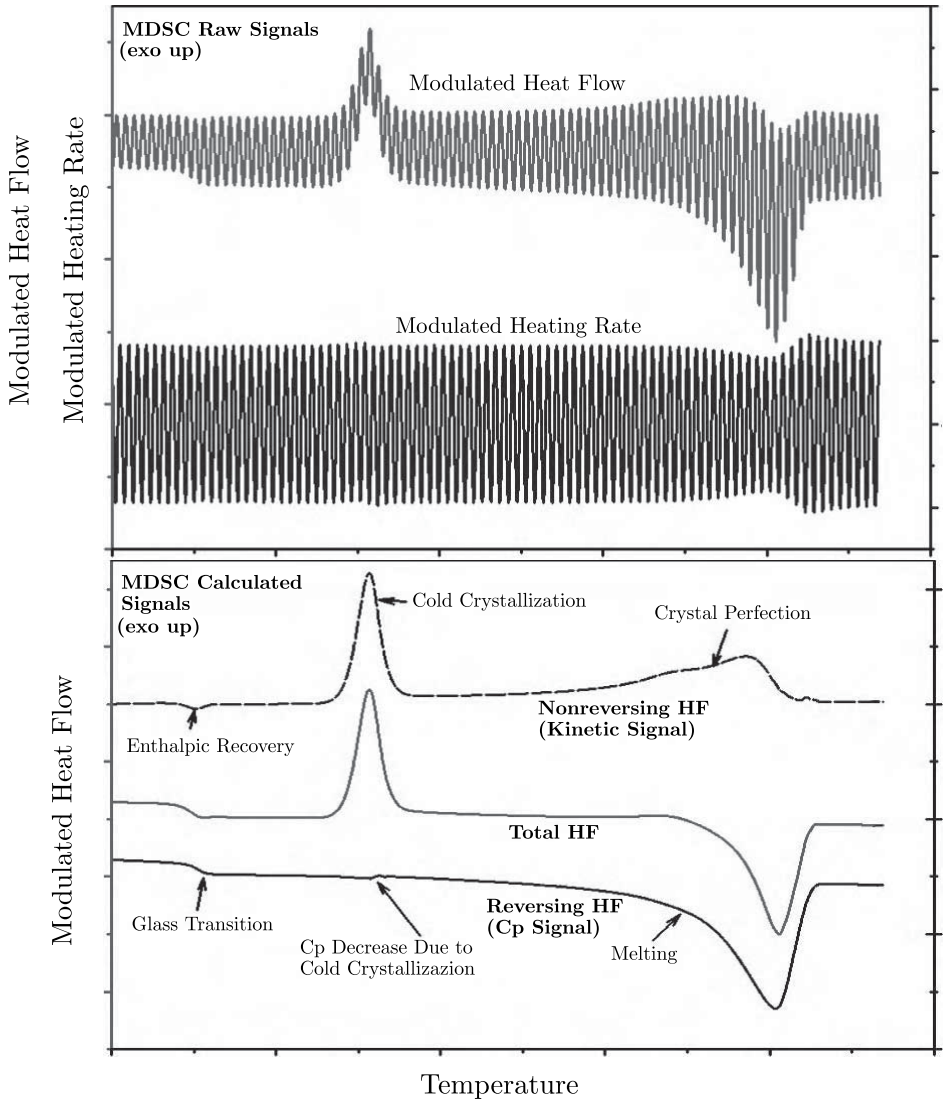

Figure 14 : Top: MDSC raw signals of modulated heating rate (applied stimulus) and modulated heat flow (measured response). Bottom: Deconvoluted heat flow components obtained from the raw data showing multiple thermal events. [41]

2.5.2 Influence of Sample Preparation on Experimental Results

Precise and reproducible DSC measurements require good heat transfer between sample, pan and measuring cell. The quality of heat transfer between the calorimeter furnace and the sample as well as the thermal history can have notable influence on material parameters obtained from DSC experiments. Therefore, standardization of these factors is necessary in order to achieve reproducible results [43].

An optimal DSC specimen is described in literature as thin, plane-parallel disc with a smooth surface and a high degree of flatness [43].

A large contact area between sample and pan leads to increased heat transfer. Thus, the sensitivity of the measurement increases, as the contact area becomes larger. Therefore, the diameter of the sample should be as large as possible. However, there should be

some space between pan walls and specimen, to avoid wetting of the walls by molten material. This would increase the contact area during the measurement and is known to cause artifacts [43].

Thermal Contact and Time-Temperature History

Rieger [44] published round-robin test results of glass-transition measurements of a high molecular-weight polystyrene. This material was chosen because it shows a well defined, narrow glass-transition. Ten different institutions were asked to test a provided polystyrene specimen and to provide the measured data. The test revealed that the reported midpoint-values of the T_g spread around $107°C$ by $\pm 2°C$ despite the fact that the literature values from reliable sources are approximately $100°C$. Furthermore, it was found that all measured heat-flow curves significantly differed from each other. It was found that one reason for the discrepancy of the measured values from the literature values was the time-temperature history, i.e. heating and cooling history, which proved to have considerable impact on the thermal transitions, including glass transition temperature. As other influential factors, the variable apparent thermal conductivity of the sample and the imperfect contact between specimen and crucible were identified. This imperfect thermal contact persisted even after melting the sample at a temperature $50°C$ above the T_g in the first heating run, due to the high viscous melt. The apparent thermal conductivity is a function of the sample mass, the thermal resistance and the homogeneity of the sample. The quality of the thermal contact between sample and pan and the apparent thermal conductivity are therefore related. This thermal inertia effect induces variability to the measurement. Thus, also the measured T_g depends on all parameters mentioned above. In another part of the study of Rieger, smooth ground platelets were tested and compared to shavings. It was found that, due to the better thermal contact of the flat platelets, the measured values of T_g were significantly lowered. Higher sample mass had the opposite effect on T_g [44]. Similar findings were published by Frick et al., who found that the melting temperature of polyoxymethylene (POM) and the width of the melting peak both are directly proportional to the sample mass [43].

2.6 Rheology

Fully understanding the rheological behavior of the processed materials is crucial for the optimal design of polymer processing equipment. Particularly for use in process equipment flow simulation, the accuracy of the results is directly dependent on the quality and correctness of the utilized material data. Accurate simulations bear great potential for accelerating process development, reducing the need for trial-and-error experiments. Consequently, the simulation approach is less time, labor and material-consuming as traditional equipment design [45]. The mechanical response of a polymer or a polymeric pharmaceutical formulation to shear and extensional deformation has major impact on its processability. Polymer melts generally exhibit a much more complex flow behavior than Newtonian Fluids like water or oil. Generally, polymer melts show a non-Newtonian, time-dependent (viscoelastic) flow behavior. In the case of a Newtonian fluid, the relationship between shear stress (τ) and shear rate ($\dot{\gamma}$) is linear, with a proportionality factor, called *viscosity*, $\eta = \frac{\tau}{\dot{\gamma}}$. The viscosity is a strong function of temperature, and in case of some polymer melts, it also depends on pressure [46]. Accurate knowledge of the viscosity η as a function of shear-rate $\dot{\gamma}$ and temperature is of utmost importance for simulation and equipment design purposes.

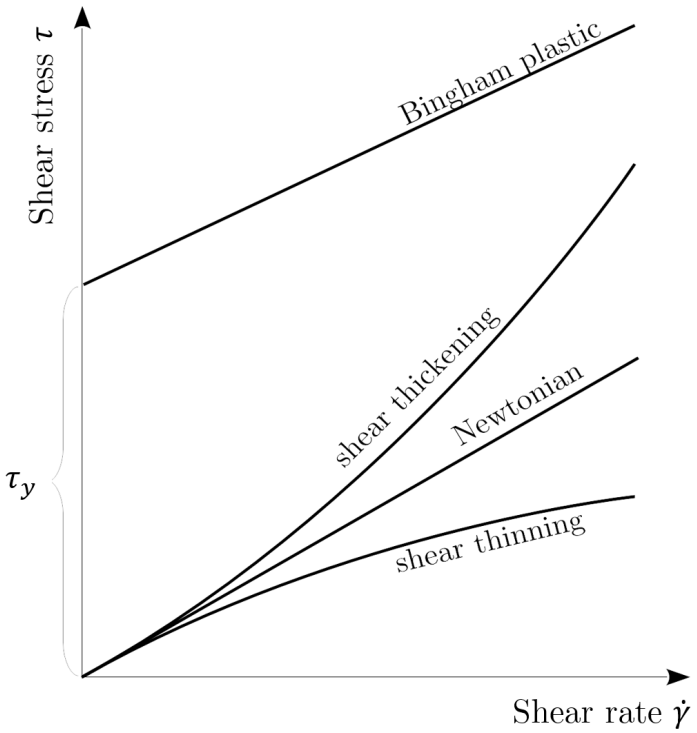

Figure 15 : Typical relationship of shear stress as a function of shear rate for different fluids [47]

For fluids with a more complex molecular structure, the shear stress τ shows a non-linear dependence on shear rate $\dot{\gamma}$. Different possible relationships of stress and strain are shown in figure 15. The slope of the curves indicates the viscosity as a function of $\dot{\gamma}$. It is possible that the shear stress τ grows with increasing shear rate. This behavior is called *shear thickening* and can be observed, e.g., when shearing concentrated aqueous corn starch suspensions. Furthermore, the shear stress τ can decline with increasing shear rate (*shear thinning*). This behavior is commonly observed for polymer melts and

-solutions. Moreover, it can be that a certain minimum stress, the so-called yield stress τ_y has to be overcome before the material can flow. Below this threshold value of stress, the material behaves like a viscoelastic solid. If a material exhibits a yield stress and subsequently flows with constant viscosity it is termed Bingham plastic. However, also shear-thinning and thickening behavior are observed for materials with a yield-stress.

Viscoelasticity

As previously mentioned, many materials, e.g. polymers and polymer melts, have a viscoelastic character. Every material which exhibits a flow behavior lying in between the two extremes of an ideal elastic solid and an ideal viscous liquid is called viscoelastic (VE), because both, elastic and viscous properties can be observed. A viscoelastic material has a certain memory of its deformation history. It is a cross between an Newtonian liquid (which forgets instantly), and an ideal-elastic solid (which never forgets). To model a viscoelastic substance, its memory has to be taken into account [48].

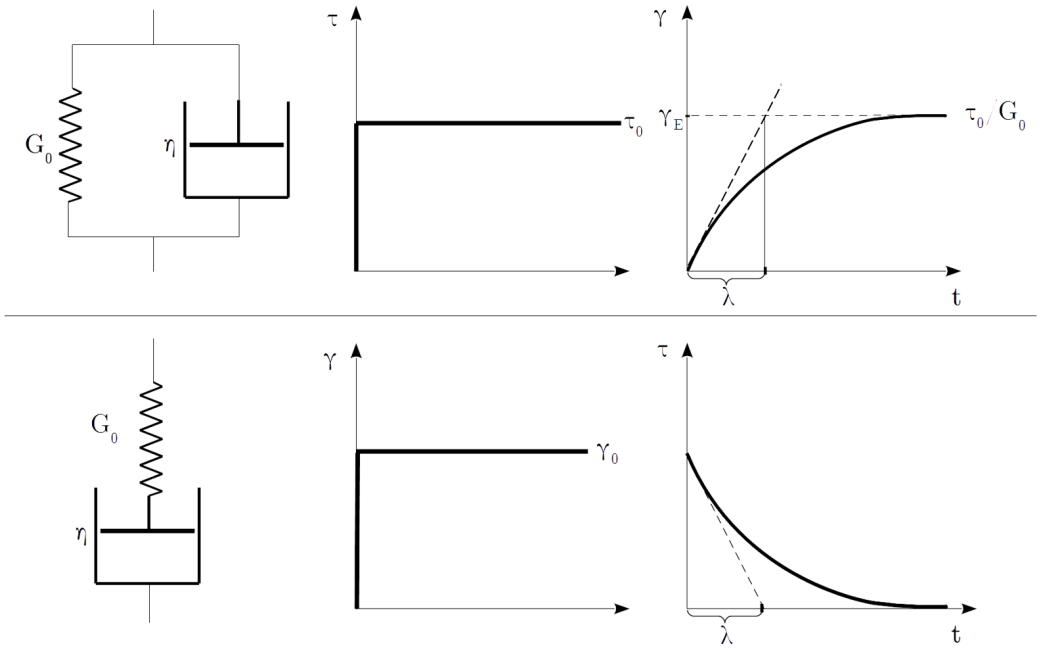

Figure 16 : Kelvin-Voigt rheological model for viscoelastic solids (top) and Maxwell model for viscoelastic fluids (bottom)[47]

Viscoelastic liquids and solids can be modelled using two linear elements. The linear elements are a spring with the stiffness G_0 which represents the elastic portion, and a dashpot with a viscosity of η representing the viscous portion. A common approach to model the behavior of a viscoelastic liquid is to serially connect these two elements (Maxwell model). Conversely, viscoelastic solids can be modelled by putting the spring and the dashpot in a parallel connection (Kelvin-Voigt model). These models and their typical response to a step-stress or step-strain, respectively, are depicted in figure 16. However, these models deliver no hint of the structural cause of viscoelasticity. If a viscoelastic solid is suddenly deformed by constant stress τ_0, the resulting strain γ does not instantaneously reach its equilibrium. Instead, there is a certain time lag

until the final strain is reached. This is commonly referred to as *creep*. The lag can be quantified by the so-called relaxation time λ, which is defined as the particular time, at which the tangent to the strain curve at time $t = 0$ intersects the equilibrium strain line $\gamma_E = \tau_0/G_0$. For viscoelastic fluids, the situation is similar. If a step-strain γ_0 is applied, the resulting stress decays exponentially and approaches zero. Again, a relaxation time λ can be defined using the time where tangent of the $\tau(t)$ function intersects a stress value of zero. The relaxation time λ is a measure for the extent of memory previous deformation history. The resulting stress-relaxation function of the Maxwell model reads:

$$\tau(t) = \gamma_0 \, G_0 \, \exp\left(\frac{-t}{\lambda}\right) \tag{2.4}$$

For real polymer melts, the Maxwell model is just a rough approximation of reality, because the stiffness of the spring and the viscosity of the dashpot are related to molecular properties such as structure and length of the polymer chains. Heavily branched polymers with long chains, usually have long relaxation times and therefore exhibit a relatively long memory of their previous deformation history. As mentioned, in processing this memory has to be taken into account. If deformation of the material during the process occur within a timescale which is in order of the relaxation time λ, viscoelastic effects start to have large influence on the flow behavior. Thus, if the material is deformed slowly within a timescale that is longer than the relaxation time, the molecules will have enough time to relax, and therefore viscoelastic effects will have little influence on flow behavior. The ratio of relaxation time and deformation timescale of the polymer describes the relative importance of viscoelastic effects in a process. This ratio is termed *Deborah Number* (De):

$$De = \frac{\lambda}{t_p} \tag{2.5}$$

where t_p is a characteristic timescale of the flow. In a shear flow, for example, the reciprocal shear rate $\dot{\gamma}^{-1}$ is the relevant timescale. This recognition is very useful to determine whether in equipment design or simulation, viscoelastic effects have to be taken into account or not. If the Deborah number is much smaller than one, viscoelastic effects will have hardly any influence on the flow and thus can safely be neglected.

2.6.1 Oscillatory Rheometry

Oscillatory testing allows to test the properties of all kinds of viscoelastic fluids over a much wider range of viscosities. Oscillatory rheometry can be idealized using the so-called Two-Plates-Model (figure 17). Via a rod, the upper plate is connected with a disk which is rotating continuously. The result is a oscillatory motion of the upper plate, while the lower plate stays at rest. The geometrical situation is illustrated in the lower part of the figure. The force $F(t)$ causes the deformation $s(t)$ of the sample, assuming the no-slip condition of fluid mechanics is fulfilled. Because of the rotation of the disk, the sample is exposed to a sinusoidal strain $\gamma(t)$ at an angular frequency of ω and a deformation amplitude of γ_A [47]:

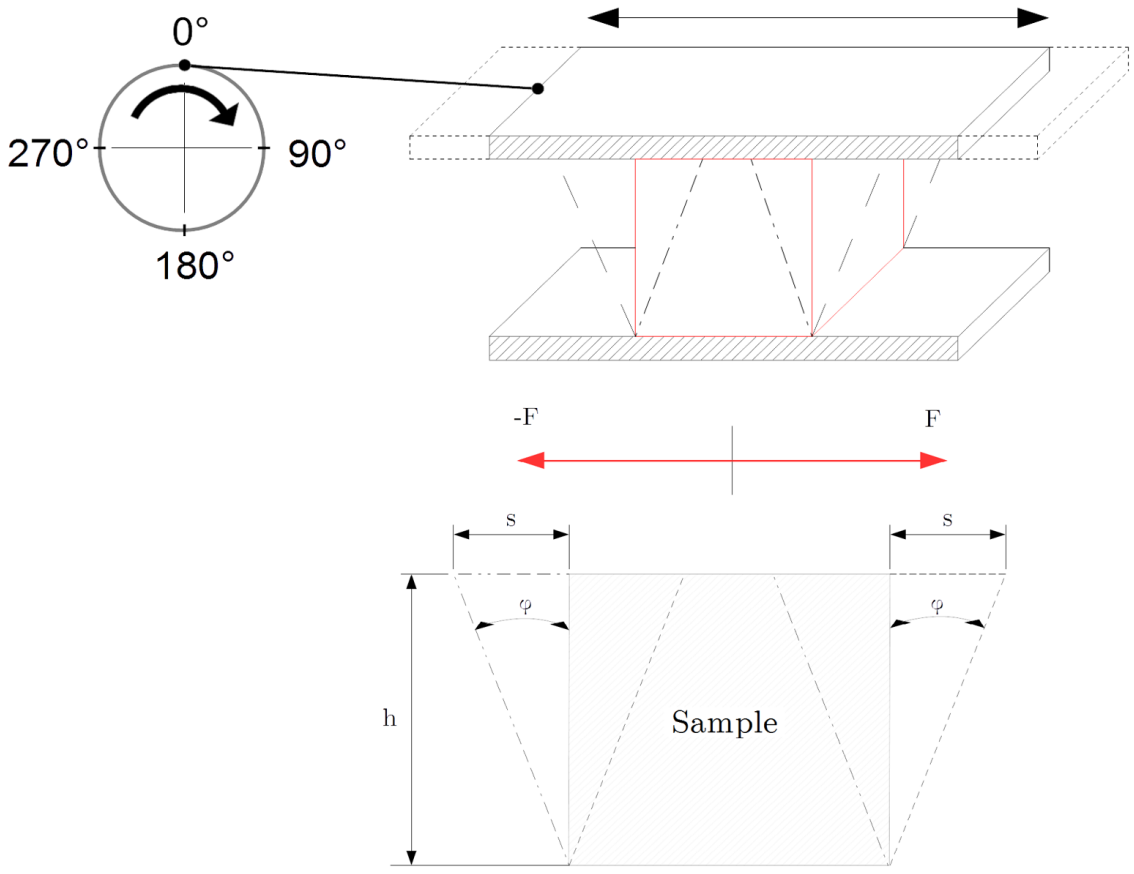

Figure 17 : Two plate model as idealization of oscillatory rheometry [47]

The strain γ as a function of time therefore can be expressed as:

$$\gamma(t) = \gamma_A \sin(\omega t) = \gamma_A \exp^{-i\omega t} \tag{2.6}$$

Where γ_A is the strain amplitude and ω is the angular frequency and t is the time. The time derivative of the strain is the shear rate $\dot{\gamma}$, which reads:

$$\dot{\gamma}(t) = \gamma_A \omega \cos(\omega t) = \gamma_A \omega \exp^{-i\omega t} \tag{2.7}$$

The shear stress, which has to be applied to achieve the preset oscillatory strain is given by:

$$\tau(t) = \tau_A \sin(\omega t + \delta) = \tau_A \exp^{-i\omega t + \delta} \tag{2.8}$$

where τ_A is the shear stress amplitude and δ is the phase shift occuring between stress and strain oscillation. The phase shift between strain signal $\gamma(t)$ and stress signal $\tau(t)$ is illustrated in figure 18.

For ideally elastic solids, the phase shift is zero, and both signals are in phase. In contrast for a Newtonian liquid, the phase shift is π and the signal are out of phase.

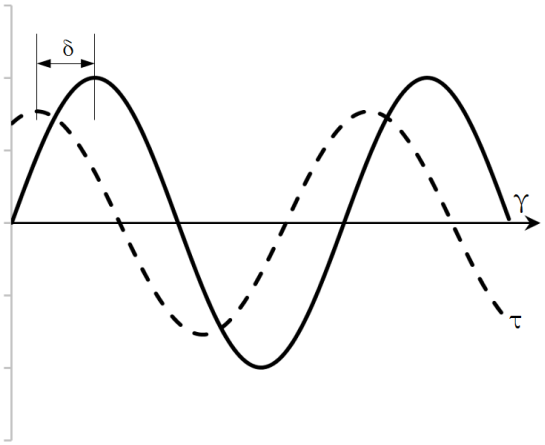

Figure 18 : Phase shift angle δ between stress and strain oscillations [47]

Viscoelastic materials exhibit a phase shift between these two extremes. The phase shift thus gives the information if a material is behaving more viscous (more liquid like) or more elastic(more solid like).

Using Hooke's law for dynamic stress and strain, inserting the expressions for $\tau(t)$ and $\gamma(t)$ given above, a dynamic shear modulus G^* can be introduced:

$$G^* = \frac{\tau(t)}{\gamma(t)} = \frac{\tau_A}{\gamma_A}(\cos(\delta) + i\sin(\delta)) \tag{2.9}$$

Analogously, using the definition of viscosity, a complex viscosity η^* can be defined:

$$\eta^* = \frac{\tau}{\dot{\gamma}} = \frac{1}{\omega}\frac{\tau_A}{\gamma_A}(\cos(\delta) + i\sin(\delta)) \tag{2.10}$$

Therefore, the relationship between these two quantities is:

$$\eta^* = \frac{G^*}{\omega} \tag{2.11}$$

η^* and G^* are termed *complex* quantifies because they can be defined in the complex plane (figure 19. Using the phase angle δ, the complex quantities can be split up into real and imaginary parts:

$$G^* = G' + i\,G'' = G^*\left[\cos(\delta) + i\sin(\delta)\right] \tag{2.12}$$

$$\eta^* = \eta' - i\,\eta'' = \eta^*\left[\cos(\delta) - i\sin(\delta)\right] \tag{2.13}$$

G' and G'' are called storage or loss modulus respectively. The storage modulus G' is a measure for the ability of the material to store elastic energy, and thus for the elastic contribution to the total modulus. Conversely, the loss modulus G'' is a measure for the dissipation of energy (i.e. transformation into heat) and hence for the viscous

contribution to the total modulus. The components of the complex viscosity η' and η'' can be regarded analogously, however they are not explicitly named.

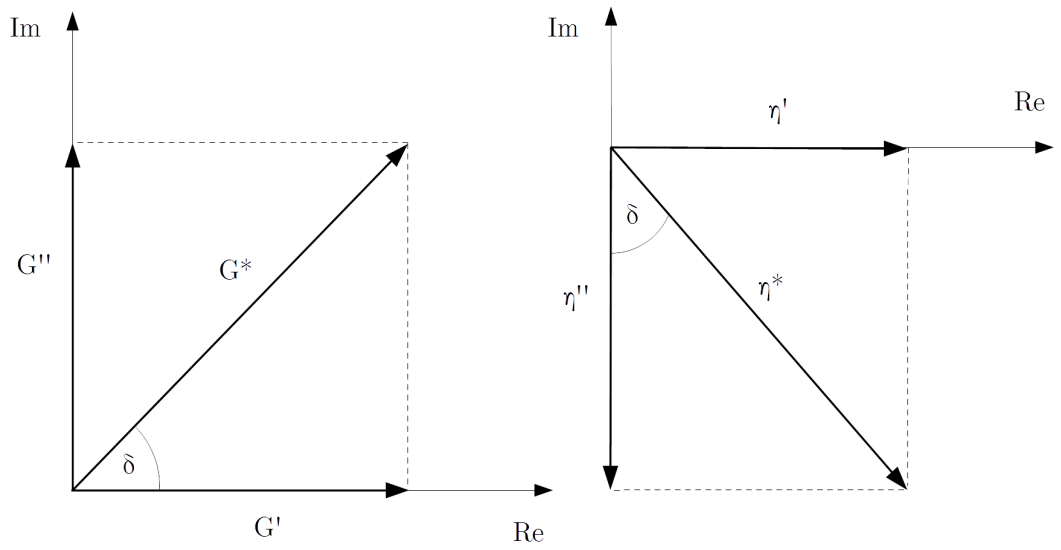

Figure 19 : Definition of dynamic shear modulus G^* and complex viscosity η^* in the complex plane [47]

The tangent of the phase angle δ is termed *loss factor* is measure for the dissipated energy due to deformation and can be expressed as:

$$\tan\delta = \frac{G''}{G'} = \frac{\text{dissipated energy}}{\text{stored energy}} \tag{2.14}$$

The flow behavior of materials can be classified using the loss factor $\tan(\delta)$ as follows:

- $\tan\delta \to 0$ ideal elastic solid
- $\tan\delta < 1$ elastic-dominant (solid-like)
- $\tan\delta = 1$ transition point
- $\tan\delta > 1$ viscous-dominant (liquid-like)
- $\tan\delta \to \infty$ Newtonian fluid

Oscillatory rheometry is particularly practical, because of an important finding of Cox and Merz, which appears peculiar at first glance. They reported that for polymer melts, the function of shear viscosity η vs. shear rate $\dot{\gamma}$, measured using a rotational rheometer, is equal to the function of the so-called *complex viscosity* η^* vs. angular frequency ω, measured using an oscillatory rheometer [49]:

$$|\eta^*|(\omega) \cong \eta(\dot{\gamma}) \tag{2.15}$$

Thus, the Cox-Merz rule allows that the dynamic data obtained using oscillatory testing is equal to steady shear data and thus can readily be used for all simulation and design purposes.

One possibility to represent flow curves of a shear-thinning polymer melt is the semi-empirical Carreau-Yasuda model [50, 51]:

$$\eta(\dot{\gamma}) = \eta_0 \left[1 + (\lambda \dot{\gamma})^a\right]^{\frac{n-1}{a}} \tag{2.16}$$

with the parameters η_0, a, n and λ. A typical flow function of a polymer melt and the meaning of the parameters are shown in figure 20.

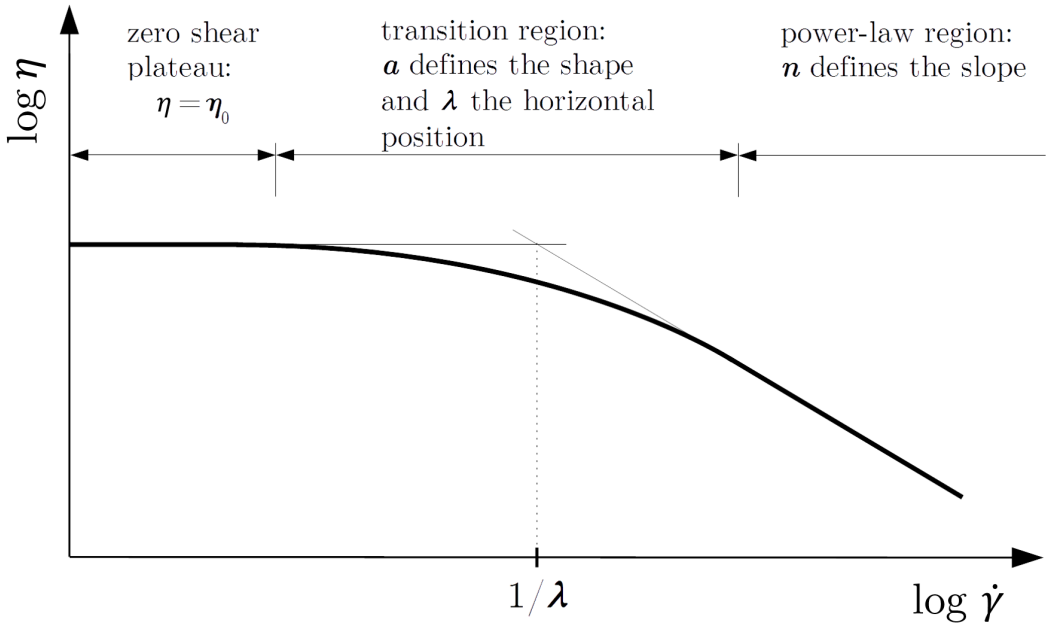

Figure 20 : Typical flow curve of a polymer melt with shear-thinning behavior. The meaning of the parameters of the Carreau-Yasuda model is indicated [47]

In figure 20, a typical flow curve of a polymer melt is depicted, together with a description of the meaning of the parameters of the Carreau-Yasuda model. At low shear rates, the viscosity does not change, because polymer chain relaxation is faster than the timescale of the flow ($\dot{\gamma}^{-1}$), thus there no significant shear thinning effect (zero-shear plateau). The viscosity at very low shear rates called zero-shear viscosity η_0. As the shear rate is increased, more and more chains cannot keep up with the rapid deformation anymore. This expresses itself in a successively decreasing viscosity with increasing shear rate. Subsequently, a power-law region is approached, which can be characterized using the power-law exponent n. The smaller the value of n, the more pronounced is the shear thinning behavior. The parameter a describes the shape of the transition between the zero-shear plateau and the power-law region. The Carreau-Yasuda model also contains the parameter λ which has the dimension of a time, and is approximately equal to the terminal relaxation time (i.e. the longest relaxation time) of the polymer.

Amplitude and Frequency Sweeps

At low strain amplitudes γ_A, the dynamic modulus G^* of viscoelastic materials has a constant value at a given frequency, i.e. it is not a function of strain amplitude γ_A. In this range, linear viscoelastic (LVE) behavior is observed, i.e. when increasing the strain amplitude γ_A by a factor of x, also the stress amplitude τ_A increases by the same factor. However, at higher magnitudes of γ_A, the dynamic modulus $G*$ starts to depend on the strain amplitude, and non-linear behavior is observed.

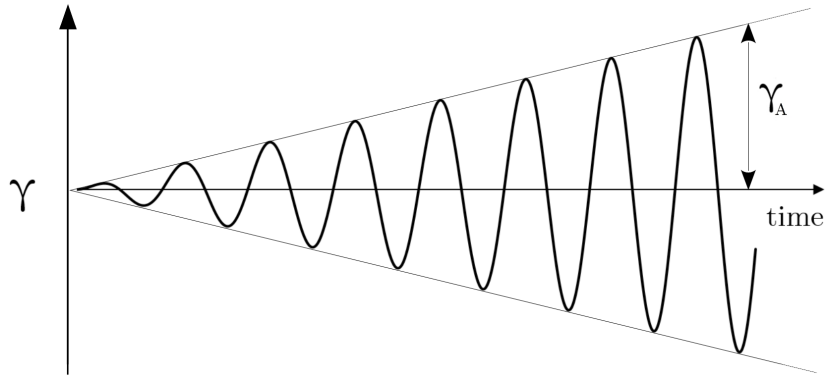

Figure 21 : Schematic illustration of the strain amplitude evolution during an amplitude sweep [47]

The limiting strain amplitude value of the LVE range is determined by successively increasing the strain amplitude at a given frequency, until G^* starts to deviate from a constant value [52]. This procedure is referred to as *amplitude sweep* (figure 21). Therefore, to ensure consistent complex viscosity or complex modulus data, the chosen strain amplitude γ_A must lie within the LVE range.

After an appropriate strain amplitude value γ_A within the LVE range is found, a frequency sweep can be performed to obtain the complex viscosity η^*, complex modulus G^* and phase angle δ as a function of angular frequency. In this test, the frequency is changed while the strain amplitude γ_A is held constant, at a value well below the LVE limit. This is illustrated in figure 22.

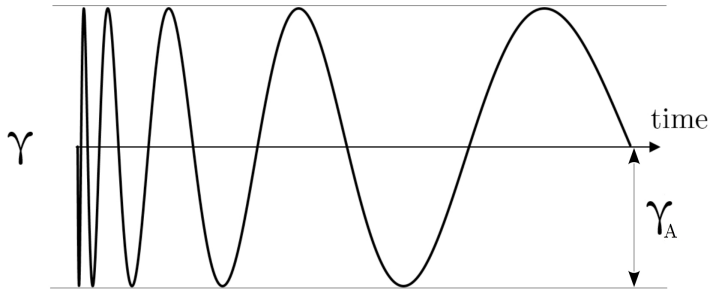

Figure 22 : Schematic illustration of the frequency change during the measurement in a frequency sweep[47]

As mentioned above, the obtained complex flow function from the frequency sweep ($|\eta^*|(\omega)$) in most cases agrees with the steady shear flow function ($\eta(\dot{\gamma})$ of the same material, according to the rule of Cox and Merz.

2.6.2 Extensional Rheology

Extensional flows occur in many polymer processing operations like film blowing, injection molding or hot-melt extrusion (HME). For example, extensional flows are encountered in HME during the flow of the melt into the die cavity, where the polymer molecules are stretched and aligned due to the flow convergence [53].

The rule of Trouton states that the viscosity in uniaxial extension is equal to three times the shear viscosity of a Newtonian fluid [54]:

$$\eta_E = 3\eta_S \tag{2.17}$$

Non-branched polymers like *linear* low density polyethylene (LLDPE) usually satisfy the Trouton rule, independent on the rate they are being extended. In contrast, branched polymers, e.g. low density polyethylene (LDPE), exhibit a strongly increasing extensional viscosity at higher rates of extension. This effect is called *strain hardening* and is a nonlinear viscoelastic effect. This effect helps to stabilize operations, in which polymer melts are stretched during processing, e.g. film blowing, blow molding, etc. This is the reason, why LDPE can easily be blown into films of uniform thickness.

Electrospinning is a rather new polymer processing method that could benefit from the gained knowledge by extensional rheology testing of pharmaceutical polymers. There exist several publications which indicate that this technique has promising pharmaceutical applications [55, 56, 57, 58, 59, 60, 61]. Electrospinning can be performed from polymer solutions or in a solvent-free process, directly from polymer melts. Both techniques have been successfully applied in the pharmaceutical field. In electrospinning the flow consists mainly of extensional components, and the extensional behavior clearly correlates with electrospinning performance, as shown by Wang et al. [62]. Thus, extensional rheometry might be a powerful tool that allows to predict electrospinning performance of polymeric formulations.

Therefore, to be able simulate complex flows (which consist of extensional and shear components) a fundamental knowledge of the material's rheological behavior under extension is necessary. However, extensional flows are difficult to realize and therefore difficult to measure in a laboratory [63]. It is reported in literature, that the uniformity of the sample can have enormous consequences on the results of uniaxial extensional tests. Homogeneous films of uniform thickness are necessary for reproducible results. Molecular orientations or inhomogeneities like air bubbles or impurities might cause a sample rupture below the maximum achievable strain, which impedes the observation of the true material behavior due to flawed data. The observed discrepancy of data obtained by different laboratories is attributed to non-standardized sample preparation procedures [64]. Therefore, it seems that also extensional rheological characterization is a field which could greatly benefit from use of specimens prepared using the VCM approach.

In openly accessible literature, hardly anything can be found concerning the extensional rheology of polymers relevant for pharmaceutical applications.

The Sentmanat Extensional Rheometer (SER)

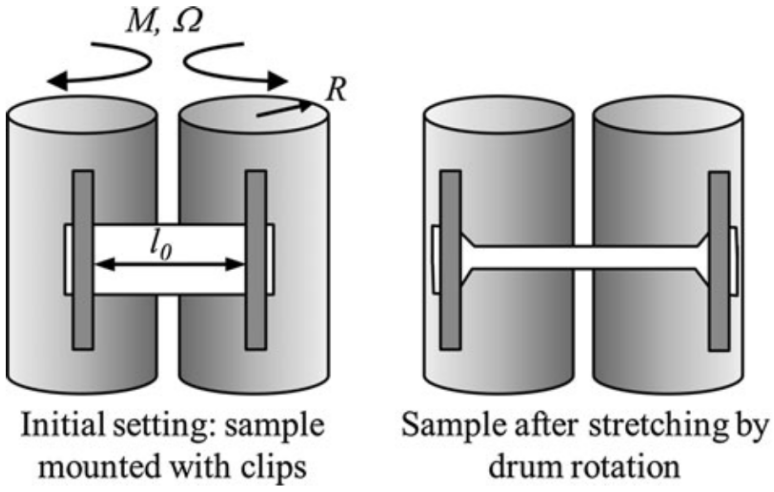

Figure 23 : Schematic illustration of the Sentmanat Extensional Rheometer (SER) principle[64]

The Sentmanat extensional rheometer fixture was introduced in 2004 by Sentmanat [65]. A schematic illustration of the device is shown in figure 23. Tangential stretching of the sample is caused by counter rotating drums, and the resulting torque M is measured by the torque transducer of the rheometer:

$$M(t) = 2RF(t) \tag{2.18}$$

where R is the drum radius (5.15mm) and $F(t)$ the tensile force.

The extensional strain rate $\dot{\epsilon}$ can be obtained using the relation:

$$\dot{\epsilon} = \frac{2\,\Omega\,R}{l_0} \tag{2.19}$$

where $\Omega = \frac{d\varphi}{dt}$ is the angular velocity of the rotating drums, and l_0 is the initial specimen length between the clips (12.7mm).

The transient extensional viscosity η_E^+ is calculated using following expression [66]:

$$\eta_E^+ = \frac{\sigma_T}{\dot{\epsilon}} = \frac{M}{2\,R\,\dot{\epsilon}_H\,A(T)\,\exp[-\dot{\epsilon}_H\,t]} \tag{2.20}$$

where σ_T is the tensile stress and the term $A(T)\,\exp[-\dot{\epsilon}_H\,t]$ represents the changing cross-sectional area of the specimen as a function of the extensional strain.

The cross-sectional area of the sample changes due to thermal expansion as it is and heated up to the measurement temperature. However, the dimensions of the sample can only be measured in solid state, before mounting the specimen. Hence, the true dimensions at the temperature of the measurement have to be considered. To that

end, the cross-sectional area is corrected using the ratio of melt density to the solid density:

$$A(T) = A_0 \left(\frac{\rho_s}{\rho_M(T)} \right)^{2/3} \tag{2.21}$$

where A_0 is the initial cross-sectional area of the specimen, ρ_s is the density at solid state (i.e. at room temperature) and $\rho_M(T)$ is the melt density at the temperature of the measurement. ρ_s and $\rho_M(T)$ have to be obtained from pvT data of the investigated material [66].

2.7 Dynamic Mechanical Thermal Analysis (DMTA)

Similar to oscillatory rheometry, dynamic mechanical analysis (DMTA) can be used to determine the viscoelastic properties of viscoelastic materials by application of a small-amplitude sinusoidal stress or -strain and measuring the resulting deflection of the sample, or the required force, respectively. DMTA is more suitable for glassy or rubbery materials while oscillatory rheometry is used for for characterization of liquid-like materials like polymer melts.

In principle, for the theory of DMTA, the same as for oscillatory rheometry holds. Also DMTA measures viscoelastic moduli (i.e. storage modulus G' and loss modulus G'') and loss factor ($\tan\delta$). Thus for the theoretical background of DMTA, it is referred to the oscillatory rheometry section.

DMTA can be carried out using various measuring geometries, e.g. in tension, torsional, three-point bending or cantilever to name a few. The particular geometry used in this work is of the torsional type. A schematic illustration of a DMTA device which uses this geometry is depicted in figure 24. The sample is mounted between two clamps and is twisted by an oscillating force generated by an air beared motor to a specified extent of strain. The necessary force to achieve this defined strain, combined with the measured phase angle and the geometry of the specimen is used to calculate the viscoelastic moduli (G' and G''). As mentioned above, stress and strain can also be related vice-versa, i.e. the resulting strain caused by a predefined stress is measured.

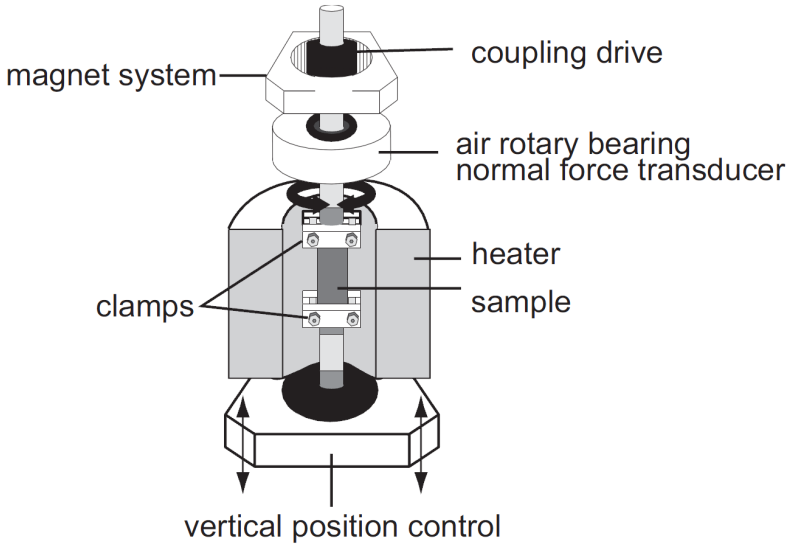

Figure 24 : Schematic illustration of the construction of a torsional DMTA instrument [67]

A typical DMTA thermogram showing a glass transition is plotted in figure 25. Glass transition causes the storage modulus G' to sharply decrease, while the loss modulus G'' show and loss factor tan δ exhibit a peak. The tan δ peak occurs at a much higher temperature than the peak in the loss modulus. There are two possibilities to define the T_g in a DMTA thermogram. One possiblity, (the more common one) is to define the temperature at which the peak of the loss modulus G'' occurs as the glass transition

temperature (T_g). Another possibility is to use the peak of tan δ. ASTM D 4065-2001[68] recommends to use the maximum of G'' as criterion for T_g, thus this convention is adopted for this thesis.

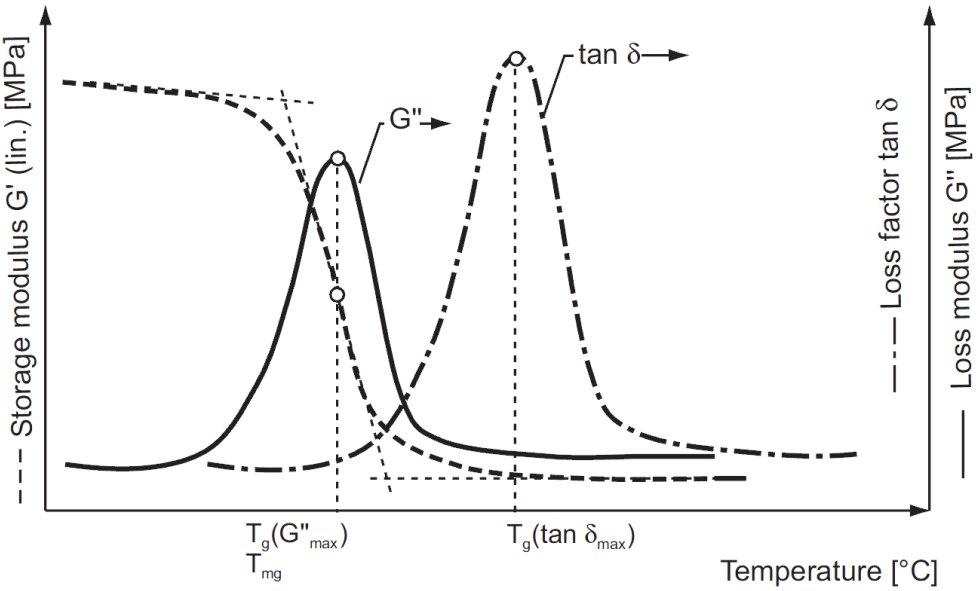

Figure 25 : Typical appearance of a DMTA thermogram showing a glass transition. Two possible definitions of the T_g are indicated.[67]

Using DMTA it is possible to capture thermal events by detecting subtle changes in the mechanical properties of a material. Using DMTA, information about relaxation processes in polymers, like glass-transition and subglass-processes can be obtained [69]. A typical DMTA thermogram of a polymer which exhibits multiple thermal events is shown in figure 26. Each relaxation (i.e. release of a constraint of molecular mobility) is accompanied with a change in the storage modulus G', and thus can be measured using DMTA. At very low temperatures the mobility of the polymer chains is constrained and only local motions of the molecules are possible. When increasing the temperature, γ, and β transitions occur for some polymers (sub-glass relaxations), which are due to release of bending/stretching- or side-group constraints. These sub-glass relaxations often only cause a very subtle change in heat capacity and are thus hard to detect using DSC. A further increase of temperature causes the main-chain constraints to be released (glass transition, or α transition), and the rubbery plateau is approached. At temperatures above the glass transition, for semi-crystalline polymers, a melting transition (T_m) is observed [70]. This example shows, how DMTA can be used to obtain a comprehensive picture of the molecular mobility of polymers as a function of temperature. Because the storage modulus often changes by orders of magnitude due to glass-transition, it is reported that DMTA is 100 times more sensitive than DSC in the glass transition temperature T_g, however DMTA has the disadvantage of requiring a larger sample mass [71].

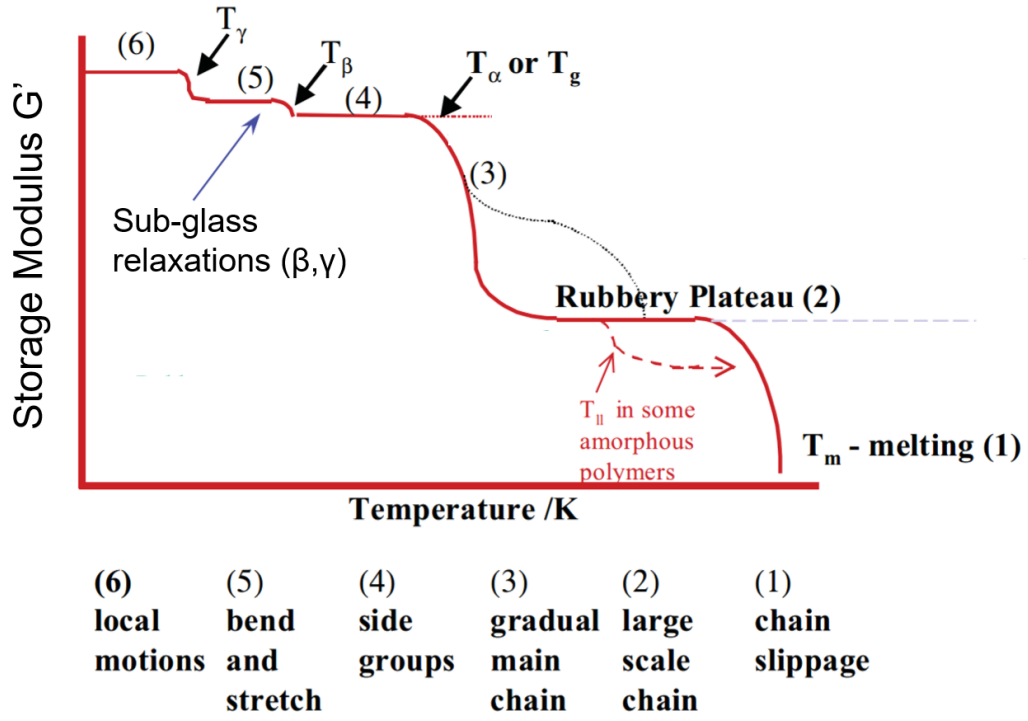

Figure 26 : Change of the storage mdulus (G') caused by different relaxation mechanisms as a function of temperature. Adopted in modified form from [70].

Pharmaceutical Applications

There is currently growing interest in DMTA for the characterization of pharmaceutical materials. For example, DMTA can be used to investigate structural properties of amorphous solid dispersions (ASD). Subtle changes in molecular mobility, such as β and γ transitions can be detected with higher sensitivity than calorimetry, because the change in heat capacity is often small. Knowledge about these transitions can give valuable information about the molecular mobility and thus, the stability of ASDs. Complementary to DSC, it can be used to study polymer/API miscibility and crystallization rates of ASDs [72, 73]. However, sample preparation is often named as restrictive factor of this technique in terms of investigation of systems with pharmaceutical relevance [74]. Due to the lack of appropriate preparation of solid samples for DMTA, in pharmaceutical research, DMTA is often carried out using special powder-pocket measurement geometries [75]. These fixtures have the disadvantage that mechanical perturbations can introduce an error (e.g. due to particle-particle friction or particle sintering/densification during a heating ramp), i.e. no intrinsic material properties can be measured using this approach.

Another pharmaceutical application is to utilize viscoelastic material data obtained using DMTA for the modelling or prediction of the compaction/tabletting behavior of polymeric formulations. One work established a relationship between viscoelastic material parameters of a type of Eudragit® and its compaction behavior [76]. Another study showed that it is possible to model the tensile strength of pharmaceutical compacts based on viscoelastic properties [77].

Another application of pharmaceutical DMTA is the characterization of polymeric formulations used for intravaginal rings (IVR). IVRs are torus-shaped drug-eluting devices designed to release API to the vagina. The main application of IVR is delivery of contraceptive hormones. Other applications include, for example, HIV prophylaxis [78, 79]. Malcolm et al. used DMTA to determine the solubilities of a range of APIs and formulation components in a silicon elastomer used for IVRs. The solubility of the drug in the elastomer at saturation depends on the length of the polymer chains and the cross-linking degree. These are typical properties which can be quantified using DMTA. Conventional measurement of the saturation would require filtering of undissolved material from a drug-saturated polymer network, which is is not possible, according to the authors. The conclusion of their study is, that the saturation solubility can be estimated using DMTA data [80]. The mechanical properties of IVRs are an important factor in the design of this particular dosage form. User discomfort or even epithelial barrier damage may be caused by inflexible IVRs. On the other hand, overly flexible IVRs might be expelled during use [81, 82]. Thus, the mechanical behavior of IVR polymers and formulations should be characterized. The flexibility of the ring in static deformation depends on its tensile modulus and the geometry. If the ring is dynamically deformed, like in the human body, it starts to exhibit viscoelastic properties where a certain portion of deformation energy is stored, while rest is dissipated. Thus, likely the viscoelastic behavior will have an influence on how well the IVR feels, when worn. Therefore, it seems that DMTA could be a method that allows to differentiate between IVR formulations with good or bad wearing comfort, respectively.

3 Materials and Methods

3.1 Materials

This section provides an overview of the different pharmaceutical polymers which are characterized in this thesis. In table 1, the chemical names, the structure types, the trade names and the manufacturers of the polymers are listed.

3.1.1 Pharmaceutical Polymers

Table 1 : Chemical names, structure, trade names and manufacturer of the polymers that are characterized in this thesis

Chemical Name	Structure	Trade Name	Manufacturer
Butyl-methacrylate dimethylaminoethyl-methacrylate methyl-methacrylate copolymer (1:2:1)	amorphous	Eudragit® E	Evonik Industries AG
Ethylene-glycol caprolactam vinylacetate graft copolymer	amorphous	Soluplus®	BASF SE
Vinylpyrrolidone-vinylacetate copolymer	amorphous	Kollidon® VA 64	BASF SE
Ethylene-vinylacetate copolymer	semi-crystalline	Ateva® 1820	Celanese Inc.
Ethylene-vinylacetate copolymer	semi-crystalline	Greenflex® ML60	Versalis S.p.A.
Ethylene-vinylacetate copolymer	semi-crystalline	Evathene®UE654-04	USI Corp.
Hydroxypropyl methylcellulose (HPMC)	amorphous	Methocel® E5	Dow Chemical Co.
Hydroxypropyl methylcellulose (HPMC)	amorphous	Affinisol® 100 LV	Dow Chemical Co.
Hydroxypropyl methylcellulose acetate succinate (HPMCAS-LF)	amorphous	AQOAT®	Shin-Etsu Chemical Co.Ltd.

Eudragit® E

Eudragit® E is a cationic, amorphous, statistical copolymer consisting of dimethylaminoethyl methacrylate, butyl methacrylate and methyl methacrylate monomers. It dissolves quickly in acidic aqueous medium below pH values of 5. It is used as a tablet coating material for taste masking and moisture protection and as a matrix material in pharmaceutical hot-melt extrusion [83].

Soluplus®

Soluplus® is a non-ionic, hydrophilic, amorphous graft copolymer of ethylene glycol, caprolactam and vinylacetate. It is used as carrier matrix for hot-melt extruded and injection molded formulations [13, 84].

Kollidon® VA64

Kollidon® VA64 is an amorphous copolymer polyvinylpyrrolidone and vinyl acetate. It is used as carrier matrix for hot-melt extruded formulations It is also used as binder for tablets and granules, as dry binder for direct compression as granulating agent and as film-former [12].

Poly-Ethylene Vinyl Acetate (EVA)

EVA is a semi-crystalline statistical copolymer of ethylene and vinyl acetate. The fraction of vinyl acetate is variable from grade to grade. A higher vinyl acetate content usually leads to a less crystalline structure. EVA is commonly used industrially, e.g. for coating foils of solar panels,for hot-melt adhesives, and in the pharmaceutical industry as a matrix material for drug-eluting devices such as contraceptive vaginal rings (NuvaRing®).

Hydroxypropylmethylcellulose (HPMC)

Hydroxypropylmethyl cellulose (HPMC), commercialized as Methocel® E5 is a non-ionic cellulose ether with methoxyl and hydroxypropyl side groups. HPMC is a hydrophilic polymer with various uses in pharmaceutical dosage forms, such as immediate-release and modified-release products. It is also used as tablet binder, as component of tablet coatings, matrix material for hot-melt extrusion [85, 86].

Hydroxypropylmethylcellulose Acetate Succinate (HPMCAS)

Hydroxypropylmethyl cellulose acetate succinate (HPMCAS-LF), commercialized as AQOAT® is a cellulose ester comprising acetyl and succinoyl groups [87]. It is used as coating material and as polymeric matrix for HME [88].

3.1.2 Model APIs

Itraconazole

Itraconazole is an anti-fungal agent with an extremely low aqueous solubility in its crystalline form. A possibility to enhance bio-availability of the substance is to form an amorphous solid dispersion. Itraconazole is the active ingredient of one of the few FDA approved drug products made by hot-melt extrusion, commercialized as Onmel^{TM} [89]. Due to the high thermal stability and low solubility, itraconazole is a widely utilized model compound for thermal processes. The melting poin (T_m) of the crystalline form is at 165°C, the T_g of the amorphous form at 62°C [90]. In this work, a formulation of 15wt.% itraconazole with Kollidon® VA64 is investigated.

Ibuprofen

Ibuprofen is a non-steroidal anti-inflammatory drug for treatment of mild to moderate pain and fever. It is poorly soluble in water and has a relatively low melting point T_m of about 60°C. In this work, a formulation of 20wt.% ibuprofen with Soluplus® is investigated.

3.2 VCM Setup and VCM Tools

The VCM process is a batch process which yields solid specimens of thermoplastic materials starting from powder or pellets. In particular, the VCM process enables to achieve this task in a much shorter time ned traditional compression molding. Also mixtures of polymer powder with active pharmaceutical ingredients (APIs) can be used as feedstock for this process.

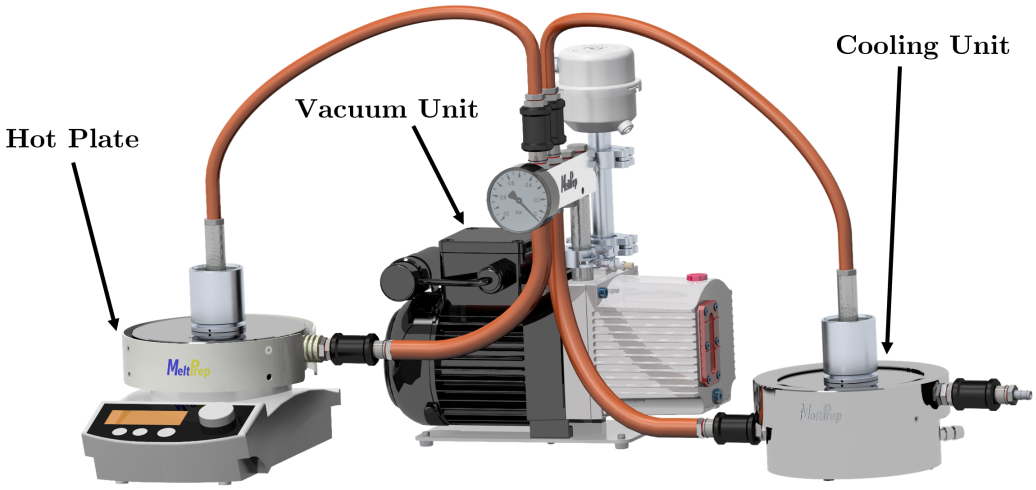

Figure 27 : Vacuum Compression Molding Setup (MeltPrep GmbH)

The VCM setup is depicted in figure 27. It consists of a hot plate which acts as heat source, a two-stage rotary vane vacuum pump, a cooling unit and a mold tool (VCM Tool), where the fusion of the particles occurs. The VCM Tool is evacuated by the vacuum pump and heated on top of the hot plate during molding.

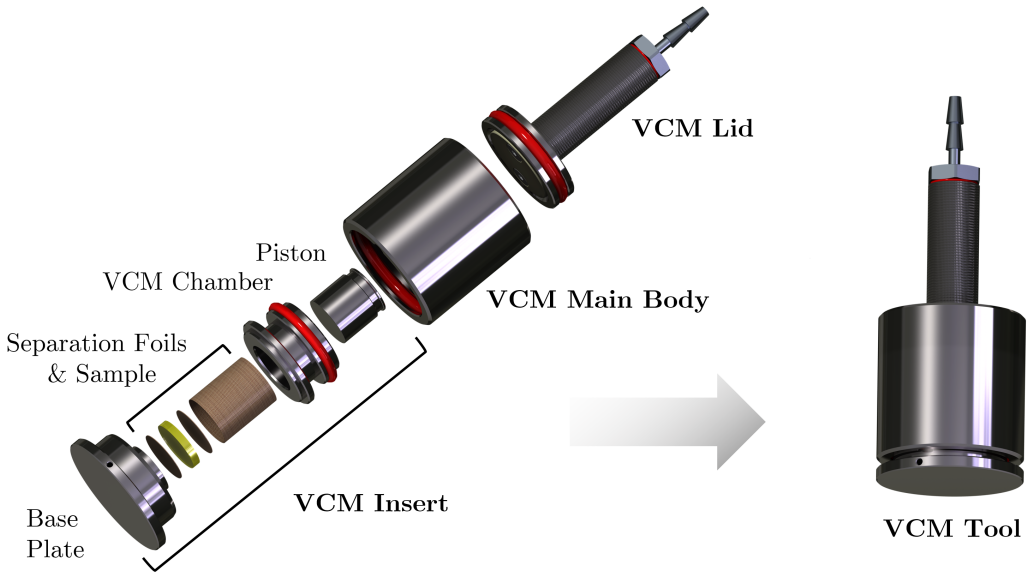

Figure 28 : Vacuum Compression Molding (VCM) Disc Tool (MeltPrep GmbH)

The design of the device depicted in figure 28 . Basically the VCM device is a small scale evacuated press consisting of a hollow aluminum cylinder as outer shell (main body), which is closed by a base plate at the bottom and a lid with vacuum hose connector at the top. The lid and the bottom plate are sealed off by O-rings. Inside the device, there is a chamber which acts as a mold (VCM Chamber). The chamber is lined with PTFE coated separation foils to prevent sticking and can be filled with specimen powder or pellets once the foils are inserted (figure 29).

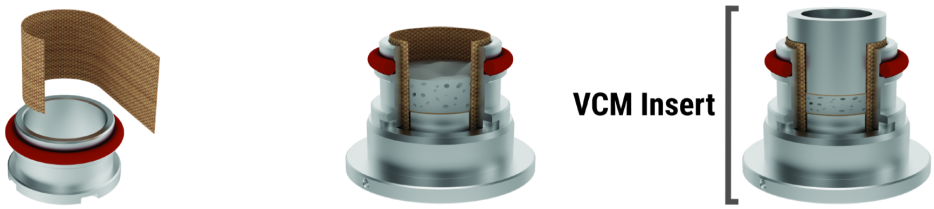

Figure 29 : Assembly and filling procedure of the VCM Tool insert. (MeltPrep GmbH)

The lid is axially displaceable within the main body and exploits the pressure differential between vacuum and the ambient pressure to generate a compressive force, which is high enough to cause complete fusion of the particles inside the chamber. This technique makes a hydraulic or pneumatic mechanism for pressure generation superfluous, which leads to a massive size reduction compared to conventional platen presses (figure 30). The vacuum pressure that can be reached during the molding cycle is approximately $2 \cdot 10^{-3}\, mbar$. The processing temperature has to be chosen according to the terminal relaxation time of the processed material. Thus, at a given temperature, the time required to achieve homogeneous fusion of the material is the combination of the time which is required to heat the material to the desired temperature (i.e. on the thermal conductivity of the polymer particles) and the terminal relaxation time of the material at this particular temperature [91]. The terminal relaxation time and heat transfer behavior usually are not known beforehand. Therefore, in most cases preliminary trials using different combinations of preparation time and processing temperature are necessary to achieve optimal results. Leakage of formed viscous polymer melt is prevented by using very narrow gaps between the separation foils and the aluminum parts. After a residence time of a few minutes on the hot plate, when it can be assumed that the material is completely fused, the VCM device is placed on the cooling unit, where it is cooled down to room temperature using heat conduction and forced convection due to compressed air flowing out of circularly arranged nozzles. The necessary heating time until the polymer particles completely fuse depends on material parameters like viscosity and thermal conductivity of the polymer.

After the VCM tool has reached room temperature, the finished sample can effortlessly be demolded from the device by removing the lid and base plate and pushing, piston down. Subsequently the specimen is extracted and the separation foils are carefully removed using pointed tip tweezers (figure 31).

Figure 30 : Size comparison between the VCM setup and a conventional platen press(MeltPrep GmbH)

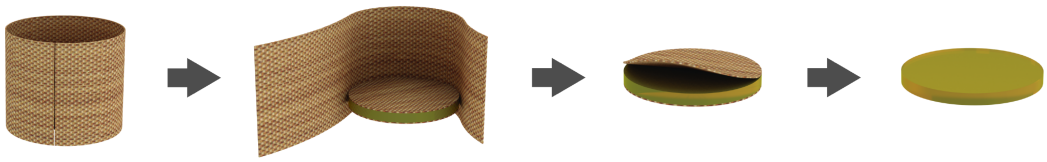

Figure 31 : Foil removal procedure from a VCM specimen after demolding, picture courtesy of MeltPrep GmbH

3.2.1 The VCM Cycle

Short cycle times are crucial if materials that are prone to thermal degradation are processed. Therefore, rapid heating of the material to its softening/melting temperature is desired. Subsequently the material has to be cooled down to room temperature, to obtain a solid specimen. The time-temperature history due to heating and cooling can have major impact on the properties of the finished specimen. For example, slow cooling favors crystallization of semi-crystalline polymers, while rapid quench-cooling leads to a more amorphous sample [92, 93]. Thus, if the goal is to produce specimens with consistent physical properties, the thermal history for all samples has to be equal in the ideal case.

A typical cycle consisting of filling of the material, heating, cooling and specimen extracting usually takes less than 10 minutes. In figure 32 the temperature curve of a typical VCM cycle and its time derivative (heating/cooling rate) are shown. The temperature profile of a typical VCM cycle (measured in the base-plate) 32. The time starts as the VCM tool is placed on the hot plate, where it is heated up very quickly.

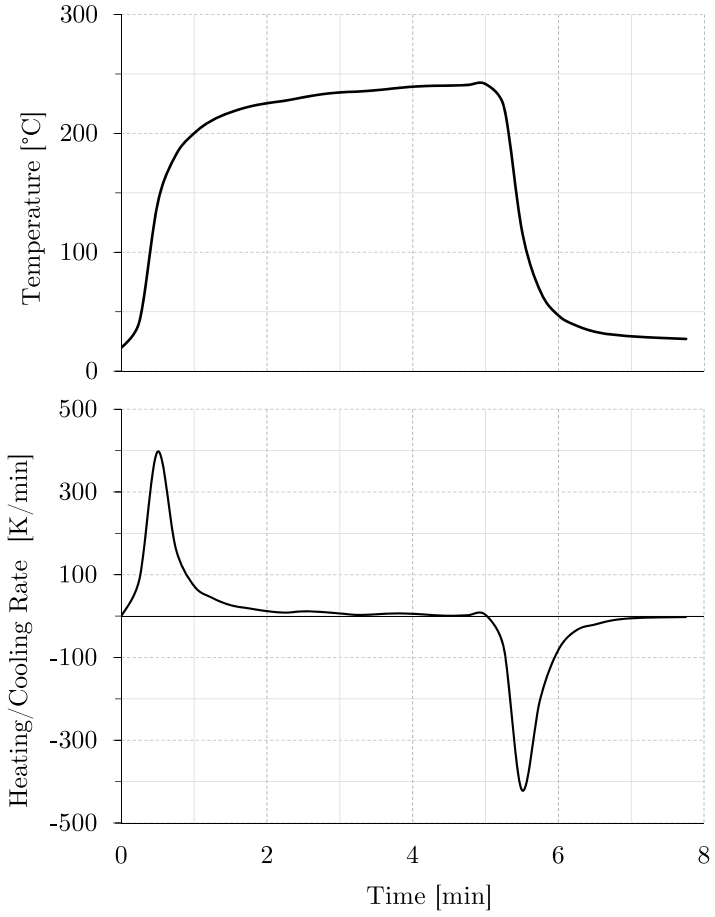

Figure 32 : Typical temperature profile of a VCM cycle (top) and the corresponding heating/cooling rate profile(bottom)

In the shown case, the set temperature of the hot plate was $240°C$, to fuse polystyrene pellets. This example should convey a feeling of the heat transfer characteristics of the VCM Tool. Initially, the heating rate increases exponentially to value of about $400\frac{K}{min}$, which reached after approximately $30s$. After passing the peak, the heating rate decreases exponentially, slowly approaching a steady state. After 5 minutes residence time on the hot plate, the VCM Tool is placed on the cooling unit, where the cooling rate again shows first a exponential increase, reaching a peak value of about $-410\frac{K}{min}$, which then decreases to approach a steady state (i.e. room temperature). Certainly, the peak values of the heating/cooling rates depend on the set temperature of the hot plate, because a higher temperature gradient between the VCM Tool and the hot plate or cooling unit will lead to faster heating or cooling, respectively. For example, a higher set temperature of the hot plate increases the peak heating rate while the cooling rate can be influenced by increasing or decreasing the temperature of the aluminum block of the cooling unit by connecting it with a thermostat.

The comparatively fast cycle time of the VCM preparation helps to minimize the thermal stress exerted on the material. Because the material is not significantly sheared within the VCM Tool, like e.g. in injection molding, there is no viscous dissipation, causing a inhomogeneous temperature field during processing. Furthermore, the residence time is exactly the same for all fluid elements in the VCM, which is also not the case in injection molding. Between the preparations of individual specimens using VCM, all heat transfer

related parameters are kept constant, leading to a highly repeatable time-temperature history. The only influence is the packing density of the powder within the chamber of the VCM device, which influences the thermal conductivity of the powder, thus the temperature rise of the material during fusion [94]. However due to the mentioned differences, the thermal history of specimens produced using the VCM approach is more well defined and reproducible compared to injection molding. Furthermore, in contrast to injection molding, no significant flow occurs during the molding cycle, so there are no flow-induced superstructures (i.e. material orientations in the specimen) present within the resulting specimens. Because neither sticking nor significant leakage happens during the process, the cleaning effort is low and the quantity of lost material during the process is close to zero. Therefore, the VCM tool allows to produce a large quantity of samples of different materials in a short time, with minimum material losses. Thus, the VCM preparation enables, in combination with the appropriate measuring instrument, high-throughput experimentation, i.e. fast screening of many differently composed materials in a short time by accelerating sample preparation, especially when only very low material quantities are available. These attributes make the VCM approach in various aspects to be superior compared to conventional approaches. These characteristics make the VCM process especially interesting for early stage pharmaceutical formulation development, where only a few grams of often outrageously expensive API is available and wasting material therefore cannot be tolerated.

Powder Compaction vs. VCM

Yang et al. reported, that they produced specimens of a polymeric formulation (Kollidon® VA64 as matrix material) for rheological characterization by compressing dry powder using die and punches [95]. To compare this approach with the VCM method, Kollidon® VA64 powder was dried for three hours at $50°C$ in a vacuum (2e-3 mbar) and then manually compressed with 25kN punch force using a Stylcam tablet press (Medelpharm, France) equipped with 12 mm punches. The resulting tablets were dried for one hour under the same conditions. A sample of the same, dried raw material was produced using the VCM Disc Tool. The Hot-Plate was set on temperature of $170°C$. The tool was heated up for 5 minutes, followed by 2 minutes cooling, which was enhanced using forced air convection. The resulting specimen had a visibly homogeneous, glass-like appearance. A comparison of the formation of a polymer melt using both samples is depicted in figure 33. Both samples were molten on top of an adhesive PTFE foil which was placed on top of the hot plate. The resulting melt was homogeneous for the specimen which was produced using the VCM tool. However, the compacted specimen had an opaque appearance, which is an indication for existence of phase boundaries. In this case, the phase boundaries are formed by inter-particulate air, which was trapped in the tabled during the compaction process. This is in agreement with the statements concerning the theory of melt formation from powder in section 2.3.2. Therefore, the VCM preparation is definitely superior compared to powder compaction.

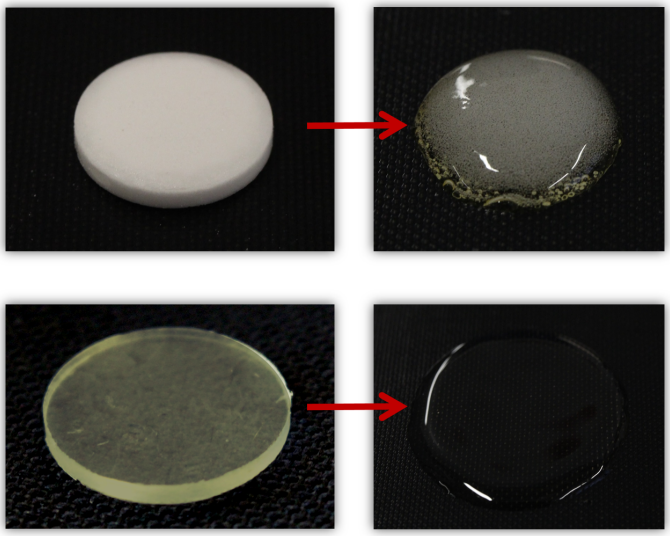

Figure 33 : Top left: Tablet of Kollidon® VA64, prepared using a tablet press. After melting (top right) a considerable amount of air stays entrapped in the high-viscous melt. Bottom left: Disc of the same material prepared using the VCM process. The resulting polymer melt (bottom right) is free of air-bubbles.

3.2.2 Mixing

Earlier work indicated that if a mixture of polymer and API is used as starting material, after the VCM process a solid dispersion or solid solution, respectively, is present [96]. Therefore, the VCM Tool could substitute, e.g., table-top extrusion processes for process development. Material quantities of few milligrams should be enough to mimic the properties of extruded formulations.

Because during the VCM process no shear-forces are applied, mixing relies exclusively on diffusion. This is a problem if for example agglomerated crystalline APIs are used, as shear forces are necessary for effective deagglomeration. Therefore, if it is desired to distribute the API homogeneously in the matrix, preliminary preparation of the powder mixture is necessary. Mixing due to diffusion can be described using the so-called random-walk model, which yields a characteristic length-scale x_D of diffusion as a function of time [97]:

$$x_D = \sqrt{2Dt} \tag{3.1}$$

The relevant characteristic diffusion length that is necessary to achieve molecular mixing of the components is in the order of the particle diameter, if one assumes a mono-disperse ideal mixture of spherical particles. Therefore, rearranging above equation yields a characteristic mixing time scale t_M:

$$t_M = \frac{x^2}{2D} \tag{3.2}$$

In the majority of cases the diffusion coefficient D is not known, however from this relationship it can be seen that the mixing time scales with the square of the characteristic

length. Thus, preliminary milling of the material, e.g. using a cryogenic mill, greatly improves mixing during the VCM process. Furthermore, the milling process also serves as a mixing step of the powder mixture, and the reduced particle size also reduces the tendency of segregation. Crystalline structures of APIs can be transformed into the amorphous state using cryogenic milling, facilitating dissolution of the API in the molten polymer matrix [98, 99].

The impact of different polymer/API mixture pretreatment methods on content uniformity of VCM prepared specimens was studied by Fiedler and Rustige using Raman spectroscopy. In figure 34, the API distributions of VCM specimens of a polymeric formulation with 10% API content are depicted. Specimen A was prepared from physical mixture, specimen B from cryomilled powder, specimen C from powder ground using mortar, pestle and liquid nitrogen and specimen D from tabletop-extruded strands of the formulation. The specimen prepared using the physical mixture (A) shows yellow and red spots, indicating that API agglomerates are present and generally poor uniformity is achieved. Cryomilling (B) and tabletop-extrusion (D) yield a similarly homogeneous distribution of the API. For mortar and pestle (C), for unknown reasons a very low API concentration was detected [100, 96].

These results indicate that cryogenic milling combined with VCM preparation yields specimens which are comparable with tabletop-extrusion in terms of mixing quality.

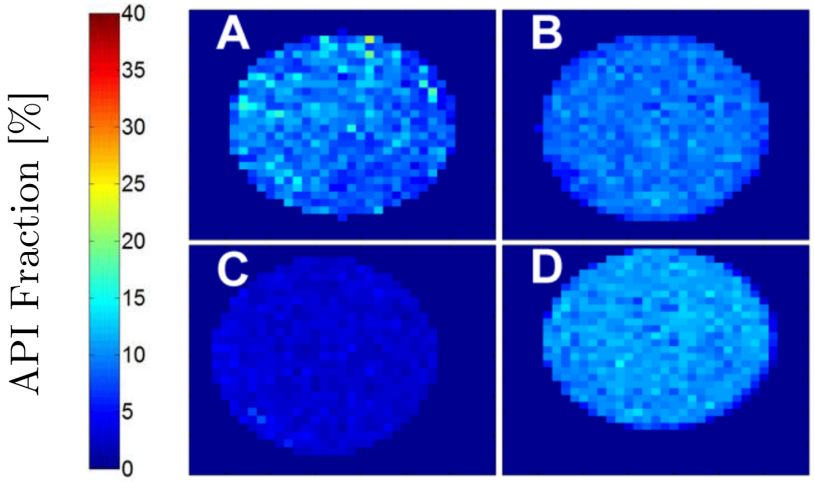

Figure 34 : Raman mappings comparing the influence on mixture pretreatment methods on content uniformity in VCM prepared specimens. A... physical mixture, B... cryomilled C...mortar and pestle with aid of liquid N_2 D... tabletop extruded [96][100]

3.3 VCM Tool for DSC Applications

n the course of this thesis, a new vacuum-compression molding (VCM) device for DSC specimens was developed and manufactured specifically for the task of producing plane-parallel, homogeneous polymer discs with a diameter of 5 mm.

The design of the VCM DSC Tool is largely based on the existing VCM Disc Tool, except the mold chamber, piston having a diameter of 5 mm. The mass of most DSC specimens is in the range of 5 - 25 mg, depending on the application.

A schematic illustration of the VCM chamber during sample preparation is depicted in figure 35. r_1 is the piston radius, r_2 is the inner radius of the chamber (including thickness of the lateral separation foil), h is the specimen height, $\dot{V}_L$ is the leakage flow rate, and F_C is the compaction force acting on the piston. As mentioned in the section above, the sealing principle is the usage of a small gap between the piston and chamber, allowing the piston to move in the chamber but minimizing the escape of the highly viscous molten specimen material. The lateral PTFE separation foil is compressed between the base plate and the chamber and acts as a static seal, thus between these two parts the chamber is tight.

In certain cases, the mass of DSC specimens has to be matched e.g. with a reference sample. Therefore, one has to make sure the filled material mass is not lost during preparation, e.g. due to leakage out of the VCM chamber. Leakage occurs at the gap between the piston and the lateral separation foil of the chamber, if materials with a low melt viscosity are processed. To understand the influential factors of leakage, a simple model can be established which is explained in the following section.

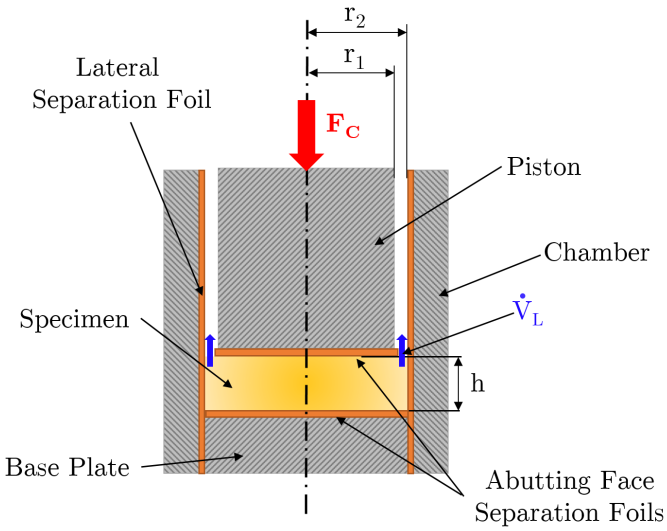

Figure 35 : Schematic illustration of the VCM mold chamber during preparation of a specimen. The gap between piston and chamber is shown strongly exaggerated for better clarity

A force F_{Lid} is generated by the lid due to the pressure differential between the the vacuum pressure inside the VCM Tool (p_{in}) and the ambient pressure (p_{out}). The friction force caused by the O-ring seal of the lid acts in opposite direction (F_F) as the resulting force F_C acting on the piston. Neglecting the influence of the vacuum connector, the force balance can be expressed as follows:

$$\underbrace{(p_{out} - p_{in})A_{Lid}}_{F_{Lid}} - F_F = F_C \tag{3.3}$$

where A_{Lid} is the projected area of the lid.

The compaction force pushes the piston down, causing a compression of the specimen with a normal stress σ:

$$F_C = A_{Piston}\,\sigma \tag{3.4}$$

where A_{Piston} is the projected area of the piston. Combination of the equations yields the relationship between the normal stress and the ratio of piston- and lid radii:

$$\sigma = (p_{out} - p_{in})\frac{A_{Lid}}{A_{Piston}} - \frac{F_F}{A_{Piston}} = (p_{out} - p_{in})\left(\frac{r_{Lid}}{r_1}\right)^2 - \frac{F_F}{r_1^2\pi} \tag{3.5}$$

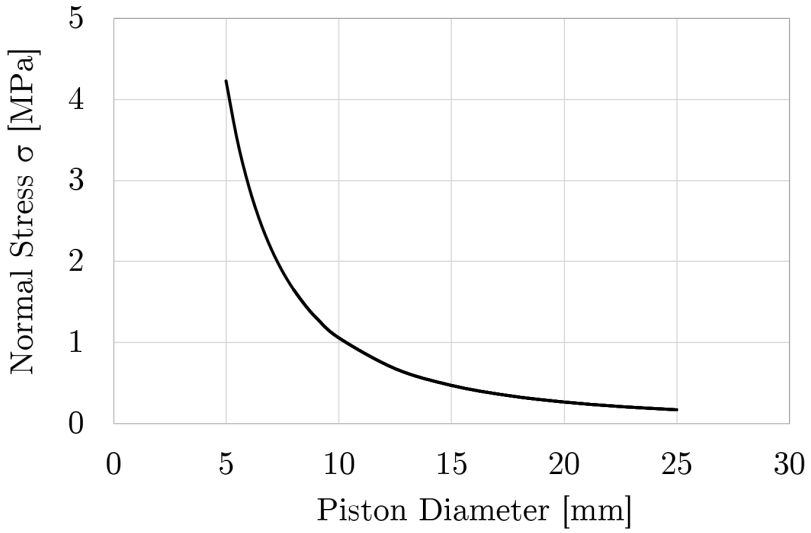

Figure 36 : Dependence of the normal stress σ which compacts the material within the VCM on the piston diameter (Standard VCM Lid)

The function is plotted in figure 36. Experience has shown that normal stresses of 0.2 MPa (i.e. if a piston with 25 mm is used) are already sufficient to obtain homogeneous specimens even for materials which with a very high melt viscosity like, e.g., HPMC. However, a excessively high normal stress causes increased leakage of the polymer melt from the mold chamber. Because the shear rate the material experiences during VCM preparation is close to zero, the sealing of the mold chamber can be idealized by assuming laminar flow of a Newtonian fluid through an annulus, which corresponds to the sealing gap between the separation foils and the chamber shown in the illustration above. In this case, the leakage flow rate $\dot{V}_L$ through the annulus has a linear dependence upon the pressure gradient $\frac{\Delta p}{\Delta x}$ and the zero shear viscosity η_0, if all geometrical parameters are assumed to stay constant [101]:

$$\dot{V}_L = \frac{\pi}{8\,\eta_0}\frac{\Delta p}{\Delta x}\left[r_2^4 - r_1^4 - \frac{(r_2^2 - r_1^2)^2}{ln\frac{r_2}{r_1}}\right] \tag{3.6}$$

It can be seen from this equations, that the leakage flow rate scales with the 4-th power of the gap between piston and chamber. Therefore, the manufacturing of the parts has to be carried out with utmost precision in order to achieve a gap which is as narrow as possible.

Calculations using this simple model showed, that if material with a volume of a fictive specimen with a height of 1mm is processed using the conventional lid ($\sigma = 4.2MPa$) approximately 20% of the material volume would be lost after 5 minutes if the zero-shear viscosity is 100 Pas or consequently 2% for 1000 Pas, respectively. As the viscosity range of typical polymer melts is in this range, the pressure (or normal stress σ) had to be lowered drastically to achieve an acceptably low leakage.

This task was accomplished by designing a new so-called low-pressure lid, which lowers the normal stress σ to approximately $0.2\,MPa$ when using a piston with a diameter of 5mm. Thus, the leakage rate using this new lid is approximately 20 times lower than with the conventional lid, i.e. negligible if materials with a viscosity higher than 100 Pas are used. This was confirmed experimentally, even for materials with a melt viscosity in the range of 100 Pas, the lost mass due to leakage was most of the times in the order of 1%, while the molding performance (i.e. quality of fusion of the particles) was not compromised. Thus, this low magnitude of leakage allows to produce specimens with very consistent mass, even if the material has a very low melt viscosity.

The DSC tool assembly is depicted in figure 37 and a cross-section is shown in 38. The already mentioned low-pressure lid is the most prominent difference to the original VCM tool construction. It comprises an aluminum outer part in which a displaceable rod, equipped with an O-ring seal and a vacuum connector at its top is installed. The aluminum outer part is equipped with two O-ring seals which, besides sealing, leads to a thermal decoupling of the low-pressure lid from the main body, because metal-metal contacts are excluded. The thermal decoupling allows to keep the lid at low temperatures during operation. The inner part (beige) of the low-pressure lid which contacts the piston is made out of the thermally insulating high performance polymer polyether ether ketone (PEEK). This prevents that heat is conducted away from the piston, which reduces the temperature gradient within the sample during the VCM cycle.

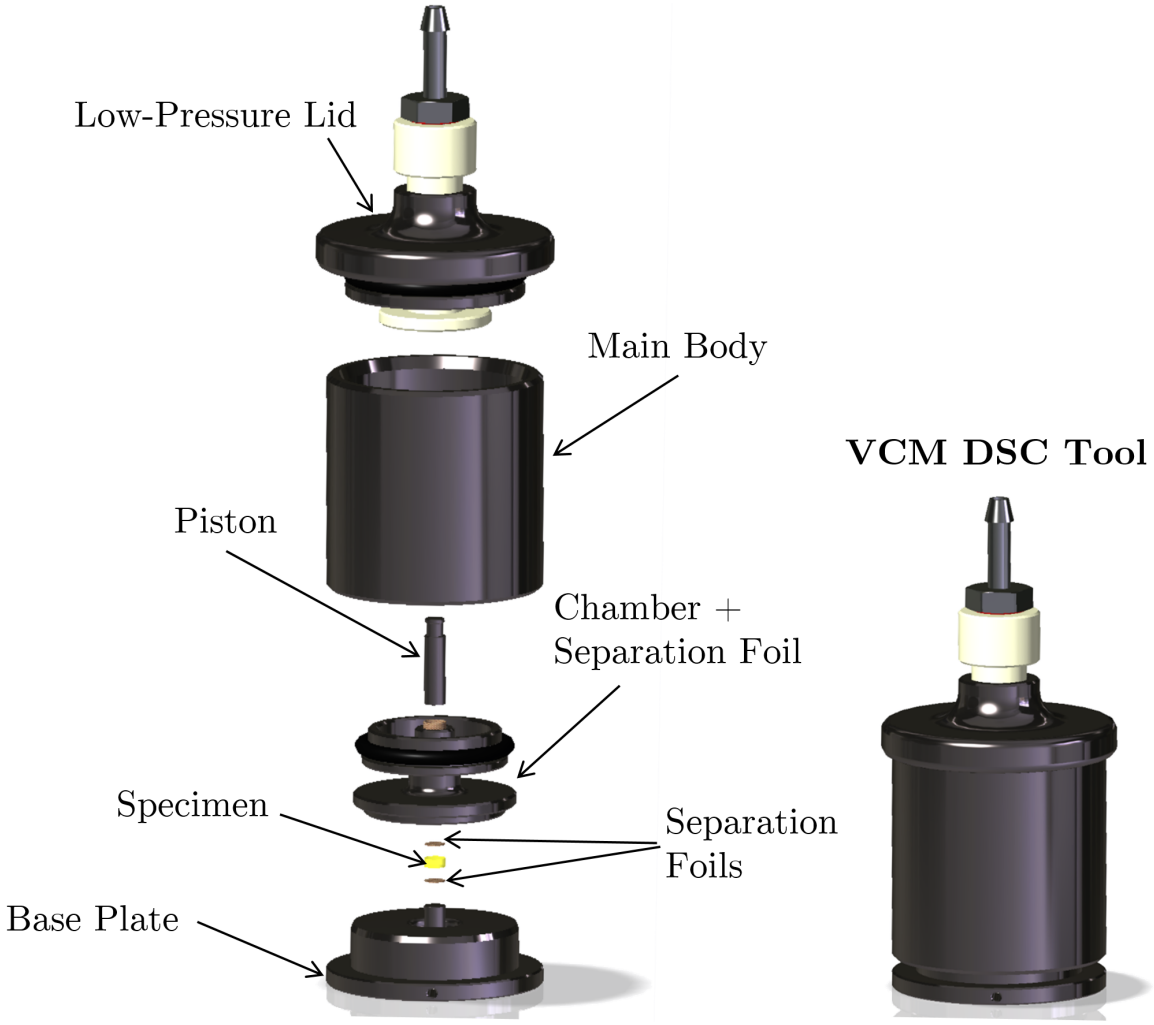

Figure 37 : VCM DSC Tool explosion view (left) and assembled (right)

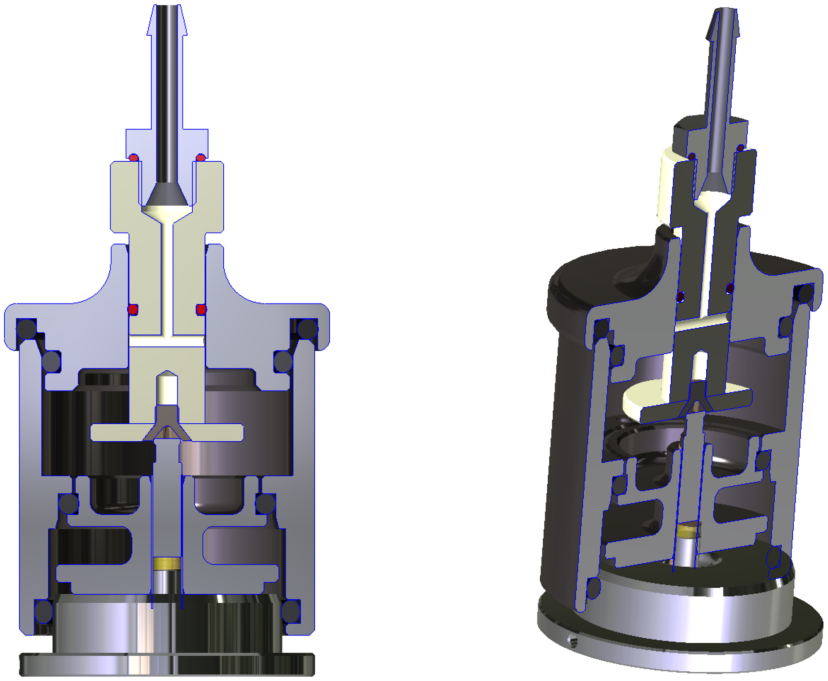

Figure 38 : Cross section of the VCM DSC Tool

3.4 Differential Scanning Calorimetry (DSC)

The motivation and benefit of DSC sample preparation using vacuum-compression molding should be explained first. In figure 39, the differences between the two approaches are illustrated. In a conventional DSC experiment in pharmaceutical research, the studied polymers or polymeric formulations are often available in form of powder or physical mixtures of polymer and API powder (illustrated on the top). In the conventional approach, the powder is simply put in the pan, the pan is sealed and is subsequently placed in the instrument. Before the measurement itself, often a preliminary heating step (1st heating) is performed to induce fusion of the particles. In case a physical mixture is used, this step is carried out to cause the API particles to dissolve in the molten polymer matrix. Analogous to the explanations in section 2.3.2, the melt formation during the 1st heating of powders with a high melt viscosity can be divided into two phases. In the first phase sintering of the particles occurs, followed by densification of the formed softened droplets which causes entrapment of inter-particular gasses. The timescale of this transient process as well as the quantity of entrapped gas depends on the magnitude of melt viscosity. Thus, for very highly viscous materials, melt formation by heating of powder occurs very slowly, so that only sintering of the particles can be achieved, even if a long 1st heating cycle is performed. If the viscosity is low enough, so densification can occur within the timescale of 1st heating, a porous 3D-network with entrapped gasses is formed. Moreover, due to the lacking external stresses, the only driving force of droplet coalescence during densification is the surface tension of the formed melt, which is counteracted by viscous forces and the pressure forces of the entrapped gas. Thus, after 1st heating of the mentioned materials, the state of the material within the pan is heterogeneous, and has not reached an equilibrium state, as the melt formation processes might not be fully completed after 1st heating. In the subsequent 2nd heating (the actual measurement), the mentioned melt formation processes continue to occur. Moreover the entrapped gas bubbles expand thermally when temperature is increased. They rise very slowly to the surface of the melt, where they are expelled successively. It is also possible that the gas diffuses into the molten material, causing alteration of the material properties. The concentration gradient of gas between bubble and melt is enhanced massively due to the capillary pressure within the bubble. These factors encourage suspicion, that some artifacts might be introduced by usage of powder as DSC specimen. A way to get rid of these artifacts is to pre-load a homogeneous sample prepared using VCM to the DSC pan.

In DSC it is important that, on the one hand the contact area of the specimen to the bottom of the pan is maximized, so optimum thermal contact is achieved, on the other hand the melt should not be able to form a meniscus due to capillary forces at the wall of the pan [43]. A diameter of 5 mm of the VCM samples was therefore chosen as a trade-off between contact-area maximization and enough distance from the wall to prevent meniscus formation. The initial state and the geometry of VCM samples are more well defined than for powder. No disturbances due to incomplete particle fusion or gas inclusions should influence the measurement in this case. Furthermore, it is avoided that the walls of the pan are wetted by the sample, which increases the sensitivity of the measurement[43].

In order analyze the characteristics of this new preparation approach, DSC measurements of both traditionally prepared samples (i.e. placing powder in the DSC pans) and samples

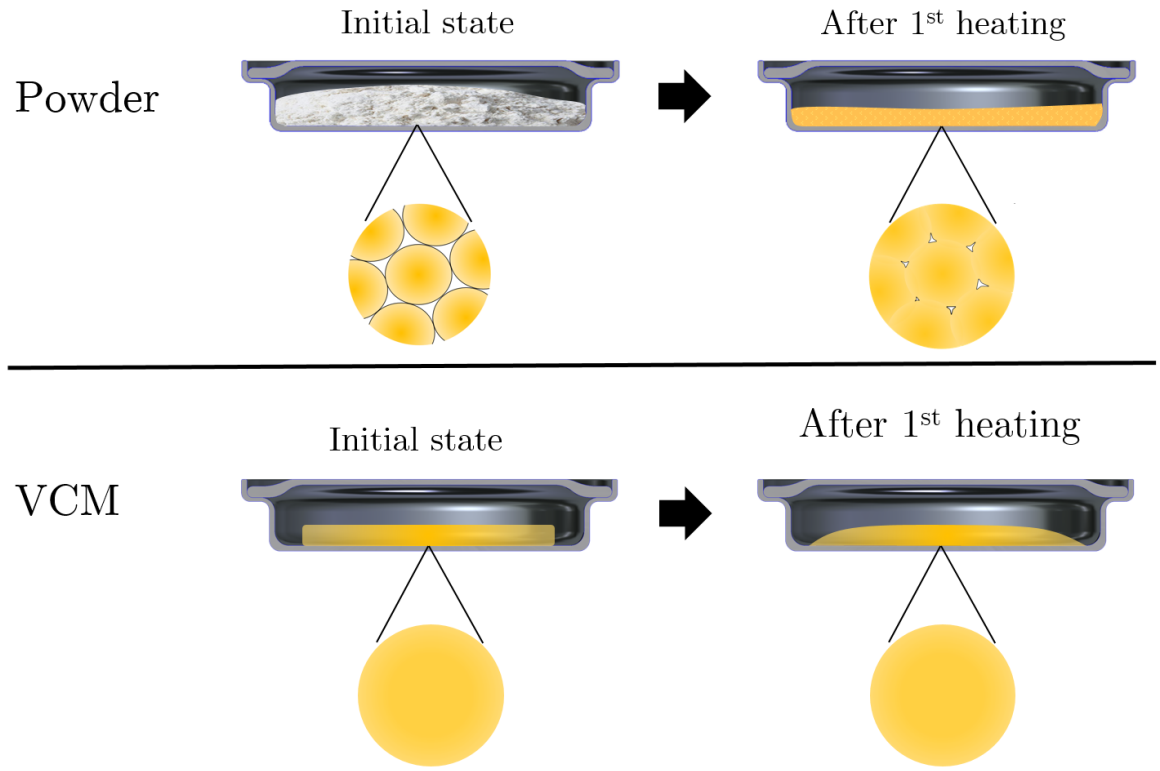

Figure 39 : Melt formation in DSC pan. Top: Untreated powder. After heating, particle fusion is not completed and air is entrapped in a porous air-polymer network. Bottom: A homogeneous melt is achieved due to usage of a VCM - prepared specimen. Wetting of the pan walls is prevented.

prepared by the VCM approach are compared.

All DSC measurements were performed on a Phoenix 204 F1 differential scanning calorimeter (NETZSCH GmbH, Germany) equipped with an automatic sample changer (autosampler). The mass of all specimens was carefully determined using a high-precision laboratory balance (XP205, Mettler Toledo GmbH, Switzerland).

Investigated Materials

First, the thermal transitions of specimens prepared by powder and VCM specimens are compared. Different typical pharmaceutical polymers which are used as carrier matrices in polymeric formulations were chosen as test subjects. These are Soluplus®, Eudragit® E, Kollidon® VA64, HPMCAS-LF and HPMC Methocel® E5 . For example, HPMC Methocel® E5 is known for his weak change in heat capacity during glass transition, which makes it especially hard to detect its T_g. Furthermore, it does not exhibit spontaneous sintering and densification during heating if no external force is applied. This makes Methocel® E5 a good candidate to study the influence of VCM preparation.

A method to measure the thermal conductivity using modulated DSC is introduced in a subsequent section. A different type of HPMC was used for the thermal conductivity measurement (HPMC Affinisol® 100 LV), because it is more suitable for hot-melt extrusion than HPMC Methocel® E5.

3.4.1 Thermal Transitions

To compare the thermal characteristics of vacuum-compression molded specimens with those of powder, MDSC scans of both powder samples and VCM samples were performed. Various pharmaceutical polymers were investigated, in order to obtain a comprehensive picture of the consequences of the VCM preparation.

Sample Preparation

The neat polymers were all supplied as powders and were used without further treatment. The API/polymer mixtures were cryogenically milled using a CryoMill (Retsch, Germany) to achieve a homogeneous mixing of the components during the VCM preparation. The grinding beaker was filled with approximately 5 g of mixture. Three milling cycles of 2.5 min with a frequency of 25 Hz were performed. Between the cycles, an intercooling step of one minute at a frequency of 5 Hz was carried out. All materials were dried at least for 24 hours in a vacuum oven before measurement/preparation.

The traditional sample preparation procedure in DSC is to simply fill powder in a pan and perform a preliminary heating step before the actual measurement. Thus for all powder samples, a first heating step was performed in order to soften the material. Each powder sample was heated to a temperature of $T_g + 40°C$ with a heating rate of $20\,K/min$ and held isotherm at this temperature for 5 minutes, followed by cooling at a rate of $20\,K/min$ to the starting temperature of the MDSC measurement ($0°C$). VCM samples of each investigated material with diameter of 5mm a mass of around 10 mg were prepared using the VCM DSC tool. The preparation temperatures were chosen sufficiently high above the glass transition temperature of the polymers to achieve complete particle fusion within a 5 minute heating cycle. All specimens had a homogeneous glass-like transparent appearance, except HPMC Methocel® E5, which had a white, opaque appearance. Increasing processing temperature and cycle times did not lead to more transparent samples of HPMC Methocel® E5. The VCM specimens were directly measured, i.e. without first heating. Therefore, a direct comparison between the currently established sample preparation procedure and the VCM preparation is achieved.

Measurement Procedure

The measurements were performed with an underlying heating rate of 2 K/min, a temperature modulation period of $40\,s$ and an amplitude of $0.212°C$, which corresponds to heat-iso conditions. Heat-iso conditions means that during temperature modulation no cooling with respect to the underlying heating rate occurs, i.e. the heating rate never goes below zero. A nitrogen gas flow rate of $50\frac{ml}{min}$ was used to purge the DSC cell during measurement to prevent oxidation and provide a moisture-free atmosphere.

It was tried to match the sample masses of powder and VCM within a tolerance of $\pm 0.5\,mg$, to exclude effects due to a different specimen mass. All pans were crimped and subsequently pierced, to allow the N_2 purge gas to circulate and to allow potentially released gases to escape the pan. This prevents inflation or even bursting of the pan due do excessive pressure, which might even contaminate the DSC sensor.

The pans were placed in an automatic sample changer, and the measurement was started immediately after sample preparation. Due to the fact that one MDSC measurement takes about 2h in total, the time until the measurements were completed was approximately 14h of continuous DSC operation. During this time, the specimens which were still to be measured were exposed to the laboratory atmosphere (approx. $22°C$ and 25% relative humidity).

3.4.2 Quasi-isothermal Heat Capacity Measurement using MDSC

Modulated DSC - in contrast to conventional DSC- allows to measure the heat-capacity at quasi-isothermal conditions. These conditions are characterized by setting the underlying heating rate to zero, i.e. applying a small amplitude temperature oscillation around a constant temperature.

A method to determine *thermal conductivity* using modulated DSC, which is introduced in a later section, requires to measure the heat capacity in so-called quasi-isothermal mode.

The advantage of the quasi-isothermal method is, that the heat capacity is determined at a steady state of the modulated heat flow, therefore any transient influences (e.g. influence of heating or cooling rate, respectively) are excluded. Thus, the values of c_p measured using this method are a more true representation of heat capacity [102]. A typical heating program of a quasi-isothermal heat capacity measurement at several temperatures is illustrated in figure 40. At each temperature of interest, for 20 minutes an isothermal-modulated segment is performed, with an amplitude of $\pm 0.5K$ and a period of $80s$. Afterwards, heating with $5K/min$ to the next higher temperature of interest is performed. In this case the temperature step-size is $10°C$. The disadvantages of this technique are that it is very time-consuming compared to conventional DSC, and the resolution of the heat capacity with respect to temperature is limited by the finite step-size between the isotherms.

The apparent reversing heat capacity for the quasi-isothermal case can be expressed as follows [103]:

$$C_{app} = \frac{A_{HF}}{A_{HR}} = \frac{1}{\omega}\frac{A_{HF}}{A_T} \quad \left[\frac{J}{K}\right] \tag{3.7}$$

where A_{HF} is the amplitude of the modulated heat-flow (i.e. only the cyclic component), and A_{HR} the amplitude of modulated heating rate and A_T is the amplitude of the modulated temperature. The angular frequency ω is calculated using the well-known relationship:

$$\omega = \frac{2\pi}{P} \tag{3.8}$$

where P is the period of oscillation, in this case $80\,s$.

Applying a calibration factor K_{c_p} and dividing by the specimen mass m yields the specific reversing heat capacity:

$$c_p = \frac{K_{c_p}}{\omega\, m} \frac{A_{HF}}{A_T} \quad \left[\frac{J}{kgK}\right] \tag{3.9}$$

This calibration constant is determined by comparing the measured values of a well-known material with respective reference values, e.g. from literature:

$$K_{c_p} = \frac{c_{p,ref}}{c_{p,meas}} \tag{3.10}$$

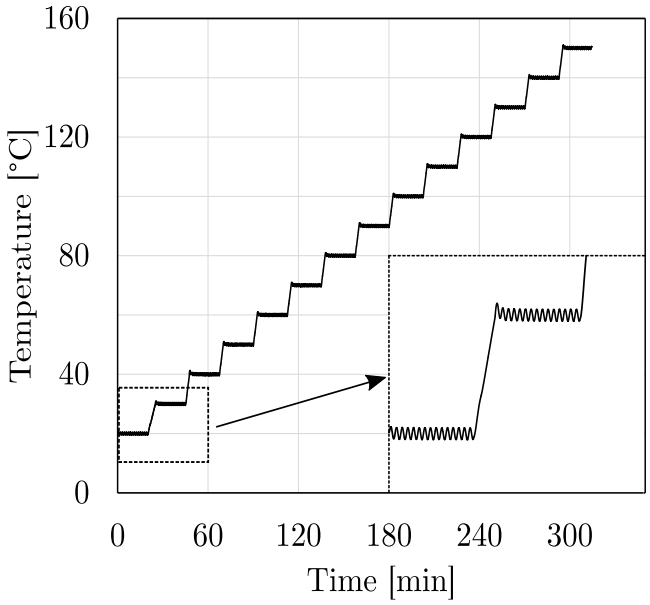

Figure 40 : DSC temperature program used for quasi-isothermal heat capacity measurements. 20 minutes of modulated isothermal segments with a modulation period of $80s$ und an amplitude of $\pm 0.5K$ are followed by heating at $5\frac{K}{min}$ to the next temperature of interest.

The quasi-isothermal heat capacity measurement was performed with a temperature program following the recommendations given in ASTM-E1952-11.

The mean heat flow ($\overline{HF_i}$) has to be subtracted from the total heat flow in each interval (i.e. at each temperature step) to isolate the oscillating component of the heat-flow ($\widetilde{HF_i}$). For one exemplary isotherm, this process is shown in figure 41. For each isotherm, the subtraction is performed for every data point, to an oscillation of the heat flow about zero is achieved.

$$\widetilde{HF_i}(t) = HF_i(t) - \overline{HF_i} \tag{3.11}$$

$\overline{HF_i}$ is calculated for all n data points of one isotherm as follows:

$$\overline{HF_i} = \frac{1}{n}\sum_{t=0}^{n} HF_i(t)\Delta t \tag{3.12}$$

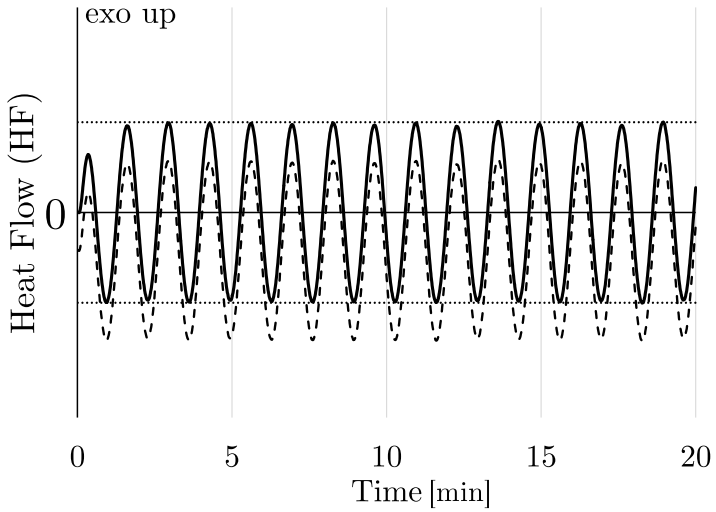

Figure 41 : Subtraction of the mean heat-flow from the total heat-flow signal (dashed line) to obtain the oscillatory part of the heat flow (solid line)

Now that the oscillating part of the heat-flow is isolated, the amplitude can be determined. According to ASTM, for evaluation the last 10 minutes of the interval should be used, to make sure a steady state has been reached. Using MATLAB, the peak values of the oscillating heat-flow in the last 10 minutes of the interval are determined, and the arithmetic mean of all peak values is calculated. This mean value is regarded as heat-flow amplitude A_{HF}, to be inserted in equation (3.9).

The amplitude of temperature oscillation is determined analogously. The mean temperature is subtracted from the total temperature at each isotherm, to isolate the oscillating part. From this part the temperature amplitude (A_T) peaks are determined.

Baseline Correction

To obtain accurate heat capacity results, a potential asymmetry of the DSC cell has to be corrected. Due to this asymmetry of the DSC cell, a finite heat flow is measured, even if two empty pans having exactly the same mass are placed on the sample and reference sensor. Therefore, a measurement run with two empty pans (so-called blanks) was carried out using the same temperature program as the specimens. Care was taken to exactly match the masses of blank- and reference pan, to eliminate a possible heat-flow contribution due to pan mass difference. An apparent heat capacity can be calculated analogously as for a regular specimen using equation (3.7).

Literature states that if modulated heat-flow and heating rate are out of phase for the blank measurement, the apparent heat capacity of the baseline has to be subtracted from all subsequent runs. In contrast, if the modulated heat-flow and heating rate are in phase, the apparent heat capacity of the baseline has to be added to all subsequent runs

[41]. Results showed that the latter is the case, so the baseline apparent heat capacity was added to the apparent heat capacity of all subsequent runs.

Heat Capacity Calibration

To accurately calibrate the heat capacity, a disc of synthetic sapphire (Al_2O_3) with a diameter of 4 mm, supplied by the instrument manufacturer. A table of reference heat capacity values for this material was available in the DSC software. These values were taken as literature values and fitted to a polynomial of 6-th order, valid in a range covering $0 - 220°C$, which is sufficient for most pharmaceutical applications. The following expression was obtained for the fit:

$$\begin{aligned} c_{p,ref}(T) = 3.514 \cdot 10^{-14}T^6 - 1.832 \cdot 10^{-11}T^5 - 6.935 \cdot 10^{-9}T^4 + 1.143 \cdot 10^{-5}T^3 \\ -6.592 \cdot 10^{-3}T^2 + 2.493T + 717.907 \ (R^2 = 0.999) \end{aligned} \tag{3.13}$$

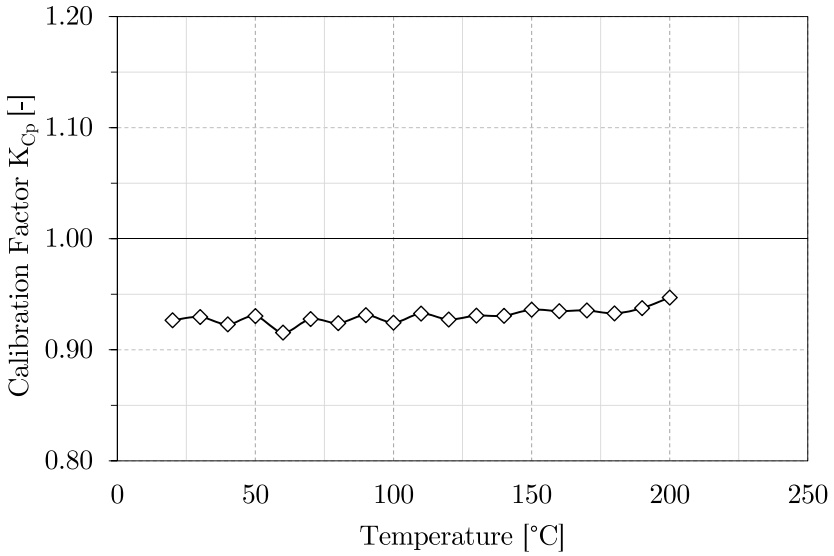

Figure 42 : Heat Capacity Calibration Factor K_{c_p} as a function of temperature, determined using a sapphire standard

The sapphire was measured using the same temperature program as the specimens. The apparent heat capacity of the sapphire was then compared with the reference c_p value of sapphire from literature to obtain the dimensionless heat capacity calibration factor K_{c_p} using equation (3.10). The determined calibration factor as a function of temperature is shown in figure 42. K_{c_p} does not change much with temperature, thus there seems to be an approximately constant bias between the measured and true heat capacity of the sapphire. ASTM-E1952-11 recommends to use a constant, representative value of K_{c_p} for calibration [104]. Therefore, the arithmetic mean of all values is used as a constant calibration factor for all temperatures. The determined average value $\overline{K_{c_p}}$ is 0.933 [-].

3.4.3 Thermal Conductivity Measurement Method using MDSC

One possibility to measure the thermal conductivity (κ) of low-conducting materials (e.g. polymers), is to use modulated DSC. The basic principle of this method is to compare the heat capacity of two measurements of the same material. One measurement is carried out under optimized conditions, to obtain the intrinsic heat capacity of the material. These optimal conditions are fulfilled if small, thin specimens encapsulated in highly conductive pans (e.g. aluminum) and long oscillation periods are used. When test conditions differ from these recommendations, the accuracy of the measured heat capacity declines. In this case, non-uniform temperature conditions across the test specimen arise due thermal conductivity of the material. If one maximizes his non-uniform temperature conditions by using of thick specimens in open pans, thus applying the temperature modulation only to one side of the specimen, the thermal conductivity directly influences the measured heat capacity. This principle can therefore be used to measure the thermal conductivity of solid specimens, correlating the intrinsic c_p of the material, determined under optimal conditions and an apparent heat capacity determined under conditions which maximize the influence of thermal conductivity on the result. This measurement method has gained sufficient attention to be approved as an ASTM standard test method (E1952-11) [104].

The benefit of this DSC method compared to established thermal conductivity measurement methods is, that differential scanning calorimeters are a commonly available instrument and that the measurement can be automated using automatic sample changers. Furthermore, a sample mass lower than 100 mg is sufficient for one measurement run. Thus, many differently composed samples can be screened in a short time. The disadvantages are that homogeneous samples cylindrical samples are an essential prerequisite and that for data analysis, no method is implemented in the software belonging to the DSC instrument. Therefore, a MATLAB routine had to be developed, which provides fully automated and unambiguous data analysis. The program is briefly described hereinafter.

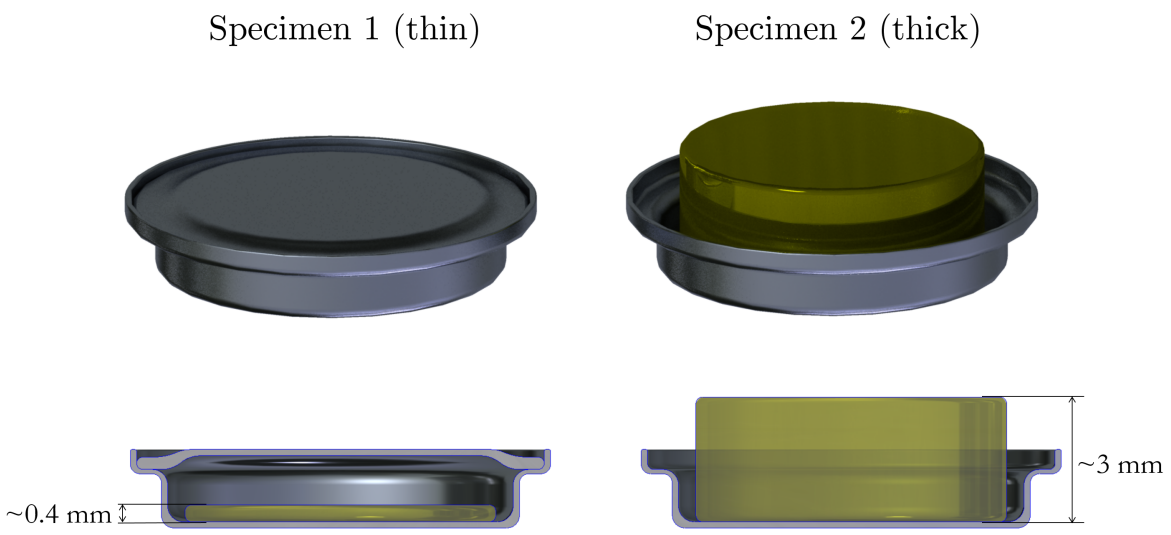

Figure 43 : Two specimens are used for the thermal conductivity measurement. A thin sample, encapsulated in a hermetically sealed pan (left), and a thick sample in an open pan(right)

The theoretical basis for this method was derived by Marcus and Blaine [105] The theory is based on a one-dimensional heat conduction model. Details concerning the underlying theory can be found in [106].

From the one-dimensional model, following expression for the apparent thermal conductivity κ_0 can be derived [105]:

$$\kappa_0 = \frac{8\,L\,c_p}{d^2\,P}\left(\frac{C}{c_p}\right)^2 \tag{3.14}$$

where L is the thickness of the thick specimen, C is the apparent heat capacity of the thick specimen, m is the mass of the thick specimen, c_p is the specific heat capacity of the thin specimen, d is the diameter of the thick specimen and P is the oscillation period. The calculation of the specific heat capacity of the thin specimen (c_p) was already in the section explained above. The apparent heat capacity C of the thick specimen was determined similarly:

$$C = \frac{K_{c_p}}{\omega}\frac{A_{HF}}{A_T} \tag{3.15}$$

The thickness and diameter of each thick specimen were measured using a micrometer screw.

The assumptions and simplifications of the presented model are as follows:

- One-dimensional heat flow in the specimen
- The specimen is a circular cylinder with parallel end-faces
- The specimen has a known density ρ and heat-capacity c_p and both properties are constant within the whole material
- The face of the specimen follows the applied temperature modulation
- The heat flow through the opposing face and the sides of the specimen is zero

In reality, however, heat is lost to the purge gas through the sides of the specimen and the material thermally expands as the temperature is increased. To correct these effects, calibration has to be performed using a reference material with well-known thermal conductivity. Thus, a correction factor that takes into account the heat losses to the purge gas has to be introduced. This correction factor is obtained by calibration with a material with well-known heat capacity. In literature, it is proposed to use polystyrene as calibration material, as its thermal conductivity as a function of temperature is well-known [105, 107]. To that end, analytical grade atactic polystyrene with a mean molecular mass of 192000 $\frac{g}{mol}$ in form of granules was purchased at Sigma Aldrich. Atactic polystyrene is an amorphous thermoplastic polymer with well-known physical properties, including heat capacity and thermal conductivity. It is therefore suitable as a reference material to check the plausibility of the measured heat capacity. Furthermore, it is a recommended calibration material to calibrate the thermal conductivity using modulated DSC [105].

The correction factor, denoted D, is calculated from the calibration data using the following expression [105]:

$$D = \sqrt{\kappa_{obs,PS}\ \kappa_{r,PS}} - \kappa_{r,PS} \tag{3.16}$$

where $\kappa_{obs,PS}$ is the observed thermal conductivity for a known reference material and $\kappa_{r,PS}$ is the reference value from literature.

The thermal conductivity (after correction) can finally be calculated using following formula [105]:

$$\kappa = \frac{1}{2}\left[\kappa_0 - 2D + \sqrt{\kappa_0^2 - 4D\kappa_0}\right] \tag{3.17}$$

Sample Preparation

A restrictive aspect of this thermal conductivity measurement approach using modulated DSC is, that two small cylindrical, plane-parallel, homogeneous samples, with different thickness are required. In literature, different sample preparation approaches for this measurement method were reported, including cutting from extruded rods [105], injection molding [107], or even compression of powder[108]. These approaches are all rather time- or material consuming, or in case of powder compression, definitely yield erroneous results. The VCM DSC Tool that was introduced in the last section allows to freely choose the specimen height by changing the filling weight, and it yields exactly the demanded specimen geometry for this technique at very low material expense and very short times. Therefore, it seems to be almost ideally suitable for production of specimens for this measurement method.

Thin and thick (0.4 and 3mm thickness) specimens with a diameter of 5mm of different polymers were prepared using the VCM DSC Tool. All materials were dried for at least 24 hours in a vacuum oven. The mass of the thin specimen was matched with the sapphire standard of the c_p measurement. The necessary filling weight of the VCM tool to achieve a thickness of exactly 3mm for the thick specimens was estimated by first producing larger disc specimens with a diameter of 20mm of all materials. As the sample geometry in good approximation is a plane parallel cylinder, its volume can easily be calculated. Thus if the exact mass, thickness and diameter of the disc are known, one can very easily calculate the true density of the material. The resulting 20mm specimens were accurately weighed using a precision scale and subsequently their thickness and diameter was carefully determined using a micrometer screw to estimate the solid density. Using the determined values of the density, the required filling mass to obtain a height of 3mm was calculated. The resulting height of the thick specimens was remarkably close to the nominal value. All specimens could be produced within a thickness range of $3 \pm 0.05mm$.

The thermal contact between pan and specimen has to be well defined to obtain good thermal conductivity results. An undefined thermal contact was shown to lead to declining reproducibility of the measurement [105, 109]. Samples prepared using VCM tools usually have a smooth surface with a high degree of evenness. However, due to the surface roughness of the DSC pans, the thermal contact is disturbed by the inevitable air gaps that are present between sample and pan (figure 45). The air gaps can be avoided by either using a small amount of heat conducting oil between specimen and

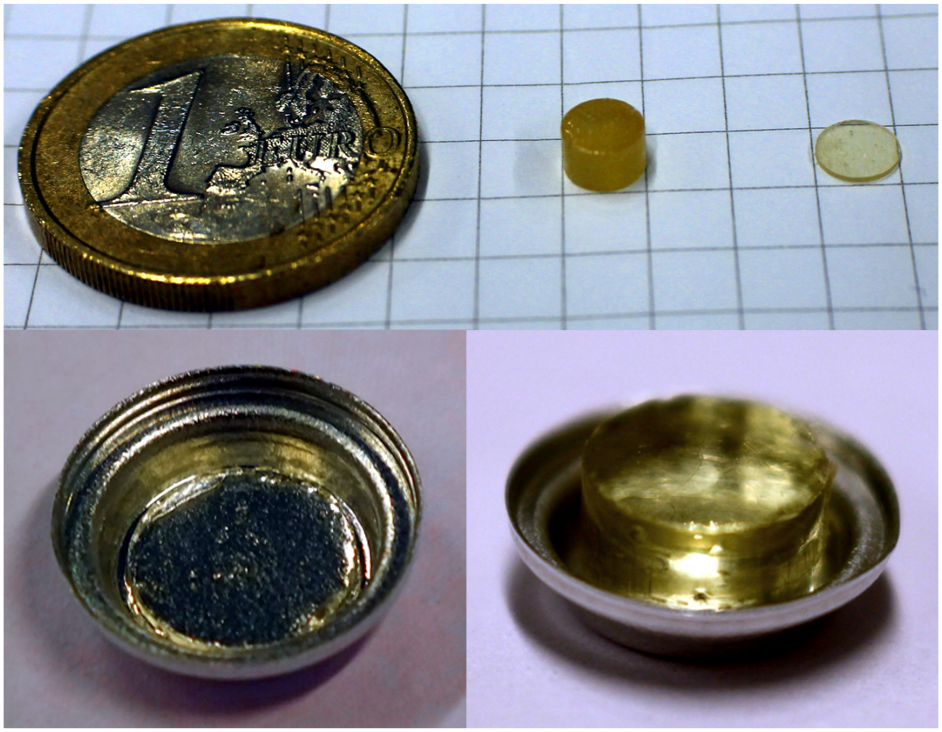

Figure 44 : Top: size comparison between thin and thick specimens of HPMC Affinisol®100LV prepared using VCM and the one euro coin. Bottom left: thin VCM specimen of Soluplus® placed in a DSC pan. Bottom right: thick VCM specimen of Soluplus® placed in a DSC pan

pan, or by softening the polymer sample at the contact surface by a short, but rapid heating of the sample in the pan, so wetting of the surface occurs. The interactions of silicone oil with pharmaceutical polymers are unknown, therefore the latter approach is chosen, which is realized by placing the pan containing the sample on a pre-heated hot plate for a 1-3 seconds, depending on the viscosity or relaxation time, respectively. Due to the thermal insulating properties of polymers, only the layer directly adjacent to the bottom of the pan is thermally affected in such short times. The plate thus has to be at temperature at which the polymer relaxes within a timescale of seconds. Subsequently, the pan is put on a block of aluminum to quench the pan. This procedure, however, has the disadvantage that the thermal history of the material is affected, that a human factor is involved and that the required temperature is not known in the first place. For most of the investigated polymers, approximately the same set-temperature of the hot plate as used for their VCM preparation yielded good wetting behavior. An exception are the cellulosic polymers HPMC and HPMCAS, which generally do not exhibit flow if no external forces are applied, thus no wetting can occur. The influence of this surface-wetting step on specimen thickness was negligible, as was confirmed by precisely measuring the thickness of pan and sample before, and after the procedure. Thus, it is sufficient to measure the specimen thickness directly after producing it using the VCM DSC tool.

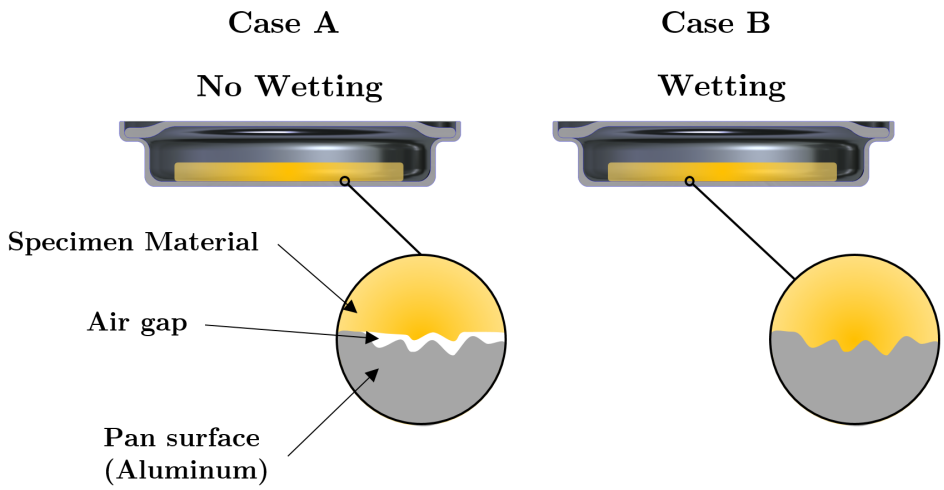

Figure 45 : Case A: irreproducible thermal contact between specimen and pan due to air gaps between specimen and pan. Case B: the polymer has wetted the pan material and fills the microscopic surface depressions, enabling a better thermal contact

Data Analysis using MATLAB

A MATLAB script was developed in order to evaluate the raw data of the MDSC thermal conductivity measurement. The script can be used to import raw data files of MDSC measurements, which were previously exported as .csv files using NETZSCH Proteus Analysis Software. Subsequently, data analysis can be carried out fully automatically, the only parameters that have to be put in manually are the thickness and diameter of the thick specimen used in the thermal conductivity measurement. All other parameters, like sample masses, are extracted automatically from the exported data files. Also the calibration etc. is automatically adapted to the temperature range of the measured data. After execution of the script, the results are written into a spreadsheet and a diagram of thermal conductivity vs. temperature is displayed. Therefore, this script enables rapid processing of the raw data with minimal user input, and unambiguous results are obtained. The code is given in the appendix.

3.5 VCM Tool for Production of Rectangular Bars

Analysis methods such as dynamic mechanical analysis (DMTA) require rectangular bars as specimen geometry. Typical specimen dimension for DMTA is 40x10x1mm. To enable high-quality production of specimens with this geometry, a new device called VCM Bar Tool was developed and successfully manufactured. The resulting design is depicted in figure 46.

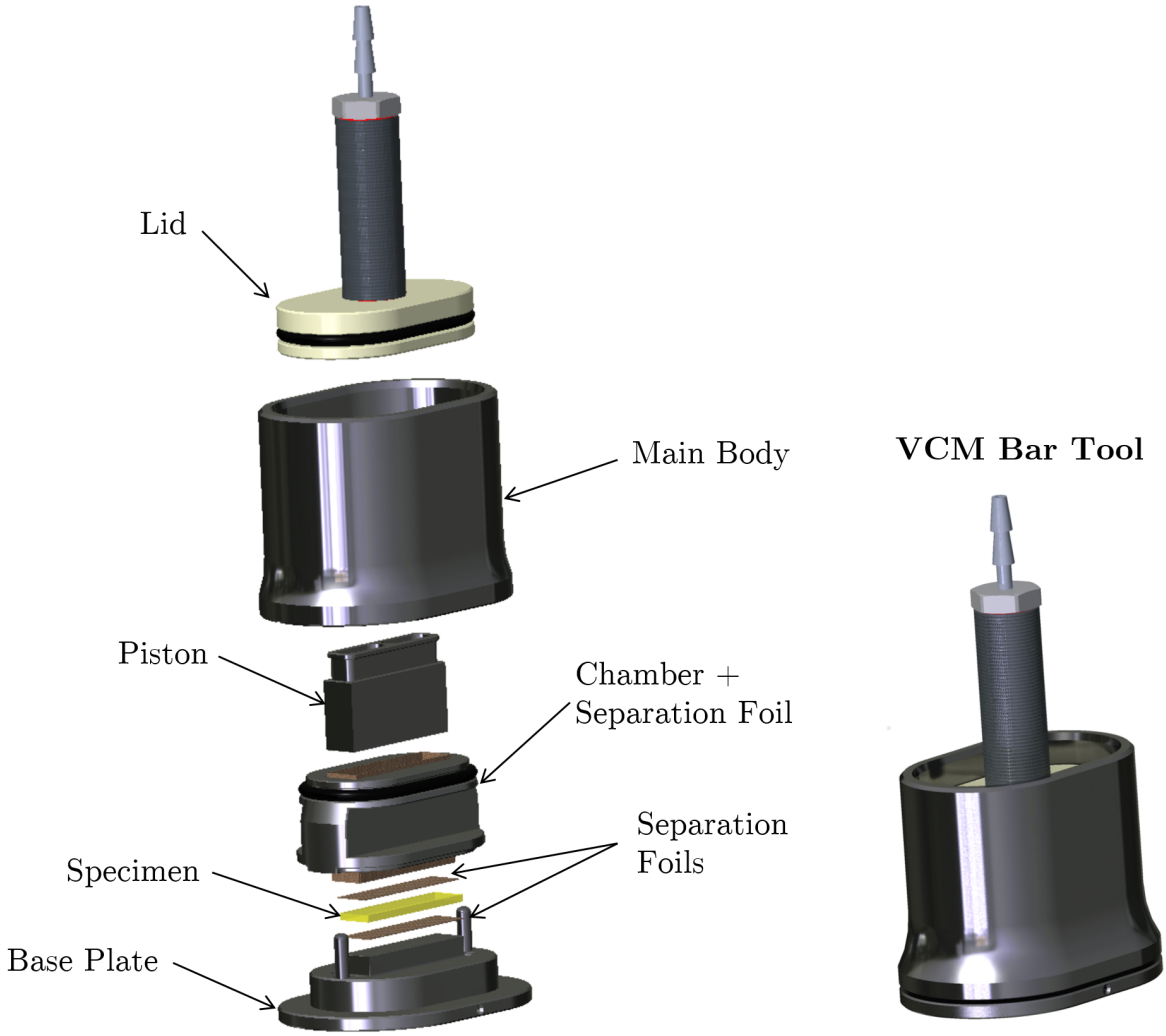

Figure 46 : VCM Bar Tool explosion view (left) and assembled (right)

The size and mass of the device should be as small as possible to minimize thermal inertia. Furthermore, the device should be user-friendly to operate, and the generated compressive force by the lid should be of similar to the VCM Disc Tool to exclude possible leakage of the material. The circumferential separation foil design had to be adapted to the square mold chamber.

A cylindrical design, like the VCM Disc Tool, would have required an outer diameter of the device of at least 75mm, leading to a relatively large and heavy device. Furthermore, the projected area of the lid plate would have been too large in a circular design, generating a compressive force which would have caused an unnecessarily high material leakage.

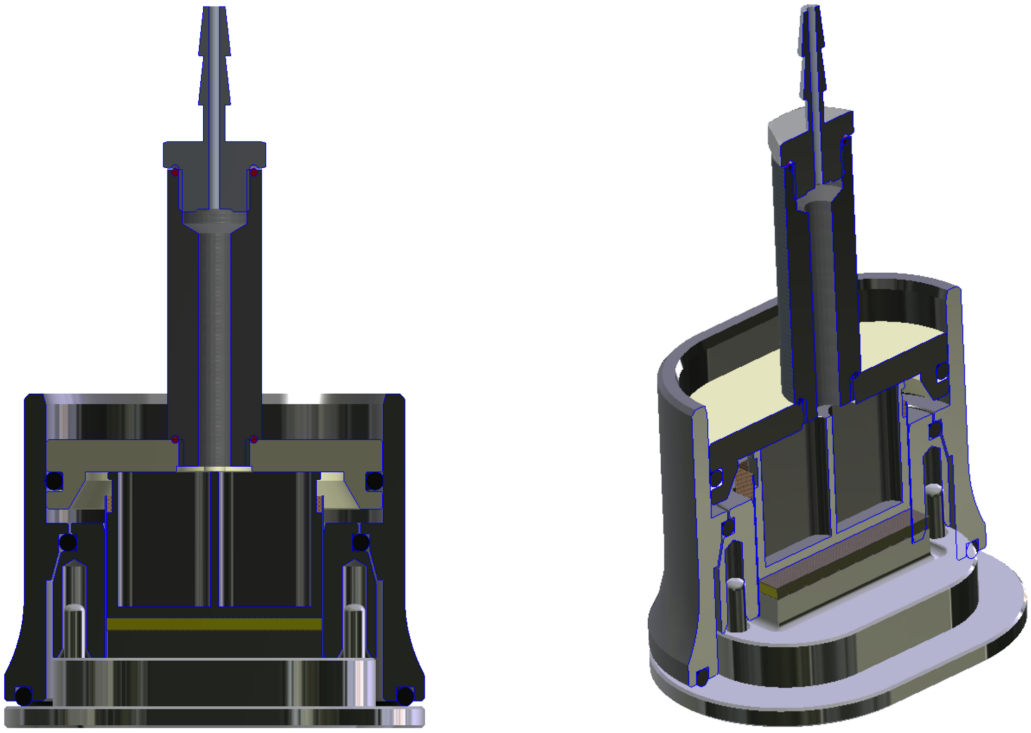

Figure 47 : VCM Bar Tool cross-section

Therefore, the smallest possible mass and size is better achieved with a non-circular design. The non-circular lid builds up a compressive force with a magnitude comparable to the VCM Disc Tool. However, one disadvantage of a non-circular design is that it has to produced using CNC milling, which is more expensive than turning. Furthermore, there exist no standard-approaches for design of O-Ring seal grooves for the given geometry. Therefore, some assumptions had to be made in first calculations, which were validated using several prototypes, before the final device could be built (figure 48).

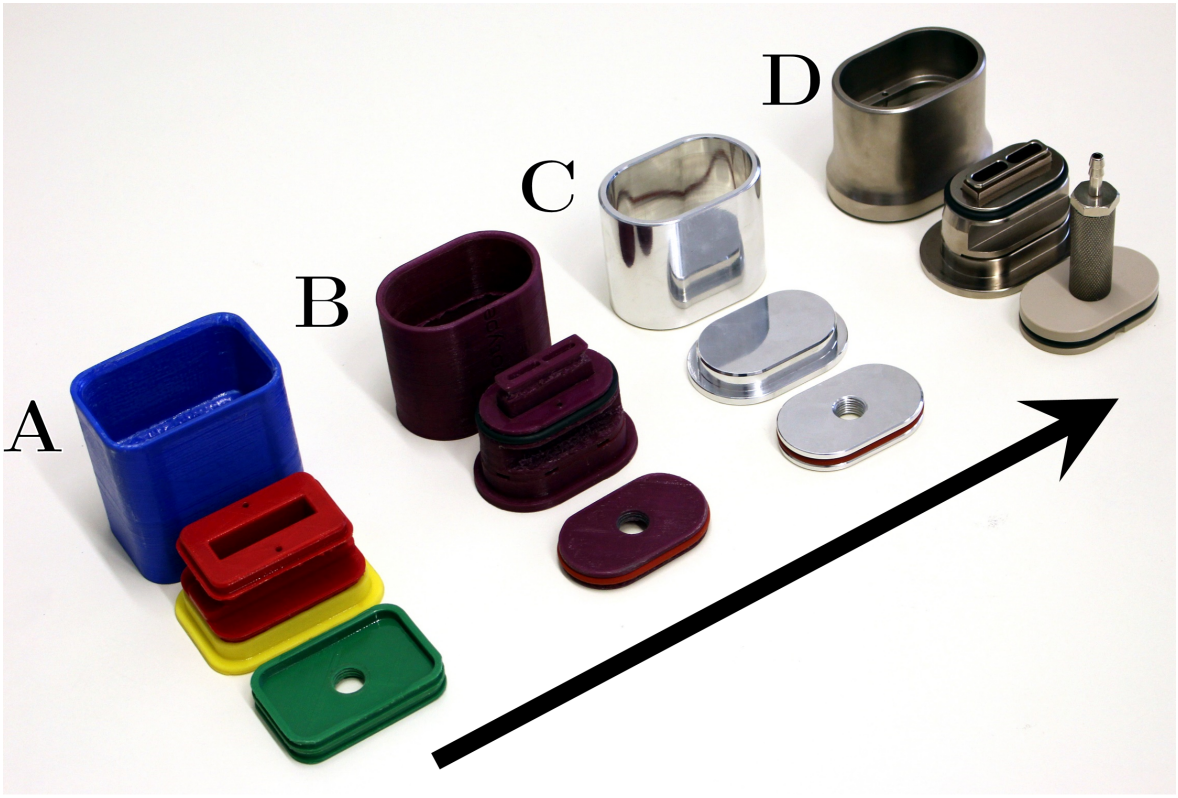

Figure 48 : Protoype evolution of the VCM Bar Tool

The evolution of the prototypes is shown in figure48. The first two prototypes on the left (A,B) were manufactured using 3D-printing on the one hand to evaluate the user-friendliness and on the other hand to check the fit of the O-rings. However, due to the low accuracy of 3D-printing, only qualitative statements concerning the O-rings could be made. To test the tightness and to validate the O-ring calculations, the third prototype (C) was machined from aluminum. Force measurements showed a good agreement with the calculated values of the O-ring friction force. The check of the tightness yielded satisfactory results as well. With the knowledge gained from the prototypes, the final VCM Bar Tool (D) could be built.

3.6 Dynamic Mechanical Analysis (DMTA)

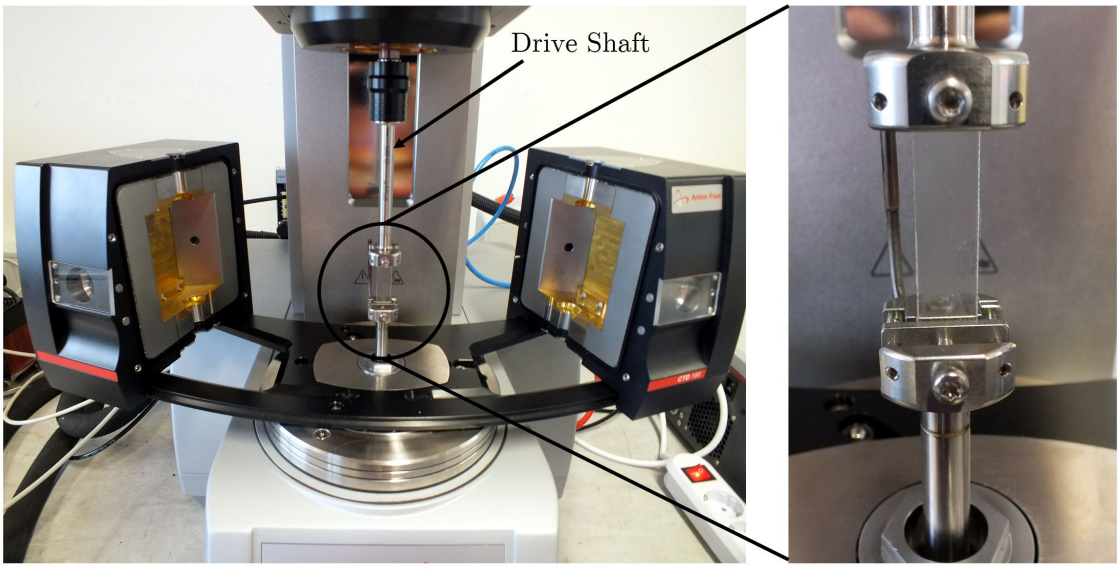

Figure 49 : The used Anton Paar MCR 702 rheometer with Solid Rectangular Fixture (SRF) for torsional DMTA of rectangular bars with mounted Soluplus® specimen shown in closeup view

Dynamic mechanical thermal analysis (DMTA) measurements were carried out in combination with rectangular-bar specimens produced using the VCM Bar Tool. Due to the tedious preparation of specimens using conventional methods, only little DMTA data of pharmaceutical relevance are published in literature. Usually special laboratory injection molding machines is necessary to achieve this task, which entail drawbacks like residual stresses, flow induced material orientations and the skin-core structure of the finished specimens, like they were explained in section 2.4.2. Thus, these conventionally prepared specimens will not reflect the intrinsic material behavior of a polymer, especially if semi-crystalline polymers are regarded. Poly ethylene-vinylacetate (EVA) is a semi-crystalline copolymer, which is used in pharmaceutical hot-melt extrusion as matrix material for contraceptive intravaginal rings (IVR). As already mentioned, the thermo-mechanical properties are an important factor in the design of this particular dosage form. Thus three different grades of EVA were selected as test subjects. To check the feasibility of thermal analysis of polymeric formulations and to be able to compare the results with available DSC data, also typical polymers which are used as hot-melt extrusion matrices, namely Kollidon® VA64, Soluplus® and Eudragit® E, were chosen for investigation.

Sample Preparation

Rectangular bar specimens of the chosen polymers with a geometry of $40x10x1.5mm$ were prepared using the VCM Bar Tool. All materials were dried for at least 24 hours in a vacuum oven. The mass of polymer powder to be filled into the tool was chosen, such that a thickness of $1.5 \pm 0.1mm$ is achieved. The preparation temperatures were chosen sufficiently high above the glass transition temperature of the polymers to achieve

complete particle fusion within a 5 minute heating cycle. The samples prepared from amorphous polymers (Kollidon® VA64, Soluplus®, Eudragit® E) all had a transparent glass-like appearance, without any visible inclusions. As an example, a rectangular bar of Eudragit® E prepared using the VCM Bar Tool is shown in figure 50. The samples made from EVA were also homogeneous, but slightly opaque (figure 51). The opacity arises due to crystalline structures of EVA, which are opaque because of light scattering on the boundaries between the crystalline and amorphous phases of the polymer.

For correct data evaluation, it is required to precisely determine the width and thickness of all specimens. Thus these values were measured using a slide gauge. The width of all specimens was within a range of $9.95 \pm 0.02mm$. The specimen length $39.95 \pm 0.02mm$. To evaluate the evenness of the specimens, the thickness was measured at multiple points along the length of the specimen. For the investigated materials, the degree of flatness, i.e. the deviation of the lowest and highest measured thickness from the mean value, is approximately $\pm 0.03mm$. Therefore, homogeneous specimens with a highly reproducible geometry can be produced using the VCM Bar Tool. Preparation of the specimens was carried out directly next to the DMTA instrument and each sample was immediately subjected to the DMTA measurement after its preparation.

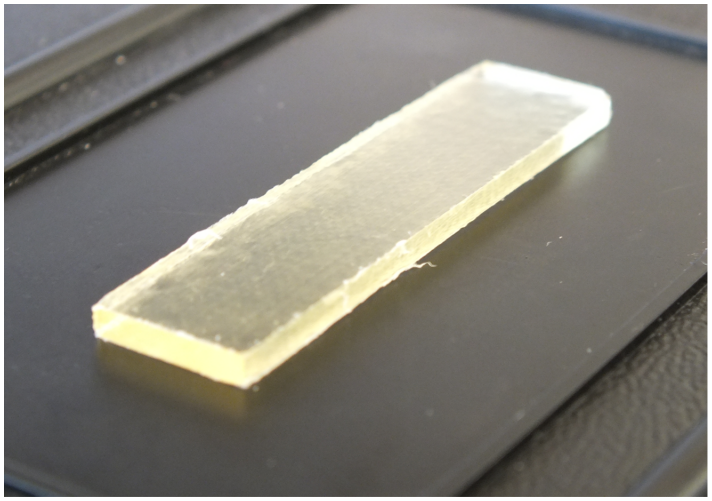

Figure 50 : Recangular bar sample (10x40x1.5mm) of Eudragit® E prepared using the VCM Bar Tool

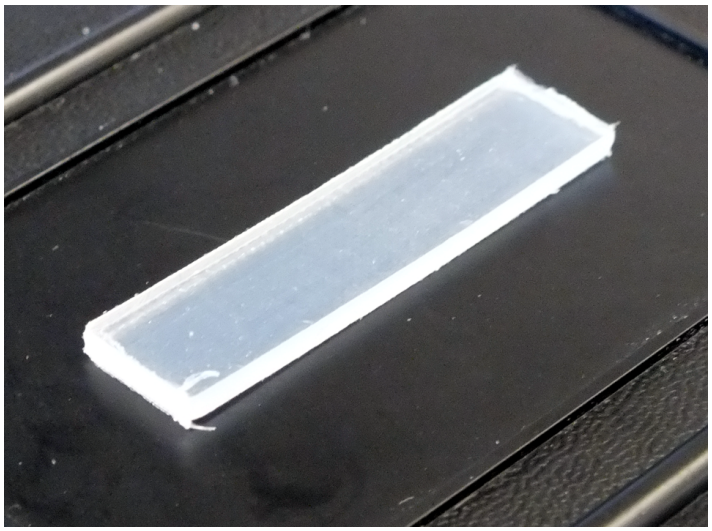

Figure 51 : Recangular bar sample (10x40x1.5mm) of EVA Ateva® 1820 prepared using the VCM Bar Tool

Measurement Procedure

Dynamic mechanical analysis was carried out using an Anton Paar MCR 702 rheometer equipped with a CTD180 convection oven and a solid-rectangular fixture (SRF) for torsional DMTA of rectangular specimens. The used DMTA fixture with a mounted specimen of Soluplus® depicted in figure 49. The standard oscillation frequency of 1 Hz was used as measurement frequency for all runs. As strain amplitude, 0.01% was selected, in order to stay within the linear viscoelastic (LVE) range of the materials . A constant tensile force of 0.5N was applied during the measurement, and this force was controlled to compensate the thermal expansion of the sample during heating, like it is recommended by the manufacturer of the instrument. All measurements were carried out twice, using two consecutively prepared samples to check the repeatability of both the measurement and the sample preparation. To hold the specimen in place during the measurement, the screws of the SRF fixture were tightened using a torque wrench to a torque of 0.3 Nm.

Residual Stresses

As mentioned in previous sections, the minimization of residual stresses is important to be able to measure intrinsic material properties, instead of, e.g. possible residual stress relaxations during heating. One possibility to visualize residual stresses is to exploit the stress-induced birefringence, exhibited by many polymers. The mentioned stress can be applied externally or is frozen due to processing (e.g. during cooling in injection molding).

When a sample is placed between two polarizers with crossed axes, a color pattern is observed, because the polarization of light is is rotated after is passes through the specimen. The magnitude of rotation depends on wavelength (i.e. on the color), which leads to dispersion of the ray of light, similar to a prism. This experimental method

is called *photoelasticity* and can be used to analyze the residual stress distribution of parts. In this case, the residual stresses of VCM specimens are of interest.

A simple experimental setup to visualize residual stresses is shown in figure 52. As first polarizer, a LC display with white background is used, because it emits linear polarized light. The second polarizer is mounted on a standard digital camera, and is adjusted by hand so be crossed with the screen, which lets the screen appear dark when taking a photo of it, because the linearly polarized light emitted by the screen is absorbed by the polarizer material. When a specimen is placed between digital camera and LC display, the polarization axis of the light passing through the specimen is rotated, yielding elliptic polarized light, which can pass the polarizer of the camera, yielding a picture of the stress distribution within the specimen.

Two rectangular VCM specimens of Ateva 1820 with visualized residual stresses are shown in figure 53. In visible light, both samples cannot be distinguished visually. The sample on the top was prepared using a temperature of $130°C$ with a cycle time of 5 minutes. The patterns at the left and right edges arise due to the clamping of the DMTA fixture. Within the sample, residual stresses are observed at the grain boundaries of the fused pellets. Obviously, the relaxation was not completed during the the timescale of the VCM cycle. However, the residual stresses due to the clamping are considerably more pronounced. The sample on the bottom was prepared at $150°C$, also with a cycle time of 5 minutes. Again, stresses due to clamping are visible. The temperature was sufficiently high to bring the terminal relaxation time of the polymer below the timescale of the VCM preparation, causing homogeneous fusion of the particles, without any visible grain boundaries. The brighter edges compared to the center of the specimen indicate, that low residual stresses are present there. However, the magnitude of residual stresses is very low.

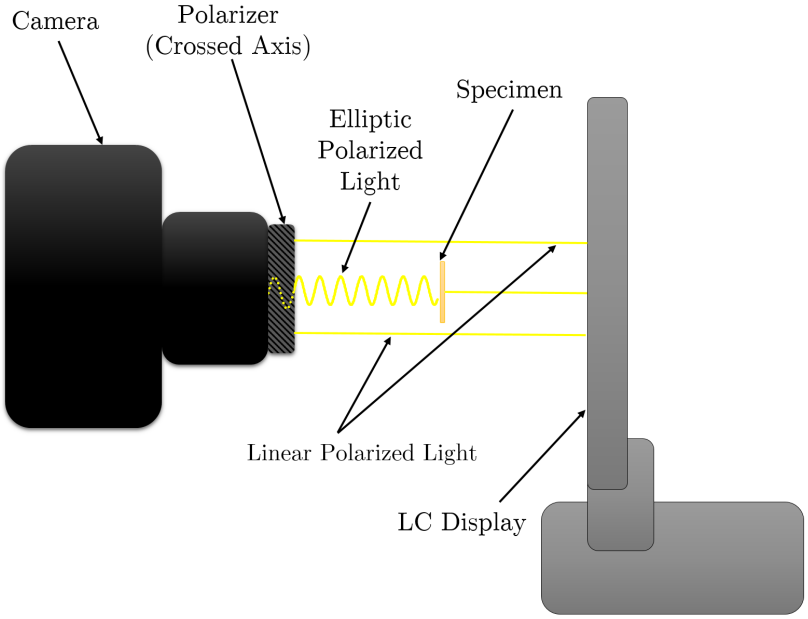

Figure 52 : Simple setup to visualize residual stresses in specimens which exhibit stress-induced birefringence

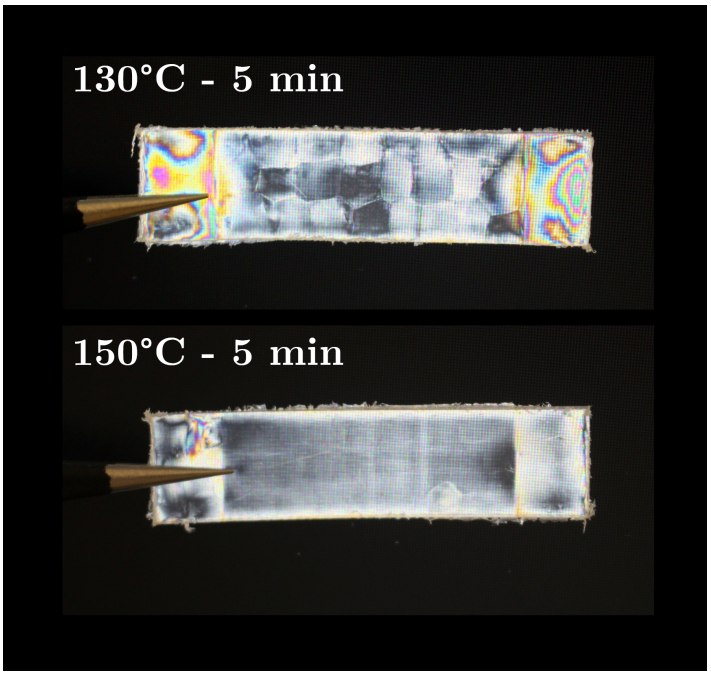

Figure 53 : Comparison of the residual stress distribution of Ateva®1820, prepared using the VCM Bar Tool at two different temperatures.

3.7 Rheometry

3.7.1 Shear Rheology

Shear rheological measurements were carried out in combination with specimens prepared using VCM to investigate the impact of the addition of an API on the rheological behavior by comparing the API-loaded systems with pure polymers. In particular, the viscosity as a function of shear rate is characterized, to investigate how the shear-thinning behavior is influenced by inclusion of API. Furthermore, it should be evaluated if the reproducibility of the measurement is compromised by addition of API. The same model formulations as for the other measurements are used, which are Kollidon® VA64 with 15% itraconazole and Soluplus® with 20% ibuprofen.

Sample Preparation

Disc specimens of the two mentioned formulations, with a diameter of 25mm and a height of 1.5mm, were prepared using the VCM Disc Tool directly next to the rheometer. Cryomilled mixtures were used to achieve a homogeneous mixing of the components during the VCM cycle. Cryomilling of the mixtures was carried out like described in section 3.4.1. All materials were dried at least for 24 hours in a vacuum oven before preparation. The Kollidon® VA64 with 15% itraconazole sample was produced using a hot-plate temperature of $170°C$. Due to the lower viscosity of Soluplus® with 20% ibuprofen, for this formulation a temperature of $150°C$ was used. The heating time for both samples was 5 minutes, following by approximately 2 minutes cooling time. All specimens had a glass-like, homogeneous appearance, indicating the absence of phase-boundaries and, in case of the Polymer-API mixtures, the dissolution of API in the polymeric matrix, i.e. no more visible crystalline structures that lead to an opaque appearance, were present. After demolding, the samples were immediately placed on the heated base plate of the rheometer.

Measurement Procedure

Shear rheological measurements were carried out using an Anton Paar MCR 301 rheometer equipped with a H-ETD400 electrical heating hood and a plate-plate geometry with 25mm diameter (PP25). The used setup is depicted in figure 54.

After heating the samples to a temperature well above their glass-transition temperature, a bubble-free melt formed for both the Soluplus®/ibuprofen and the Kollidon® VA64/itraconazole formulation, respectively. The appearance of the melt was like it is shown in the top right part of figure 54. Both melts had a slightly yellowish appearance, with a slight blue cast in case of Soluplus®/ibuprofen. Subsequently, the measuring gap of 1mm was set and trimming (i.e. removal of excess material) was carefully performed using a spatula.

To obtain flow curves, frequency sweeps in a range between 0.03 and 100 Hz (0.1 and 628 rad/s) were performed at three different temperatures, which were selected in the range of typical processing temperatures of the polymers in hot-melt extrusion. The

measured complex viscosity as a function of angular frequency is, as stated in the theory section, in very good approximation equivalent to a function of viscosity as a funtion of shear rate (Cox-Merz rule). An oscillation amplitude γ_A of 1% (with regard to the gap between bottom and top plate of the measuring geometry) was chosen in order to ensure the linear viscoelastic (LVE) range is not exceeded. The LVE limit was determined for the pure polymers in an earlier work. The LVE range for the neat polymers is much wider than the used strain amplitude [47]. During the measurement, the heating hood was continuously purged with nitrogen gas, to prevent possible oxidation of the polymer melt.

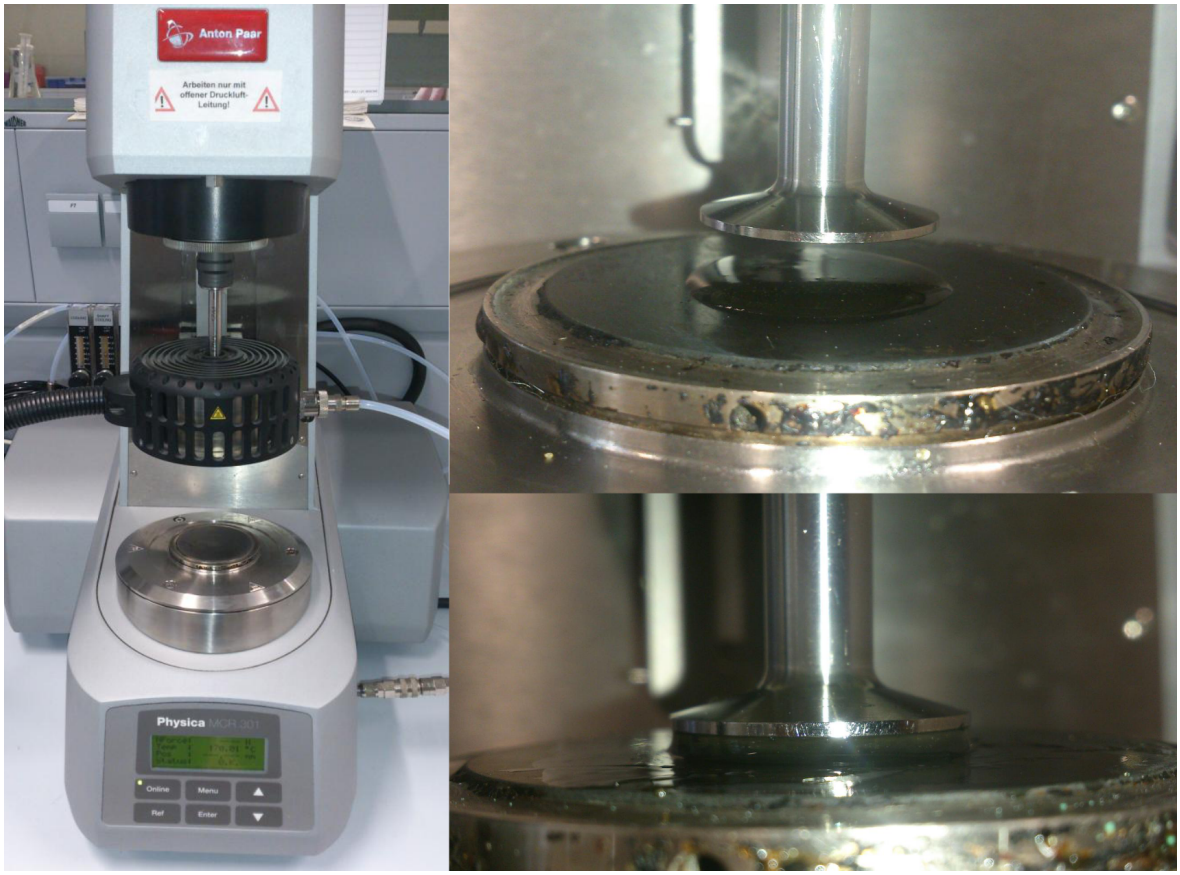

Figure 54 : Left: The used setup for the shear-rheological measurements. Anton Paar MCR 301 rheometer and a plate-plate measuring geometry with a diameter of 25mm (PP25) Top right: molten polymer specimen (prepared using VCM), before trimming, Bottom right: trimmed specimen, ready for measurement[47]

Carreau-Yasuda Model - Data Fitting

To fit the data of a certain complex viscosity isotherm to the Carreau-Yasuda model, the following steps were carried out the same way as in previous work. Thus, the following description was adopted without major modifications from reference [47].

As fitting function of the complex viscosity, the already introduced Carreau-Yasuda equation was used:

$$|\eta^*|^{fit}(\omega_i) = \eta_0 \left[1 + (\lambda\,\omega_i)^a\right]^{\frac{n-1}{a}} \tag{3.18}$$

Subsequently, by a least-squares approach, the data is fitted to the Carreau-Yasuda equation using the generalized-reduced-gradient (GRG) algorithm, which is a gradient based method for nonlinear regression. This method is implemented in the *Solver* tool in Microsoft Excel. The objective function is the squared sum of relative errors of all m data points:

$$\sum_{i=1}^{m} \left(\frac{|\eta^*|^{fit}(\omega_i) - \overline{|\eta^*|}(\omega_i)}{\overline{|\eta^*|}(\omega_i)} \right)^2 \Rightarrow MIN \tag{3.19}$$

where $\overline{|\eta^*|}$ is the measured mean complex viscosity of multiple runs at a given point of angular frequency ω_i. The algorithm varies the parameters λ, n, and a, until it converges, i.e. reaches the global minimum of the objective function. η_0 is predetermined by the value of the complex viscosity at a the lowest available angular frequency of the frequency sweep, which is usually a good assumption.

It is advantageous using the relative error, as values of the function $|\eta^*|(\omega)$ usually cover several decades. If the absolute error would be minimized, errors at large values of $|\eta^*|$, i.e. the zero-shear region, would affect the fit significantly more than deviations at small values (i.e. in the power-law region). This issue is eliminated by minimizing the relative error.

3.7.2 Extensional Rheology

Branched polymers usually exhibit nonlinear rheological behavior in extensional flow. Soluplus® was selected for extensional rheology investigation, because it is a polymer with grafted side chains, i.e. one could expect it to behave a similar rheology in extension as a branched polymer.

Sample Preparation

Rectangular bars with a thickness of 1mm were prepared using the same approach as described in section 3.6. However, a typical sample width for extensional rheology is 20mm, i.e. half the length of a specimen prepared using the VCM Bar Tool. Thus the sample were carved using a knife and carefully broken in two pieces of approximately 20x10x1mm.

Measurement Procedure

Extensional rheological measurements were carried out using an Anton Paar MCR 702 rheometer equipped with a CTD180 convection oven and a Sentmanat Extensional Rheometer (SER3) fixture. The setup is depicted in figure 55. One of the sample pieces was carefully put in the fixture. Subsequently the convection oven was closed, and heated up to soften the mounted specimen. As measurement temperature, $140°C$ was chosen, because the minimum zero-shear viscosity needed for this measurement principle are 10.000 Pas (to avoid sagging of the specimen) and because shear rheological data

of Soluplus® are available at this temperature. After the measurement temperature was reached, the measurement was started immediately. Multiple experiments were performed in a range of extensional strain rates between 0.01 and 25 s^{-1}, each requiring a new specimen. Thus, a large number of samples are required to characterize a material in extension. The VCM Bar Tool is a method, which is able to provide a large number of specimens suitable for these tests in a short time.

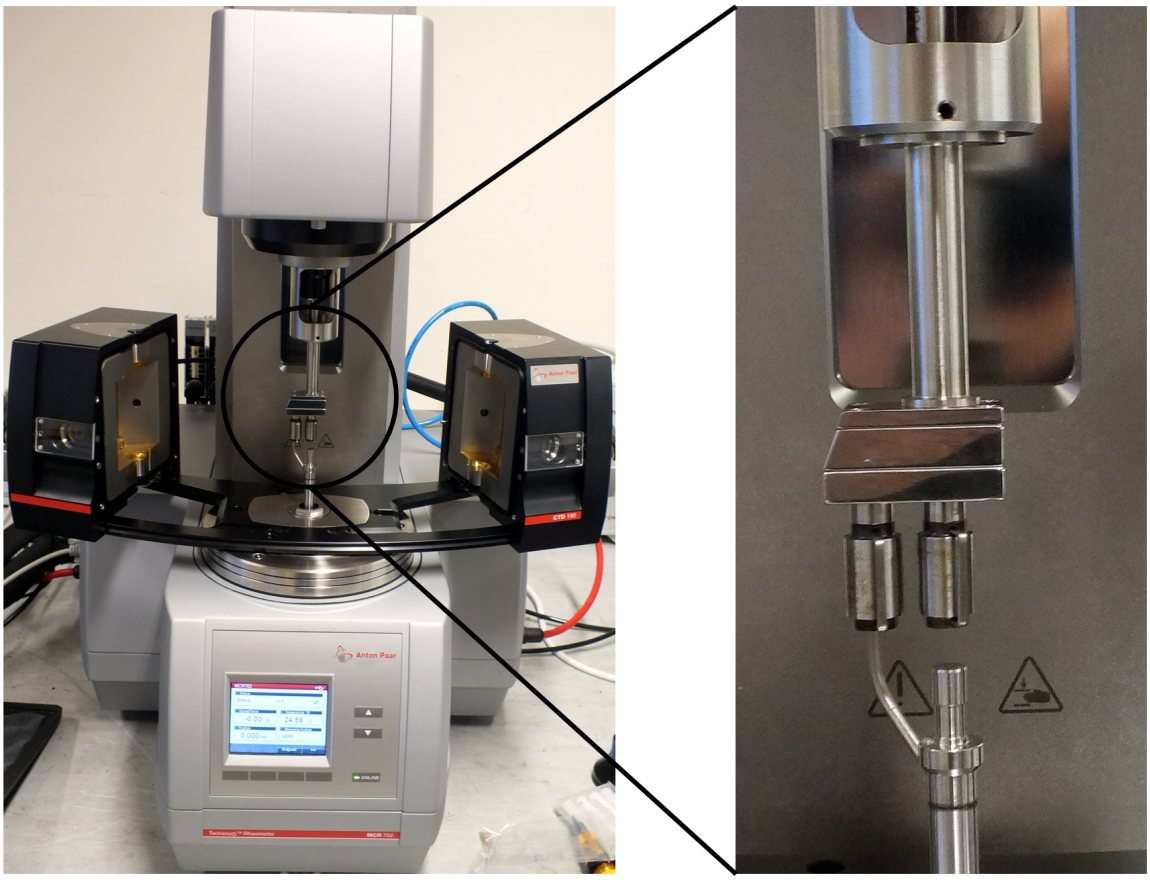

Figure 55 : Used setup for rheometry in extension Anton Paar MCR 702 rheometer, CTD180 convection oven and a Sentmanat Extensional Rheometer (SER3) fixture

4 Results and Discussion

For most measurement results presented in this chapter, a standard deviation is indicated, which is used to quantify the variation of the data values. The standard deviation (SD) of the data was was estimated using the well-known expression:

$$SD = \sqrt{\frac{\sum (x_i - \bar{x})^2}{n-1}} \tag{4.1}$$

where x_i is the i-th data point $\bar{x}$ the arithmetic mean and n the number of data points. The relative standard deviation is calculated with regard to the mean $\bar{x}$.

$$RSD = \frac{SD}{\bar{x}} \cdot 100[\%] \tag{4.2}$$

The mean relative standard deviation (MRSD) is the arithmetic mean of the RSD of all data points .

4.1 Differential Scanning Calorimetry

4.1.1 Thermal Transitions

In the following sections, the results of modulated DSC measurements of different pharmaceutical polymers are presented. Moreover, the results of specimens prepared by VCM and by simple powder are compared. The reversing and non-reversing heat flow components are presented in separate diagrams for clarity. The used sign convention is that released heat (e.g. due to exothermic processes) is denoted as positive heat flow). Thus, a heat flow due to the heat capacity of the sample material is by definition negative. This is indicated by the arrow pointing upwards (*exo up*). In literature, multiple curves on a single DSC diagram are often horizontally shifted to avoid overlapping of the curves. Thus, the values of the heat flow are not directly comparable, because the values presented on the y-axis are only valid for one reference curve. In the data presented in the following sections this is not the case, which enables to quantitatively compare the data presented in one diagram.

Evaluation of the Glass Transition Temperature (T_g)

All measured glass transition temperatures that are reported in this thesis were determined by evaluating the peak of the smoothed derivative of the reversing heat flow curve. As selected example, in figure 56 the first derivative of the reversing heat flow with respect to time is compared for a powder and a VCM specimen of HPMC Methocel® E5. For evaluation of the peak value (to determine T_g), both curves were smoothed using the same setting (H) in the DSC software (NETZSCH Proteus). The noise in the curve obtained using a VCM sample is much lower compared to the powder sample. The fluctuations in the data of the powder sample lead to a very inaccurate determination of T_g. However, this is not the case for the VCM specimen and a better defined value of T_g can be obtained.

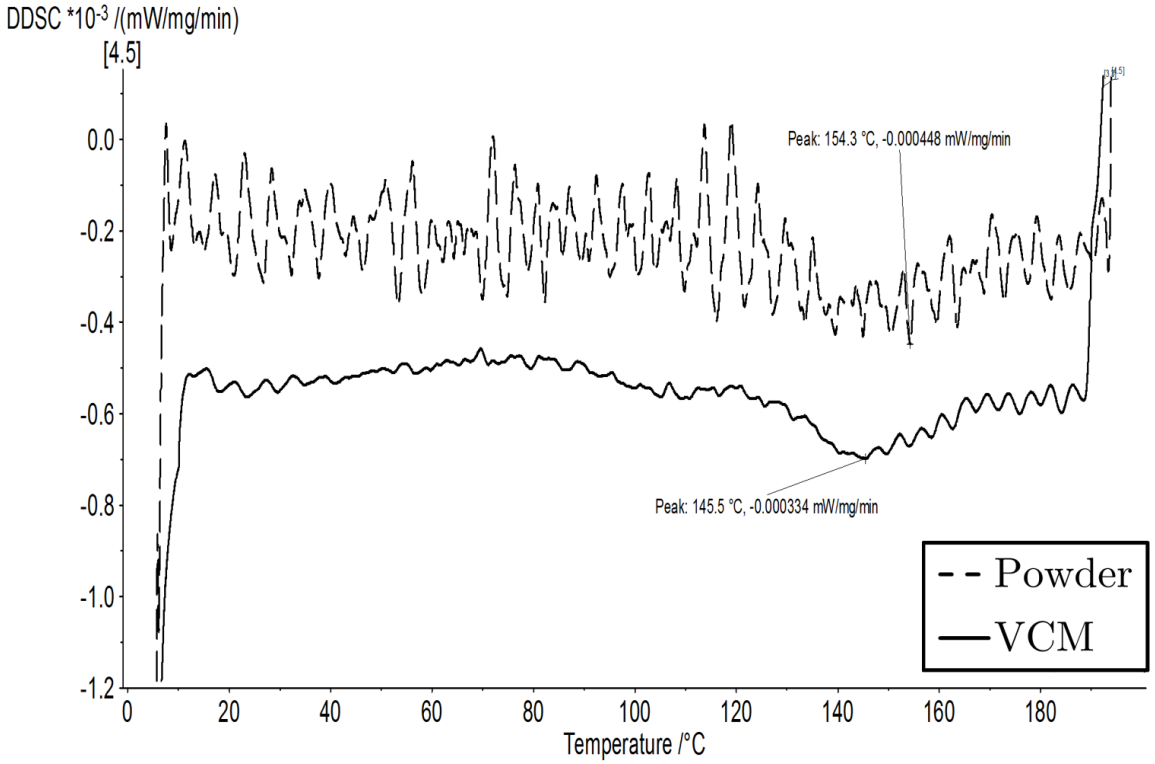

Figure 56 : Determination of the T_g of HPMC Methocel® E5 using the 1st derivative of the reversing heat flow. Solid line: VCM Sample, dashed line: powder sample. Both curves were smoothed with the highest smoothing setting in the NETZSCH software (setting H). The curves are vertically shifted for clarity.

Soluplus®

The MDSC thermogram of Soluplus® (figure 57) reveals clear differences between powder and VCM specimens. The glass transition event is similar for both specimens. Above $100°C$ the heat flow for the VCM specimen is much lower than for powder.

The non-reversing heat flow curve of powder shows a small negative deviation near the T_g, possibly due to an enthalpy recovery. The curve of the VCM sample strongly deviates from powder and indicates a small peak at approximately $45°C$. This event occurs approximately $25°C$ below T_g, and is purely kinetic-related, because it is not

seen in the reversing heat-flow curve. The reason this event is observed is unknown. The curvature of the VCM curve indicates that some moisture is released from the specimen during the measurement, which explains the strong curvature between 55°C and 125°C. Above 125°C, the moisture seems to be completely released, as the VCM curve approaches the same slope as the powder data.

Obviously, despite the short time between preparation of the VCM specimen and measurement, the polymer absorbed a certain quantity of moisture from the atmosphere. During the first heating run, the absorbed moisture was more effectively removed from the powder sample, because of its higher specific surface area which allows a more effective mass transfer and thus leads to nearly full drying of the specimen during first heating.

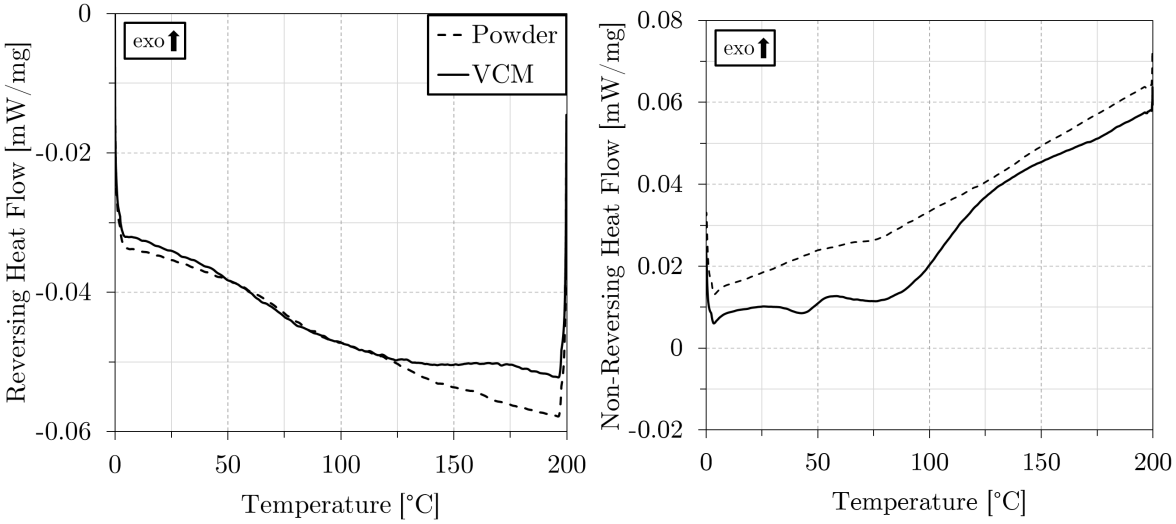

Figure 57 : MDSC thermogram of Soluplus®. left: reversing heat flow, right: non-reversing heat flow

Kollidon® VA64

The MDSC thermogram of Kollidon® VA64 is depicted in figure 57. The reversing heat flow curve of powder seems to indicate a two-step transition, whereas the VCM curve shows a clearly defined glass transition with a higher observed change in heat capacity than for powder. This effect likely arises due to ongoing powder sintering or coalescence processes, which lead to the appearance of two seemingly consecutive glass transitions. Therefore, the data obtained using the VCM specimen exhibits a better defined glass transition.

The non-reversing heat flow curve of the VCM specimen, as for Soluplus®, indicates moisture release. The powder sample clearly exhibits an enthalpic recovery at T_g, which is not seen for the VCM sample due to the large contribution of moisture loss to the non-reversing heat flow.

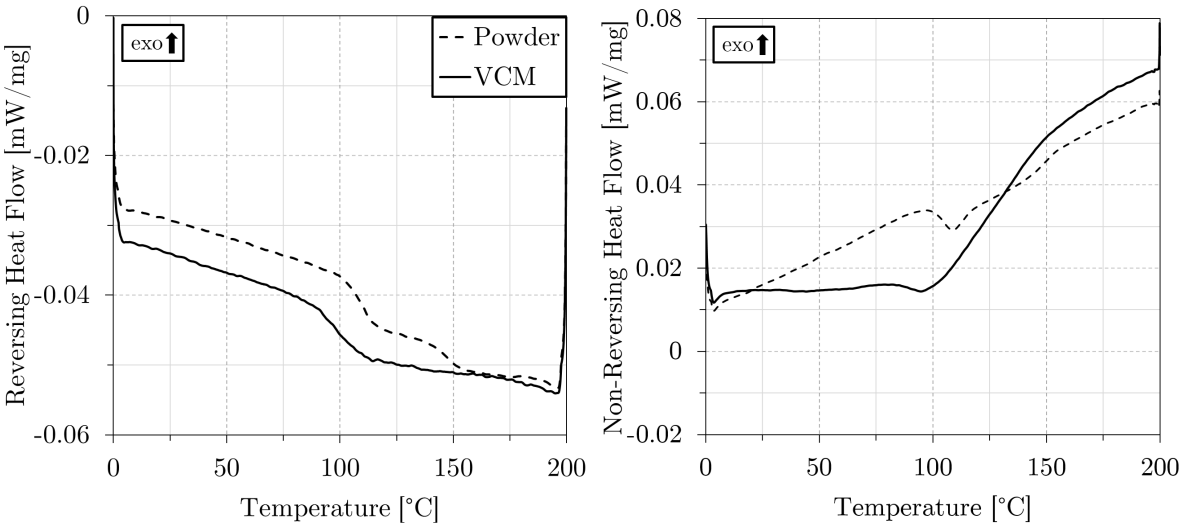

Figure 58 : MDSC thermogram of Kollidon® VA64. left: reversing heat flow, right: non-reversing heat flow

Eudragit® E

The MDSC results for Eudragit® are shown in figure 59. It can be seen in the reversing heat flow curve (left diagram) that, compared to powder, the glass transition of the VCM specimen occurs at a slightly lower temperature. Moreover, the change of the reversing heat flow due to the transition is visibly larger, which is presumably due to a more efficient heat transfer between sample and pan. At about 150° there is an onset of an event which can only be observed for the powder specimen. This might be due to air bubbles emerging from the melt.

In the reversing heat flow curve, for the VCM specimen, an endothermic peak at approximately 45° occurs. This is roughly at the glass transition temperature (T_g). Therefore, this is a typical enthalpy recovery event. For the VCM sample, a stronger enthalpic recovery compared to the powder specimen is observed. For powder, enthalpic recovery occurs at considerably higher temperature and on the other hand it is thermally much quieter, i.e. the peak is less pronounced. The higher enthalpic recovery is a sign that the specimen has relaxed (aged) during the time between preparation of the specimen and the DSC measurement. The time between preparation and measurement of this sample was approximately 10 hours due to the waiting time in the autosampler before the other measurements were finished. The enthalpy recovery is much weaker for the powder sample, because its thermal history is erased by the first heating step, and for the second heating (the actual measurement) the sample is immediately reheated, which means the material has less time to relax, causing a lower recovery of enthalpy.

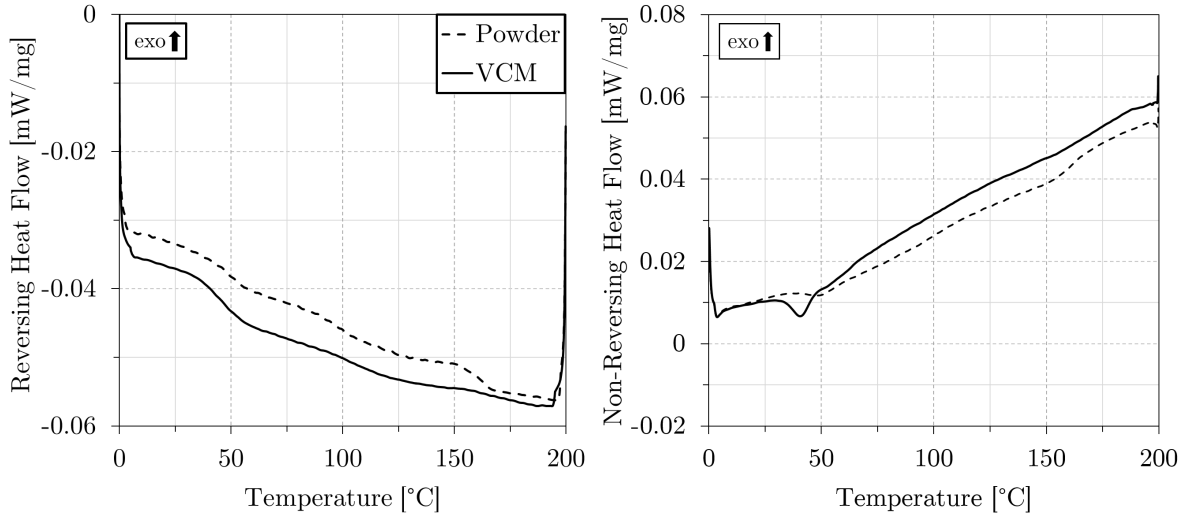

Figure 59 : MDSC thermogram of Eudragit® E. left: reversing heat flow, right: non-reversing heat flow

HPMC Methocel® E5

HPMC has a very high viscosity, even when heated to temperatures way above the T_g. Therefore, for HPMC powders sintering and densification occur very slowly if no compressive external force is applied. For HPMC, only the sintering of the particles is reached during a traditional DSC measurement. In contrast, the VCM preparation yields a homogeneous specimen disc. Therefore, the samples prepared using VCM seem to be better suitable to detect the intrinsic properties of the material, compared to powder.

The MDSC thermograms of HPMC Methocel® E5 are depicted in figure 60. The reversing heat flow curve appears similar for both samples. However, determination of the T_g is difficult for the powder sample, because the slope of the curve does not change significantly. However, for the VCM sample there is a more clearly defined change in slope and a clear peak is visible when determining the T_g via the derivative of the reversing heat flow. As shown above, the heat flow signal of the powder sample is significantly noisier, which only allows a vague determination of T_g. For the VCM device, the determined T_g can be more unambiguously determined. The value for the VCM specimen is $145.5°C$ which is approximately $9°C$ lower than for the powder specimen $154.3°C$. The T_g reported in literature is $154°C$ [110], presumably because the authors used powder as sample for the DSC measurement.

The non-reversing curve of the VCM specimen shows a bump which ends at approximately $100°C$. This bump can be attributed to moisture loss. As the glass transition temperature lies at about $140°C$, its value should thus not considerably be affected by the moisture. For the VCM specimen at the T_g an enthalpic recovery event can clearly be seen. However, no thermal event can be assigned to the non-reversing heat flow curve of the powder sample. Therefore, the VCM approach seems to lead to a higher sensitivity of the measurement in this case.

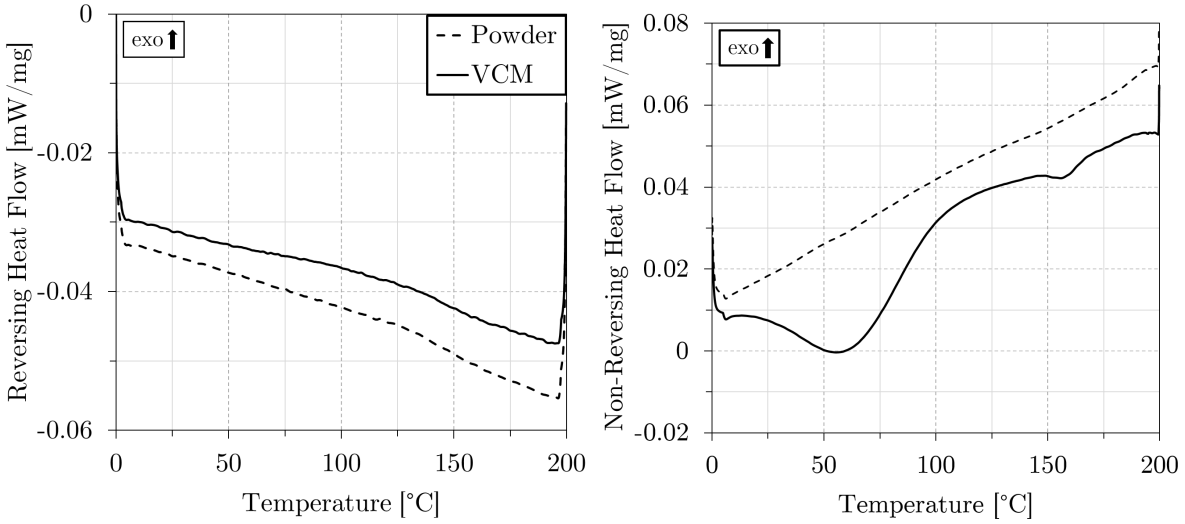

Figure 60 : MDSC thermogram of HPMC Methocel® E5. left: reversing heat flow, right: non-reversing heat flow

HPMCAS-LF

HPMCAS-LF shows similar behavior as as HPMC Methocel® E5. Its high viscosity, even way above its glass transition temperature, only allows sintering of the particles if no external force is applied. The VCM preparation yields a yellowish, homogeneous, transparent sample disc.

The MDSC thermogram of HPMCAS-LF is depicted in figure 61. The reversing heat flow curves show qualitatively the same behavior for powder and VCM samples. The glass transition temperature is similar for both specimens (around $120°C$). The non-reversing heat flow of the VCM sample again shows a bump due to moisture loss, which causes a less visible enthalpic recovery event for the VCM sample, compared to the powder specimen.

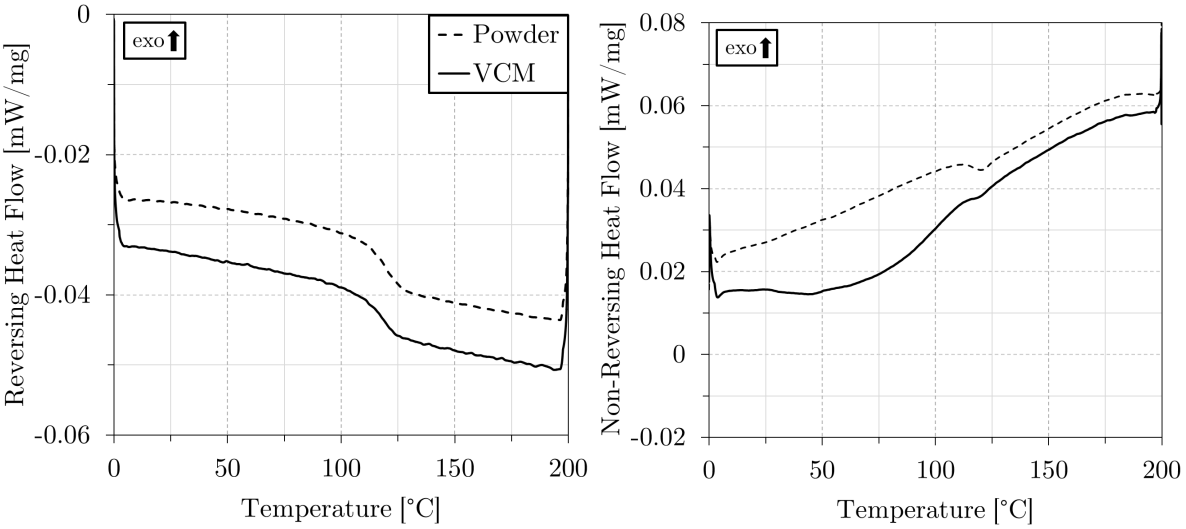

Figure 61 : MDSC thermogram of HPMCAS LF. left: reversing heat flow, right: non-reversing heat flow

Soluplus® - Ibuprofen

The MDSC thermogram of the formulation of a Soluplus® matrix with 20 wt% ibuprofen is depicted in figure 62. The reversing heat flow curve shows that the VCM specimen exhibits a more pronounced change in heat capacity (i.e. stronger changing reversing heat flow) due to the glass transition than the powder specimen. A single T_g around $30°C$ is observed for both samples, which is an indication that ibuprofen has dissolved in the polymeric matrix and is present in its amorphous form, i.e. no melting peak of crystalline ibuprofen is detected. Melting of crystalline ibuprofen would be expected at the melting point of ibuprofen crystals ($54°C$). Therefore, spontaneous fusion of a heated cryomilled mixture seems to be sufficient to dissolve ibuprofen crystals in the molten Soluplus® matrix. The T_g of the VCM sample is approximately $3°C$ lower compared to powder. Due to the addition of 20% ibuprofen, the T_g of neat Soluplus® is lowered by approximately $40°C$. Therefore, incorporation of ibuprofen into the polymeric matrix strongly plasticizes of the polymer, i.e. enables a higher mobility of the polymer chains. This shifts the glass transition temperature to a lower level compared to the pure polymer.

The non-reversing heat flow curve of the VCM sample shows, in contrast to most of the polymers described above, no signs of moisture loss. This might be due to the fact that ibuprofen is hydrophobic. However, in literature it was reported that the water uptake for a hot-melt extruded formulation of ibuprofen increased with increasing drug loading [111]. Therefore, it seems that a lower residence time in the autosampler is the reason for the lower apparent moisture loss. Compared to the powder sample, a stronger enthalpic recovery is exhibited by the VCM specimen.

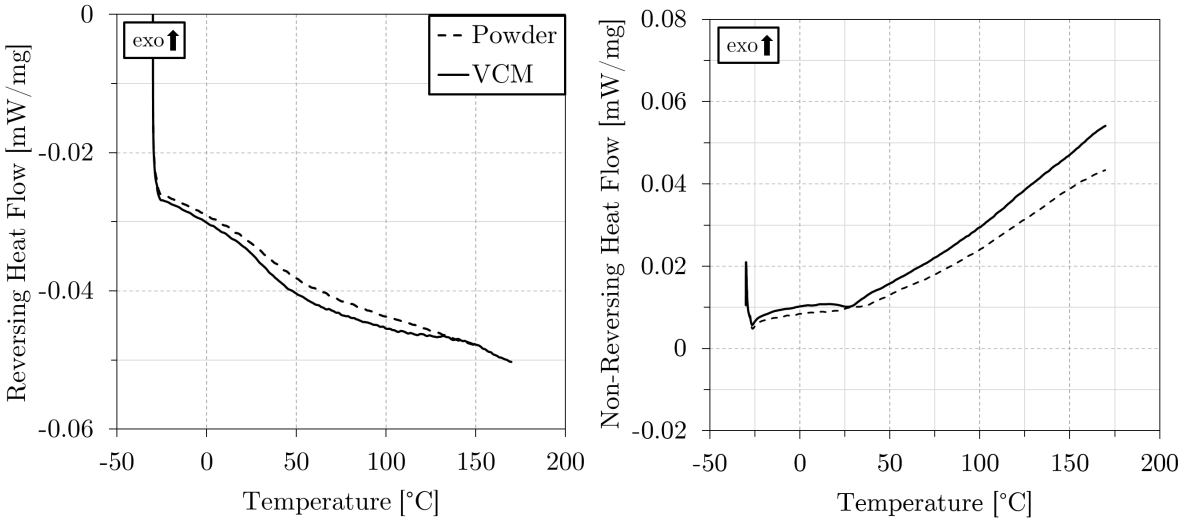

Figure 62 : MDSC thermogram of a mixture of Soluplus® and ibuprofen (80:20)

Kollidon® VA64 - Itraconazole

The MDSC thermogram of the formulation of a Kollidon® VA64 matrix with 15 wt% itraconazole is depicted in figure 63. The reversing heat flow curve shows that both samples exhibit a single T_g and no melting of crystalline itraconazole is observed (would

be expected around 166°C). Thus, also in this case the API is present in its amorphous form in both powder and VCM specimens.

The non-reversing curve shows indications of moisture loss, however much less pronounced than for neat Kollidon® VA64. This is due to a lower residence time of the sample in the autosampler compared to pure Kollidon® VA64. At about 35°C a small endothermic event is observed for the VCM sample, which is not present for the powder specimen. The reason for the occurrence of this event is unknown.

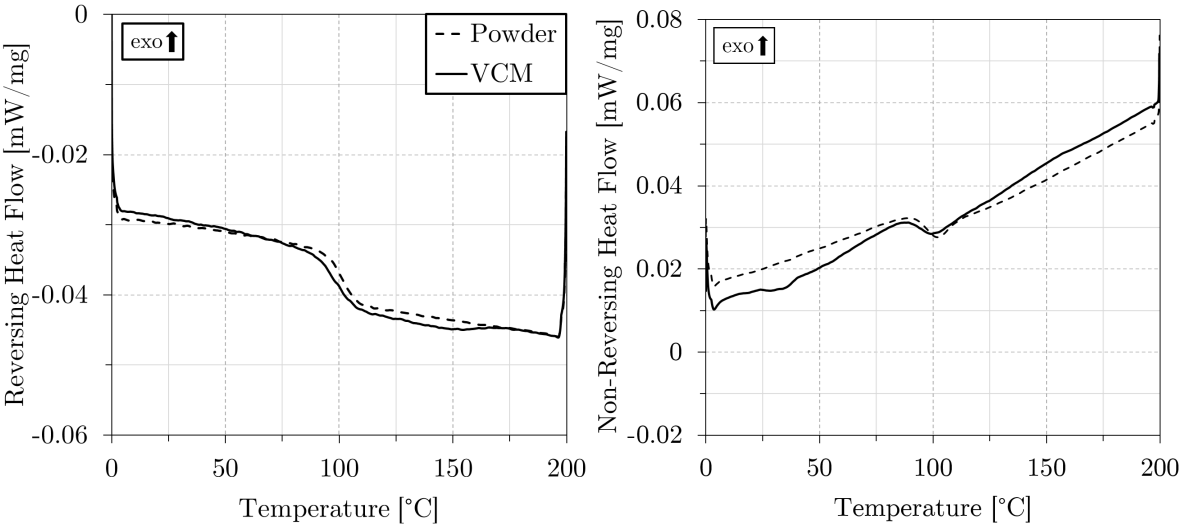

Figure 63 : MDSC thermogram of a mixture of Kollidon® VA64 and itraconazole (85:15)

Summary and Conclusion

In table 2, the T_g values, determined using the smoothed first derivative of the reversing heat flow, and the values of glass-transition *Onset*, *Mid* and *End* temperatures are summarized and compared between powder and VCM. For HPMC Methocel® E5 and Soluplus®/ibuprofen, no meaningful glass-transition *Onset*, *Mid* and *End* data could be determined due their thermally very subtle glass transitions, which resulted in a low signal to noise ratio.

For all materials, except neat Soluplus® and HPMCAS-LF, the detected T_g is lower for the VCM specimen. Also the width of the transitions differs strongly between the sample preparation methods. Except for Soluplus®, the *Onset* is observed at a lower temperature for the VCM sample. The same holds for the *Mid* values. For HPMCAS-LF and Soluplus®, VCM samples lead to lower *End* values while for the other polymers the *End* value is only slightly affected by the sample preparation method.

Material	T_g [$°C$]	Onset[$°C$]	Mid [$°C$]	End [$°C$]
Soluplus® Powder	74.6	41.2	84.2	128.7
Soluplus® VCM	75.4	49.9	87.4	95.6
Soluplus® - 20%IBU Powder	33	n/a	n/a	n/a
Soluplus® - 20%IBU VCM	29.9	n/a	n/a	n/a
Kollidon® VA64 Powder	108.5	103.2	107.6	107.5
Kollidon® VA64 VCM	96.2	90.2	100.2	108.5
Kollidon® VA64 - 15%ITRA Powder	101.8	94.7	101.2	107.5
Kollidon® VA64 - 15%ITRA VCM	98.6	90.3	98.6	106.4
Eudragit® E Powder	50.7	41.9	46.9	55.2
Eudragit® E VCM	46.9	36.1	45.4	55.3
HPMCAS-LF Powder	118.2	108.2	118	127.5
HPMCAS-LF VCM	119.1	106.4	115.9	125.6
HPMC Methocel® E5 Powder	154.3	n/a	n/a	n/a
HPMC Methocel® E5 VCM	145.5	n/a	n/a	n/a

Table 2 : Summary of T_g analysis results for powder and VCM specimens

4.1.2 Thermal Conductivity and Quasi-isothermal Heat Capacity

Polystyrene (Calibration Material)

In figure 64, the results of a heat capacity measurement of polystyrene (mean values of triplicate determination) are compared with heat capacity values from literature [112]. The measured values are very consistent, indicating good repeatability of the measurement. At approximately $100°C$, i.e. close to the glass transition temperature of polystyrene, a discontinuity of heat capacity is observed as expected. At temperatures below the glass transition the measured values show good agreement with the literature values. Above the glass transition there is a negative deviation from the literature data of about 3.5%, which decreases with rising temperature. This deviation above T_g could be due to different physical properties of the measured type of polystyrene, e.g. a different molecular weight or different tacticity. Nevertheless, the agreement of the data with the literature values is good and it can be concluded that the applied quasi-isothermal measurement method and respectice data analysis approach yields plausible and repeatable results.

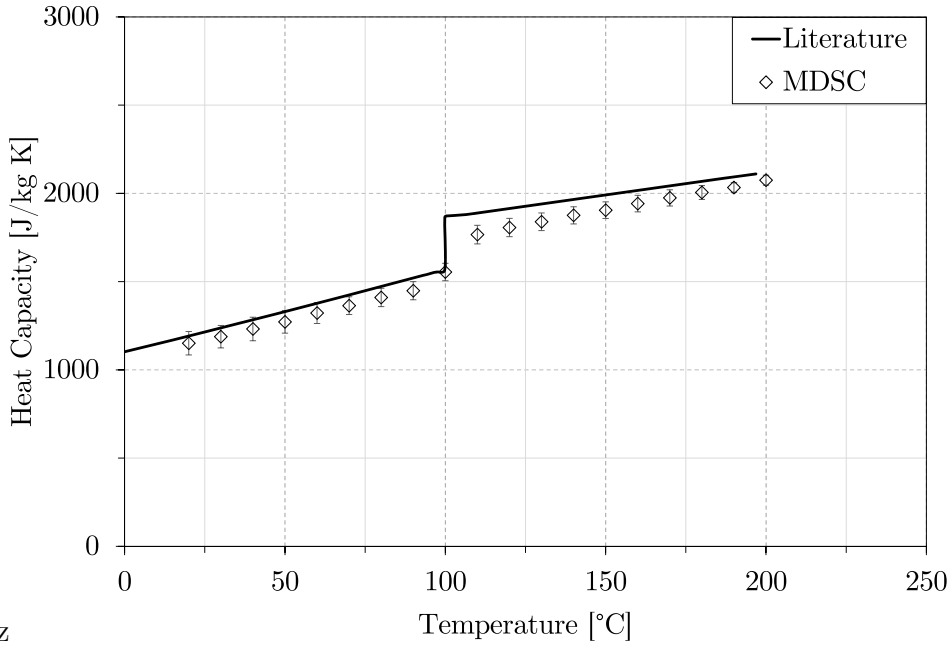

Figure 64 : Quasi-isothermal heat capacity results for polystyrene and comparison with literature values [112]

In figure 65 the results of multiple apparent heat capacity measurements of 3mm thick polystyrene specimens is shown. The mean relative standard deviation of all runs is about 3%. For polystyrene, at approximately $150°C$ the material slowly starts to flow, which causes the thickness of the specimen to decrease with time and thus the measured apparent heat capacity to increase. This is one of the major limitations of this measurement method: it can only be used in a temperature range in which the characteristic flow timescale of the measured material is larger than the timescale of the measurement.

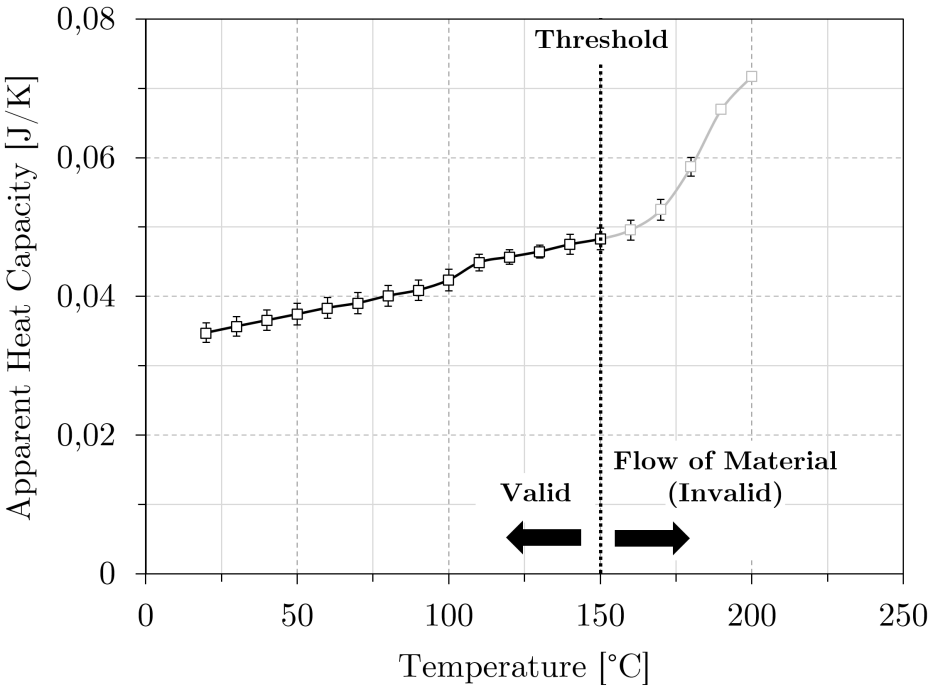

Figure 65 : Quasi-isothermal apparent heat capacity results for thick polystyrene specimens. The threshold at which the material starts to flow and the measured values become invalid is indicated

The temperature threshold, above which flow of the thick specimen occurs, marks the upper limit of determination of the thermal conductivity using the introduced MDSC method. Therefore, the thermal conductivity results presented in subsequent sections are only presented in a range below this temperature threshold, which was determined by visually inspecting the apparent heat capacity curve of each polymer and rejecting data points above the threshold.

Thermal Conductivity Calibration

The observed thermal conductivity value of the polystyrene calibrant is slightly higher than the true thermal conductivity given in literature. At $20°C$ the observed thermal conductivity is $0.185\,W/mK$. Marcus and Blaine measured observed a thermal conductivity of $0.17\,W/mK$ at $25°C$. Considering the manifold influential factors due to the instrument, the present results are roughly comparable to the results of Marcus and Blaine. The thermal conductivity calibration factor D was calculated for each individual temperature using equation (3.16). Reference thermal conductivity data of pure polystyrene were taken from the publication of Sakakibaba et al. [113]. The values for D as a function of temperature showed a fluctuation around a mean value, with no clear trend. As the value of the calibration factor D depends strongly on the quality of the literature data, it was decided to use an averaged value of D, to avoid distortion of trends in the raw thermal conductivity data. An averaged calibration factor of $D = 0.022\,W/mK$ was determined, which is considerably higher than the value reported by Marcus and Blaine ($D = 0.014\,W/mK$). Usage of a mean value of D leads to the same shift of all raw thermal conductivity values to obtain the corrected thermal conductivity as a function of temperature. Nevertheless, using this averaged

calibration factor and equation (3.17), a good superposition of measured values and literature values of polystyrene is achieved without inducing the mentioned distortion of trends in the raw data.

Kollidon® VA64

Figure 66 depicts the results of (a) the quasi isothermal heat capacity and (b) the thermal conductivity measurement of Kollidon® VA64. The error bars reflect the standard deviation of the triplicate measurement runs.

First, diagram (a) is explained. The repeatability of the measurement is excellent at temperatures below $120°C$, but becomes worse at higher temperatures. The shift in heat capacity at about $100°C$ is due to the glass transition of the material in this range. When approaching the glass transition temperature, the molecules successively gain mobility, and therefore more degrees of freedom for thermal motion are available. This causes a gradual increase of the heat capacity.

The thermal conductivity is in the range of $0.15\,W/mK$, which is comparable with other amorphous polymers like polystyrene. The error bars can hardly be seen, thus the repeatability of the measurement is excellent. The onset of flow of the thick specimen occurs at temperatures above $120°C$, which, as mentioned, marks the upper measurement limit of thermal conductivity using this technique. The thermal conductivity slightly increases with temperature, until the glass transtion temperature (T_g) is approached, where it drops marginally. This drop at T_g is also reported for other amorphous polymers in literature [114, 115].

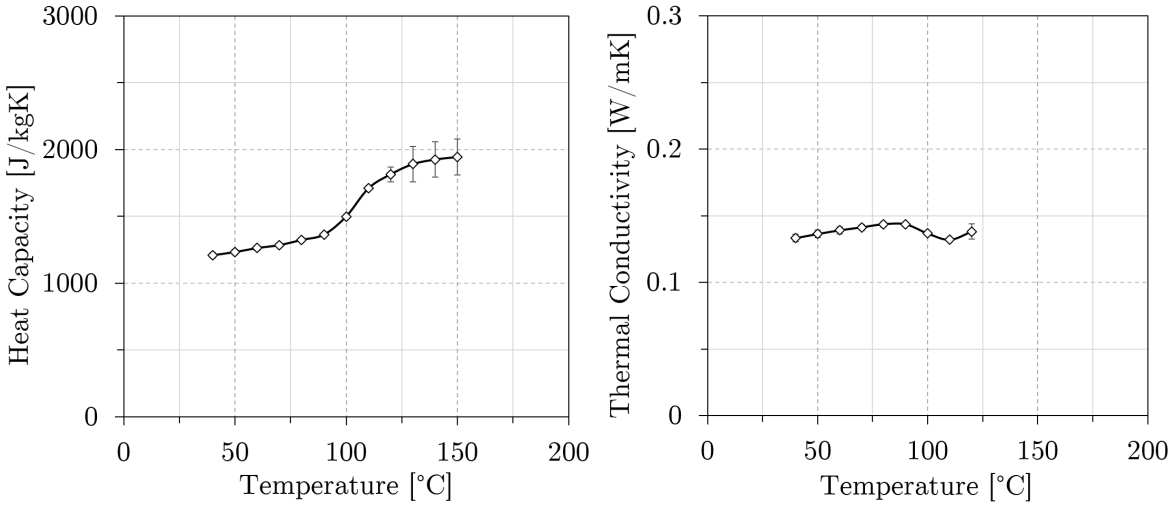

(a) Quasi-Isothermal Heat Capacity (b) Thermal Conductivity

Figure 66 : Quasi-isothermal heat capacity and thermal conductivity vs. temperature of Kollidon® VA64

Soluplus®

Figure 67 depicts the results of (a) the quasi isothermal heat capacity- and (b) the thermal conductivity measurement of Soluplus®. Also in this case, the repeatability

of both measurements is good. The upper measurement limit of thermal conductivity is 120°C. In the range of glass transition around 70°C the slope of the heat capacity curve reaches its maximum, but no pronounced discontinuity of c_p is observed, like for Kollidon® VA64. The thermal conductivity is of similar magnitude than Kollidon® VA64 and slightly increases with increasing temperature.

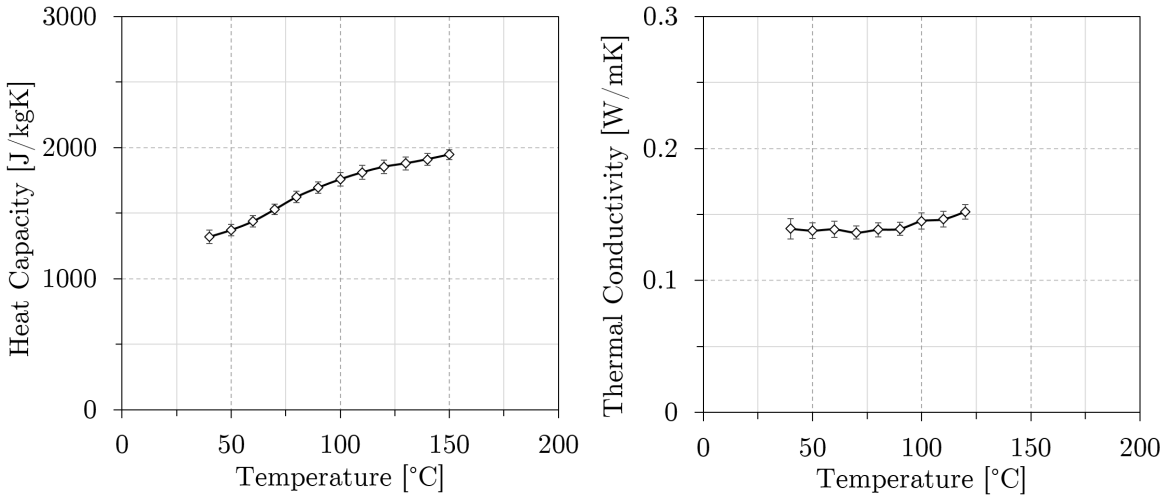

(a) Quasi-Isothermal Heat Capacity (b) Thermal Conductivity

Figure 67 : Quasi-isothermal heat capacity and thermal conductivity vs. temperature of Soluplus®

Eudragit® E

Figure 68 depicts the results of (a) the quasi isothermal heat capacity- and (b) the thermal conductivity measurement of Eudragit® E. The error bars are narrow, indicating a good repeatability of the measurement. The upper measurement temperature limit of thermal conductivity is relatively low, namely 90°C.

The discontinuity of heat capacity occurs at a slightly lower temperature as one would expect from the measured glass transition temperature (47°C). Above 50°C the heat capacity depends in good approximation linearly on temperature.

The thermal conductivity is marginally higher compared to Kollidon® VA64 and Soluplus®. In contrast to the other polymers, Eudragit® E interestingly exhibits a maximum of thermal conductivity near T_g.

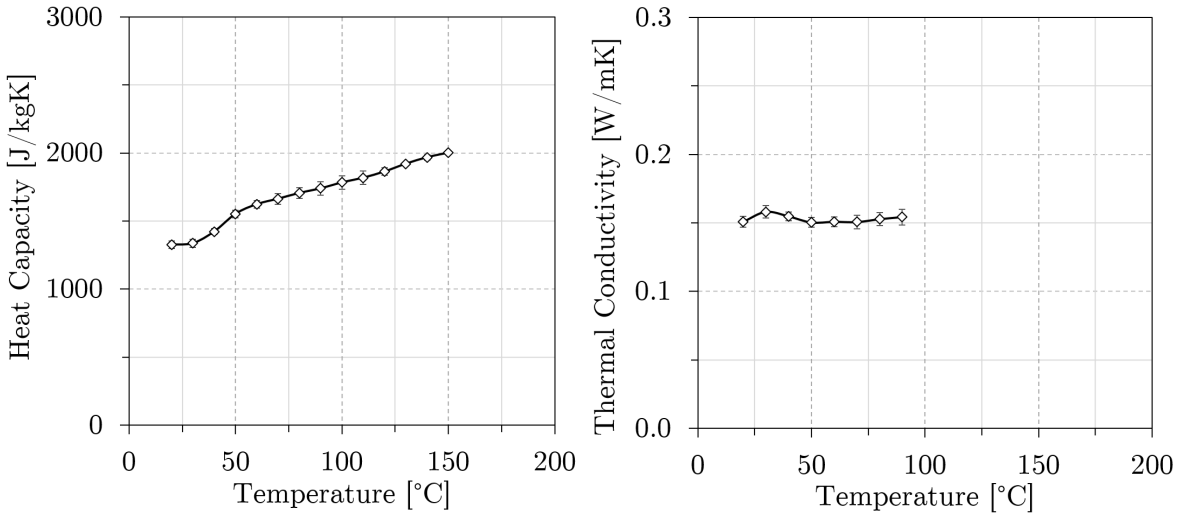

(a) Quasi-Isothermal Heat Capacity (b) Thermal Conductivity

Figure 68 : Quasi-isothermal heat capacity and thermal conductivity vs. temperature of Eudragit® E

HPMCAS-LF

Figure 69 depicts the results of (a) the quasi isothermal heat capacity- and (b) the thermal conductivity measurement of HPMCAS-LF. A discontinuity due to glass transition is visible in the heat capacity curve. At low temperatures, the thermal conductivity stays constant , then it drops at T_g, and subsequently it rises to a higher level at temperatures higher than T_g. The large error bars indicate a relatively poor repeatability of the measurement. For this polymer, there is no upper temperature limit for the thermal conductivity measurement, as it does not flow if no external force is acting. Thus, the thickness of the thick specimen does not significantly change within the whole temperature range.

However, the magnitude of standard deviation indicated by the width of the error bars is almost equal for all temperatures, indicating a systematic error to be the cause of the deviations. Most likely this is caused by a irreproducible thermal contact between the HPMCAS-LF sample and the pan. As already mentioned, cellulose ethers like HPMC and their derivatives do will not flow spontaneously, if no external force is applied. Therefore, the polymer cannot wet the bottom surface of the pan. It is likely that the non-reproducible thermal contact between sample and pan is the cause for the observed deviations. If this presumption is true, one could improve thermal contact by application of a small drop of silicone oil between pan surface and sample, like it was suggested in literature [105].

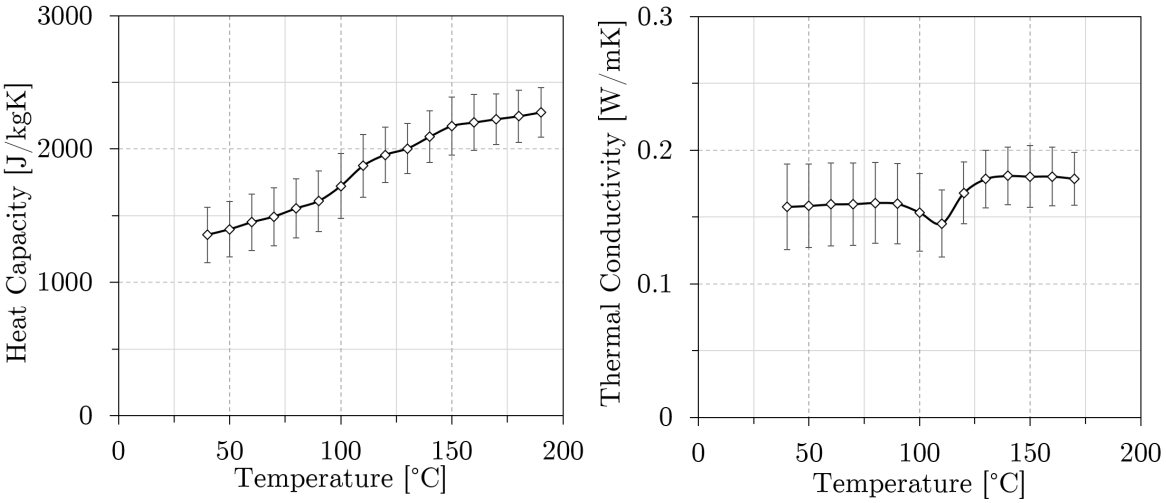

(a) Quasi-Isothermal Heat Capacity (b) Thermal Conductivity

Figure 69 : Quasi-isothermal heat capacity and thermal conductivity vs. temperature of HPMCAS-LF

HPMC Affinisol® 100 LV

Figure 69 the results of (a) the quasi isothermal heat capacity- and (b) the thermal conductivity measurement of HPMC Affinisol® 100 LV. No pronounced discontinuity in heat capacity due to glass transition is observed. The thermal conductivity is significantly higher than for the other investigated polymers, and shows a successively decreasing trend at temperatures above the $120°C$, i.e. above its glass transition temperature.

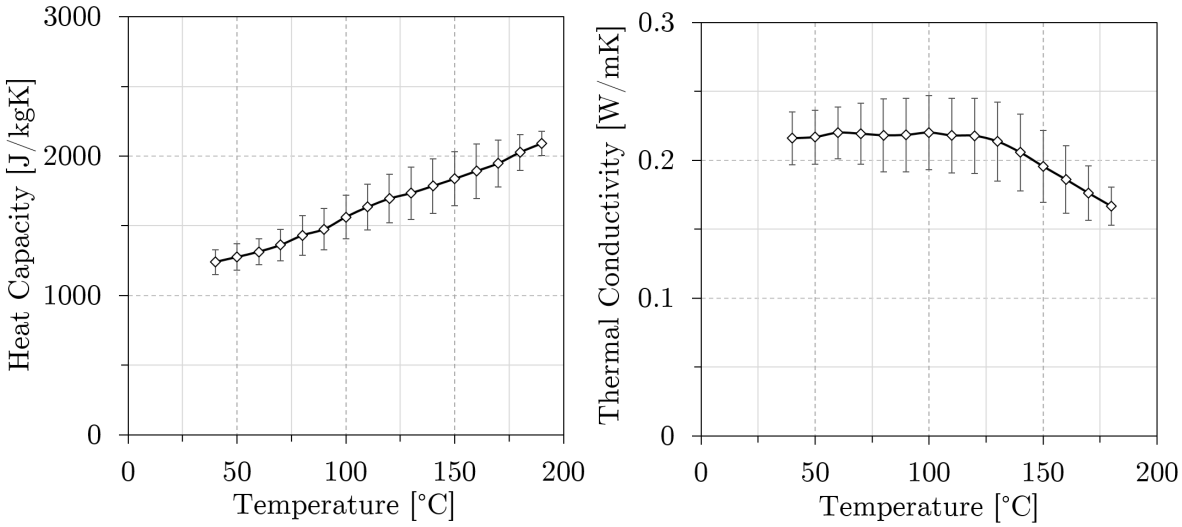

(a) Quasi-Isothermal Heat Capacity (b) Thermal Conductivity

Figure 70 : Quasi-isothermal heat capacity and thermal conductivity vs. temperature of HPMC Affinisol® 100LV

Comparison of Pure Polymers

In figure 71 a comparison of the quasi-isothermal heat capacity as a function of temperature of all investigated polymers is depicted. All polymers exhibit a distinctively

different dependence of heat capacity on temperature, especially below their glass transition temperatures. Above their respective glass transition temperatures, the difference in heat capacity for the non-cellulosic polymers (Eudragit® E, Soluplus®, Kollidon® VA64) becomes much smaller than it is at low temperatures.

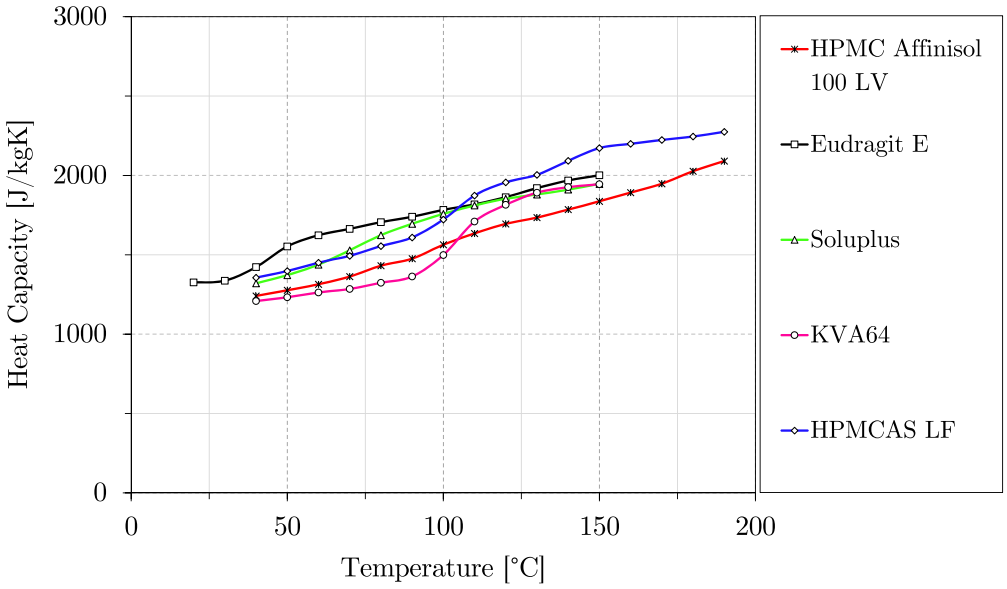

Figure 71 : Quasi-isothermal heat capacity comparison for all investigated neat polymers

In figure 71 a comparison of the thermal conductivity as a function of temperature of all investigated pharmaceutical polymers is shown. Soluplus® and Kollidon® VA64 are the worst thermal conductors, followed by Eudragit® E which conducts heat marginally better. The cellulosic polymers (HPMC Affinisol® 100 LV and HPMCAS-LF) are better conductors. Below its glass transtion, HPMCAS-LF is as thermally insulating as Eudragit® E, but above T_g it increases slightly. HPMC Affinisol® 100 LV is a significantly better thermal conductor compared to the other polymers.

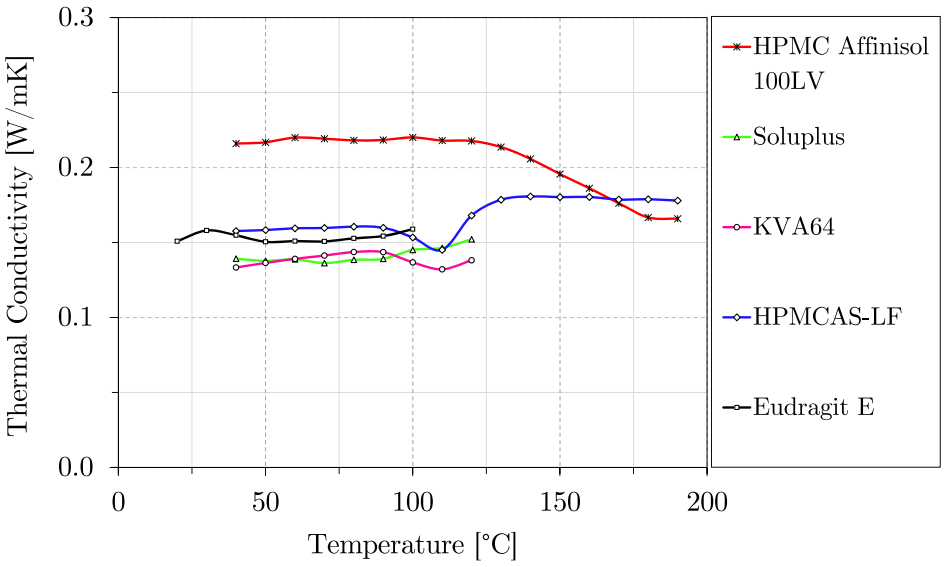

Figure 72 : Thermal conductivity comparison for all investigated neat polymers

Influence of API Loading

The influence of API loading on quasi isothermal heat capacity can be studied by comparing the measurements of two API/polymer formulations with the results obtained with the pure polymers. In figure 73 the results for the formulation of Soluplus® with 20% ibuprofen are compared with pure Soluplus®.

At first glance, one could conclude that addition of the API increases the heat capacity of Soluplus®. However, the strong plasticizing effect of the API significantly lowers the glass transition temperature of the neat polymer, which causes a shift of the heat capacity curve to the left along the temperature axis. The measurement uncertainty (i.e. the standard deviation) is significantly larger for the API-loaded system.

The thermal conductivity of the API loaded system is almost equivalent to the pure polymer, however due to the lower viscosity the upper measurement limit is $30°C$ lower. The standard deviation of the API loaded material is high compared to the neat polymer, perhaps due to variation in API dispersion in the sample. An influence of API loading on thermal conductivity can therefore not be found, because the standard deviation of the measurement is higher than the measured differences between the materials.

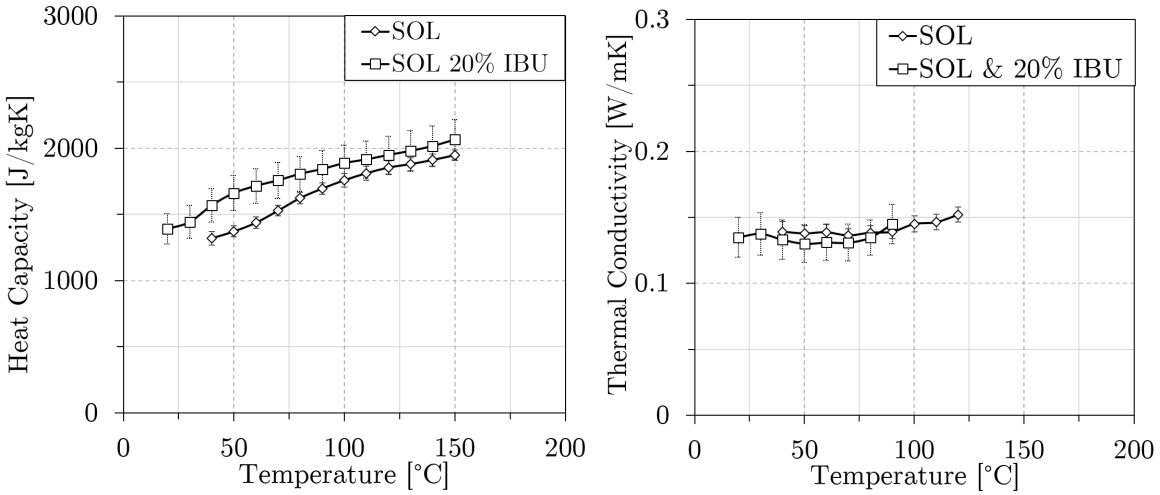

(a) Quasi-Isothermal Heat Capacity (b) Thermal Conductivity

Figure 73 : Quasi-isothermal heat capacity and thermal conductivity vs. temperature of the Soluplus® (SOL) and ibuprofen (IBU) (80:20) formulation and comparison with pure Soluplus®

Basically the same can be stated for the comparison of pure Kollidon® VA64 and a formulation of the same polymer loaded with 15% itraconazole (shown in figure 74).

Again, the data of the API loaded system exhibits a higher standard deviation. Despite addition of API, the upper measurement temperature limit of thermal conductivity measurement is not lowered in this case, compared to the neat polymer.

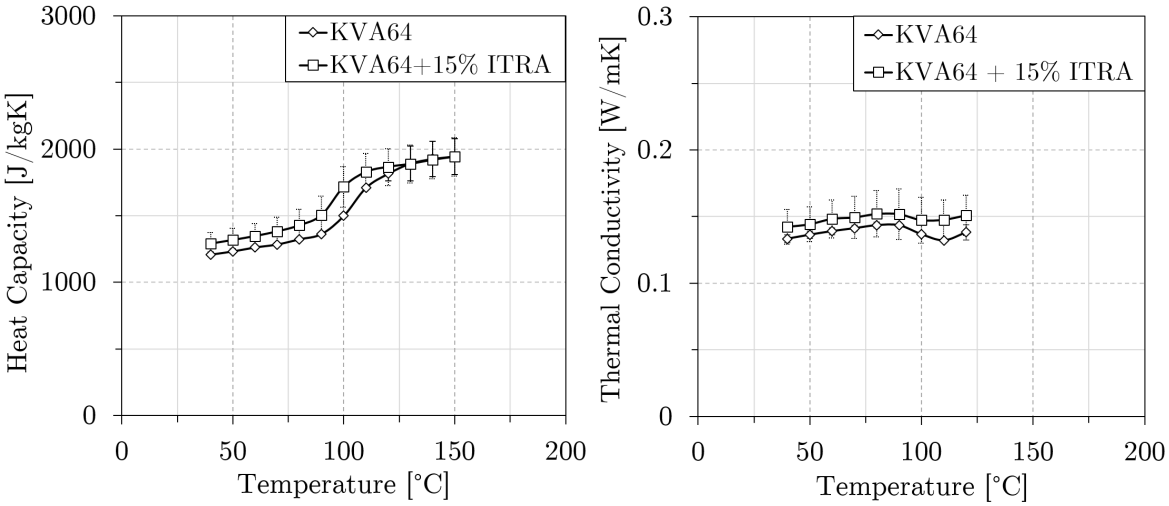

(a) Quasi-Isothermal Heat Capacity (b) Thermal Conductivity

Figure 74 : Quasi-isothermal heat capacity and thermal conductivity vs. temperature of the Kollidon® VA64 (KVA64) and itraconazole (ITRA) (85:15) formulation and comparison with pure Kollidon® VA64

Summary and Conclusion

The results of the thermal conductivity measurements are summarized in table 3, and the mean relative standard deviation (MRSD) is given for each material. As mentioned above, for many materials, the measurable temperature range of thermal conductivity was rather limited due to onset of flow of the thick specimen during the measurement. The values of thermal conductivity (at $50°C$) vary between 0.217 W/mK for HPMC 100 LV, and 0.130 W/mK for the Soluplus®/ibuprofen system. The reproducibility, characterized using a mean relative standard deviation (MRSD) is good for Soluplus® (±3.5%), Kollidon® VA64 (±3.5%) and Eudragit® E (±2.4%). The API loaded systems Soluplus® /Ibuprofen and Kollidon® VA64/itraconazole the uncertainty of the measurement is larger, the MRSD in both cases is in the order of ±10%. For HPMCAS-LF and HPMC Affinisol® 100 LV, as mentioned earlier, the bon-reproducible thermal contact between pan and sample introduces an error. Especially HPMCAS-LF showed large systematic deviations between the individual measurement runs.

For most polymers the thermal conductivity does not considerably change with temperature, however for Eudragit® E, Soluplus® Kollidon® VA64 and HPMCAS-LF, a slight drop of thermal conductivity is observed at the respective glass transition temperature, which was also reported for other amorphous polymers in literature. HPMC Affinisol® 100LV is the only polymer which stands out. It shows a considerably higher thermal conductivity than the other polymers. At temperatures above its glass transition temperature, the thermal conductivity of HPMC Affinisol® 100LV decreases successively. The thermal conductivitiy of the formulations Kollidon® VA64 and itraconazole (85:15) or Soluplus® and ibuprofen (80:20), respectively, does not significantly differ from the respective neat polymers. Thus, it seems that addition of API has little influence on thermal conductivity.

The acquired knowledge contributes to better understanding of the heat transfer behavior of pharmaceutical polymers. This is especially important for polymer processing

operations which involve transient heat transfer, e.g. injection molding, extrusion and many others. The developed method for measuring the thermal conductivity using the combination of modulated DSC and VCM DSC Tool is unprecedented, because it allows to screen the thermal conductivity of many different materials in a very short time. The VCM DSC Tool significantly shortens the time which would be needed to prepare appropriate specimens using conventional methods, e.g. injection molding. Furthermore, the method is universally applicable and is carried out using a commonly available instrument. Especially, data obtained using this method in the future could fill the missing link for unsolved problems in polymer processing or other fields.

Table 3 : Thermal Conductivity (κ) of all investigated polymers/formulations in W/mK

Material	$\kappa(50°C)$	$\kappa(100°C)$	$\kappa(150°C)$	MRSD [%]
Soluplus®	0.138	0.145	n/a	±3.5
Soluplus® - 20%ibuprofen	0.130	n/a	n/a	±10.8
Kollidon® VA64	0.136	0.137	n/a	±3.5
Kollidon® VA64 - 15%itraconazole	0.144	0.147	n/a	±10.1
Eudragit® E	0.150	0.153	n/a	±2.4
HPMCAS-LF	0.158	0.153	0.180	±15.2
HPMC Affinisol® 100 LV	0.217	0.220	0.196	±10.9

4.2 Dynamic Mechanical Thermal Analysis (DMTA)

In the following sections, DMTA thermograms of different pharmaceutical polymers are shown. The relevancy of characterizing these polymers using DMTA was explained in section 3.6. The dynamic mechanical measurements could be carried out without problems for most of the polymers.

Kollidon® VA64

For the Kollidon® VA64 specimens, cracks appeared in the very brittle polymer specimen every time after tightening the screws of the DMTA fixture, despite the fact that the quality of the samples themselves was flawless. This indicates that the brittleness of the material itself caused the problem. Thus, unfortunately it was not possible to characterize Kollidon® VA64 using this method.

Soluplus®

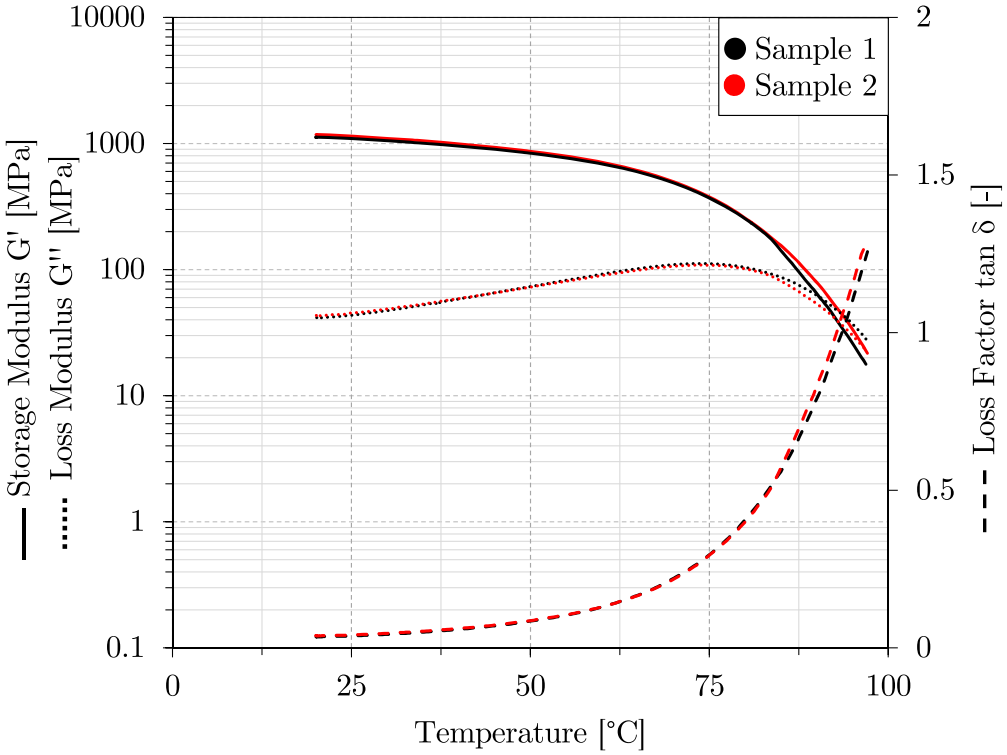

Figure 75 : DMTA thermogram of Soluplus®, tan δ is plotted on the secondary axis

Figure 75 depicts the DMTA thermogram of Soluplus®. The glass transition temperature (T_g), defined being the temperature where G'' passes a maximum, is detected at $71.3°C$. Thus the T_g obtained using DMTA is approximately $4°C$ lower than the T_g obtained using modulated DSC even though in both cases the heating rate is equal. The value of T_g strongly depends on the method of determination. The dynamic mechanical T_g and

the calorimetric T_g are therefore not equal. Despite the glass transition, no noticeable thermal events are observed.

The loss factor tan δ at room temperature ($20°C$) is 0.04, thus the material behaves predominantly elasic and only approximately 4% of the deformation energy is dissipated. The loss factor shows a steady increase with temperature, reflecting the transformation from solid-like to liquid-like behavior. The crossover point where tan $\delta = 1$, i.e. the point at which 50% of the applied deformation energy is dissipated, occurs at $92°C$.

The repeatability is excellent at temperatures below glass-transition. However, above glass transition the curves start to deviate slightly. The mean deviation of the G' between the two samples is about 6%, hence the repeatability of the measurement is, despite of the deviation at higher temperature, satisfactory.

Eudragit® E

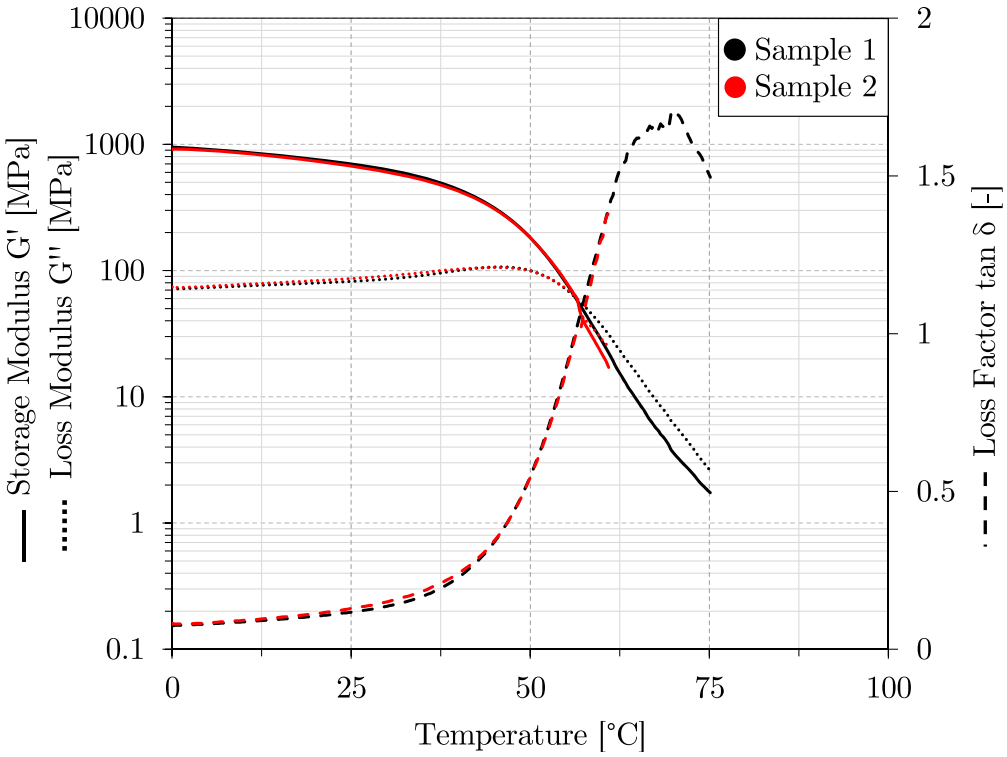

Figure 76 : DMTA thermogram of Eudragit® E. tan δ is plotted on the secondary axis

Figure 76 depicts the DMTA thermogram of Eudragit® E. No thermal events other than G'' passing a maximum (glass transition) can be seen in the temperature range of the measurement. The T_g is detected at $45.9°C$ which is close to the value obtained using modulated DSC and the VCM specimen ($T_{g,DSC} = 46.9°C$).

The loss factor tan δ at room temperature ($20°C$) has a value of approximately 0.1, which means that about 9% of the total deformation energy is dissipated. The crossover point where tan $\delta = 1$ occurs at $56°C$.

The repeatability is excellent at temperatures below glass-transition. The difference between the curves is roughly 1.5%. Above glass transition, a deviation of the curves

occurs and the difference increases to about 10%. The measurement of sample 2 stopped before reaching the final temperature. However, this run can serve as an indicator of the repeatability.

EVA Ateva® 1820

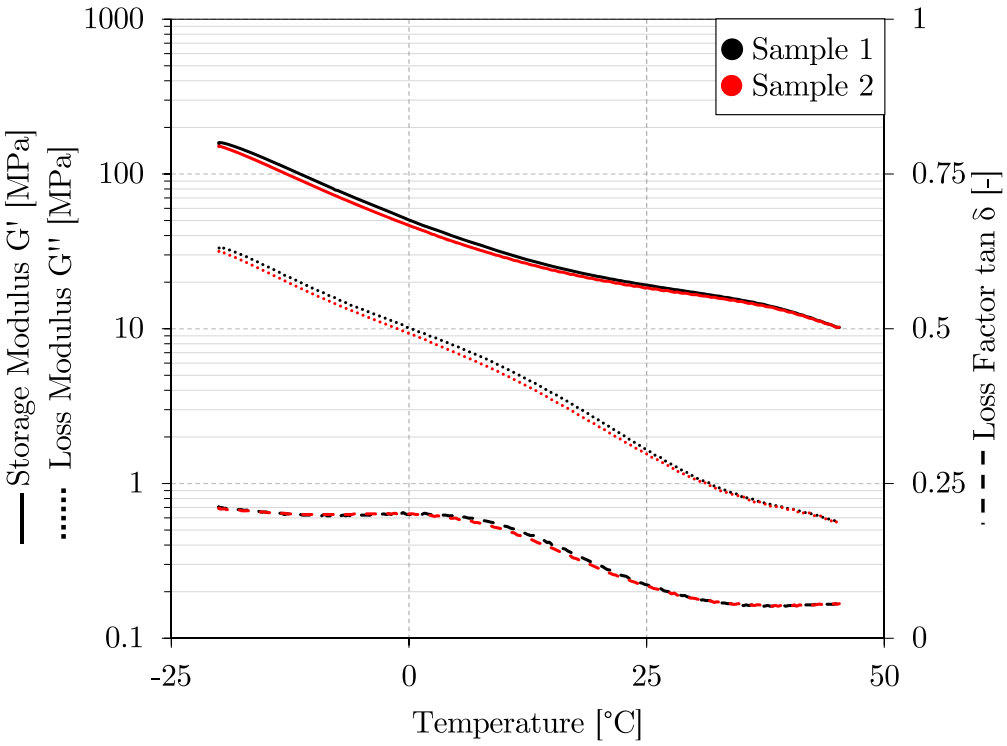

Figure 77 : DMTA thermogram of EVA 1820. tan δ is plotted on the secondary axis

Figure 77 depicts the DMTA thermogram of Ateva® 1820. The fraction of vinyl-acetate in the copolymer is 18%. The data shows that the repeatability of the measurement is reasonably good. Between the two samples, the mean difference of the measured storage modulus is approximately 5%.

In contrast to the amorphous polymers treated above, EVA is a semi-crystalline polymer which has a glass transition temperature that is below room temperature. The crystalline structures prevent the polymer from softening at temperatures between T_g and the melting temperature of the crystallites which lies at approximately $90°C$ for this polymer.

This is the reason, why this polymer displays a different viscoelastic behavior than the amorphous polymers discussed above. Unlike for amorphous polymers, the loss factor tan δ does not exhibit a steady rise with temperature. Instead it shows a plateau first, with a slight peak at approximately $5°C$ and then gradually drops, approaching a second plateau. The slight peak could be due to a thermal event with unknown cause. The observed curve for tan δ is a bit counter-intuitive because the viscous portion decreases, as the temperature is increased, i.e. the material behaves increasingly elastic dominated.

For the application of this polymer in intravaginal rings (IVR), e.g. the NuvaRing®, the viscoelastic moduli (G' and G'') and the loss factor ($\tan\delta$) at body temperature are of interest. At this particular temperature ($37°C$) the storage modulus is $14.5\,MPa$ and the loss modulus is $0.7\,MPa$, which means that the loss factor is equal to 0.05. The material behavior can therefore be classified as elastic dominated in this case. Only about 5% of deformational energy is dissipated due to the viscous portion of the material.

EVA Greenflex® ML60

Figure 77 depicts the DMTA thermogram of EVA Greenflex® ML60. The fraction of vinyl-acetate in the copolymer is 28%, which is 10% more than for Ateva® 1820. The repeatability of the runs is quite satisfactory. At low temperatures the difference between both runs is approximately 3% and it becomes smaller as the temperature is increased.

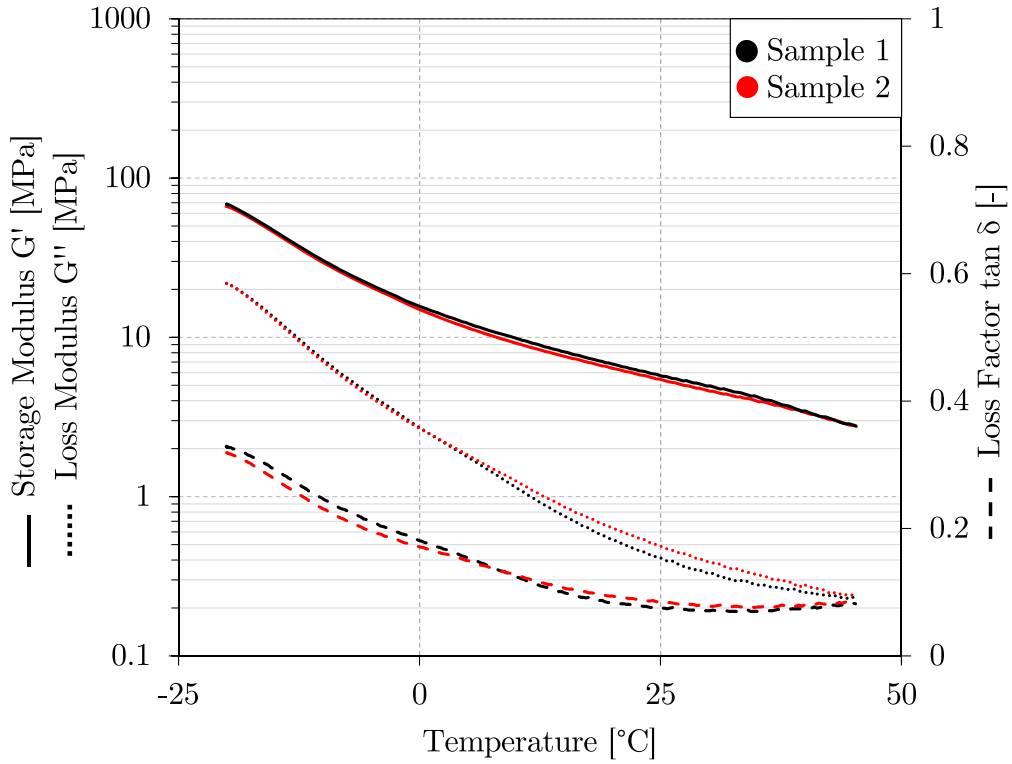

Figure 78 : DMTA thermogram of EVA Greenflex® ML60. tan δ is plotted on the secondary axis

It is known that an increasing vinyl acetate content in EVA causes a decreasing degree of crystallinity [116]. This causes the lower storage and loss modulus and the different progression of the tan δ curves of Greenflex® ML60 compared to the more crystalline type Ateva® 1820.

Evathene® UE654-04

Figure 77 depicts the DMTA thermogram of Evathene® UE654-04. This grade has a vinyl acetate fraction of 33%. The repeatability at higher temperatures is relatively poor

compared to the other EVA types as can be seen from the curves which are drifting apart at higher temperatures. Evathene® UE654-04 exhibits almost the same behavior as EVA Greenflex® ML60, despite its higher vinyl acetate fraction. Presumably, there is an upper threshold at which further increasing the vinyl-acetate fraction of the copolymer does not cause a change in crystallinity. This presumption is supported by research results which can be found in literature [116].

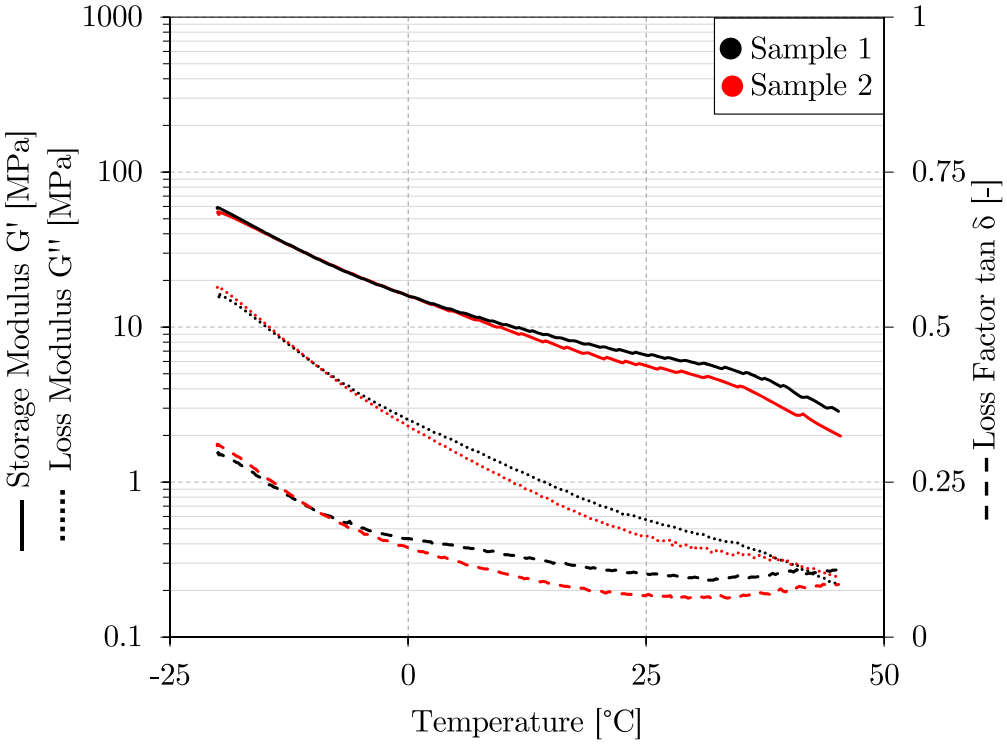

Figure 79 : DMTA thermogram of Evathene UE654-04. tan δ is plotted on the secondary axis

Comparison

To provide a quick overview, in figure 80 a comparison of the DMTA data of Greenflex® ML60 and Ateva® 1820 is depicted. This graphically summarizes the statements made in the sections above.

The viscoelastic parameters of the different EVA types at body temperature are summarized in table 4. As already mentioned Greenflex® ML60 and Evathene® UE654-04 are very similar. Ateva® 1820 as a matrix material for the intravaginal rings will yield more stiff product than the other two EVAs due to a almost four times higher storage modulus at body temperature. tan δ of all EVA types is rather low, but Greenflex® ML60 and Evathene® UE654-04 have a marginally higher viscous component than Ateva® 1820.

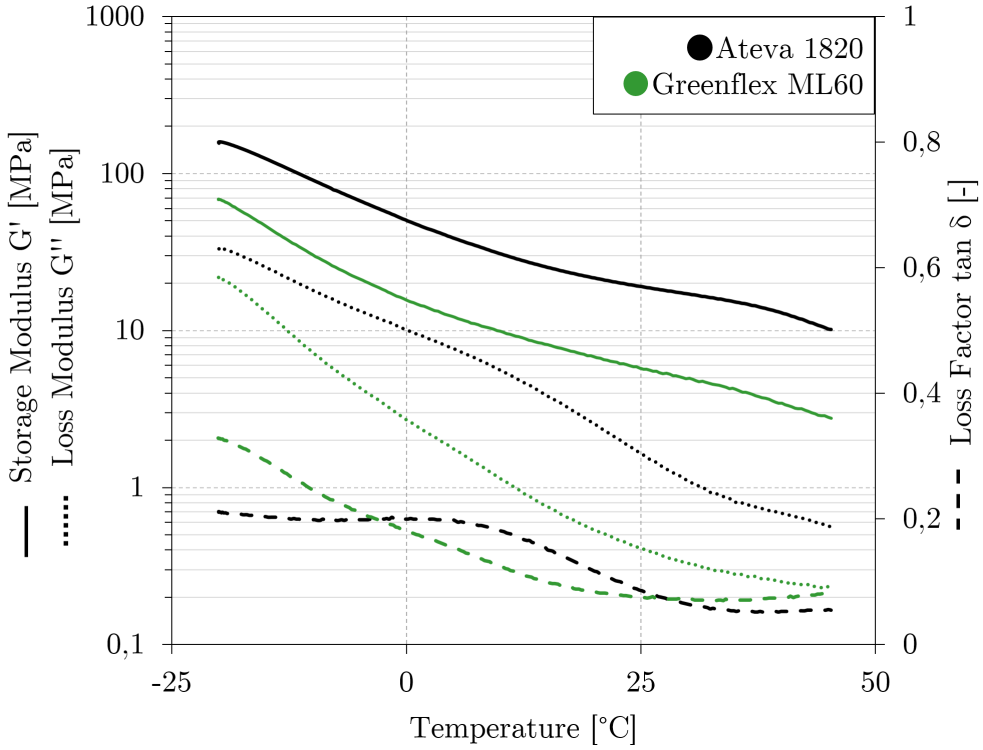

Figure 80 : Comparison of EVA Greenflex® ML60 (green curve) and EVA Ateva® 1820 (black curve). tan δ is plotted on the secondary axis. Evathene® UE654-04 is not shown for reasons of clarity because it approximately overlaps with Greenflex® ML60

Summary and Conclusion

As can be seen in the data presented above, DMTA measurements carried out with specimens prepared using the VCM Bar Tool yields repeatable results. It is possible to obtain accurate information about the viscoelastic moduli (G' and G'') and loss factors of pharmaceutical polymers, bridging the gap from shear rheology of polymer melts to glassy and rubbery materials. It is possible to detect significant differences regarding these properties.

The glass transition temperatures (T_g) of Soluplus® and Eudragit® E could successfully be determined using DMTA. Compared to the values obtained by DSC, the T_g measured by DMTA is slightly lower for both mentioned polymers. Due to the narrow temperature range which was investigated, no secondary relaxations were observed.

For the different EVA types, considerable differences could be found. Ateva 1820, with a vinyl-acetate fraction of 18%, exhibited a different thermo-mechanical behavior and a three times higher storage modulus as the two other grades. Likely, this is caused by a higher degree of crystallinity, due to the comparatively low vinyl-acetate fraction, which yields a stiffer polymer. Furtermore, the loss factor $\tan\delta$ is slightly lower. Greenflex ML60 and Evathene UE654-04 exhibit very similar moduli in DMTA, despite the vinyl acetate fraction of the former and the latter are 28 or 33%, respectively. Obviously, there is an upper threshold of vinyl-acetate content at which the degree of crystallinity is not affected by the vinyl acetate content. Using the information obtained from DMTA tests, for example it could be possible to correlate the viscoelastic moduli with wearing comfort properties of intravaginal rings (IVR) like the NuvaRing®.

Table 4 : Comparison of vinyl acetate (VA) fractions and viscoelastic parameters of the investigated EVA types at body temperature (mean values of two runs)

Material	VA [%]	$G'_{(37°C)}$ [MPa]	$G''_{(37°C)}$ [MPa]	$\tan(\delta)_{(37°C)}$ [-]
Ateva® 1820	18	14.5	0.7	0.05
Greenflex® ML60	28	3.8	0.3	0.08
Evathene® UE654-04	33	4	0.3	0.08

The possibility to produce rectangular bar specimens of polymeric formulations might yield valuable information for formulation- and process development in the future. In pharmaceutical processes where the mechanical behavior of polymers that are undergoing vitrification during processing or that are processed in glassy state is of interest, DMTA measurements in combination with the VCM Bar Tool might contribute to a better process understanding. In future work, the VCM Bar Tool and DMTA measurements can be applied to study the molecular mobility of polymers and polymeric formulations in a wide range of temperatures. As mentioned in the theory section, sub-glass relaxations ($\beta-, \gamma-$ transitions) which are hard or impossible to detect using DSC can be more easily detected by DMTA. This might help to improve the investigation of stability of amorphous solid dispersions (ASDs), for example. Moreover, as mentioned in the theory section, DMTA testing might be used to study polymer/API miscibility and crystallization rates of ASDs. These possibilities of future research are very relevant in the field of pharmaceutical science and engineering and underline the tremendous research potential that is enabled by the VCM Bar Tool.

4.3 Rheometry

4.3.1 Shear Rheology

For comparison purposes, shear-rheological data of the pure polymers were taken from previous work[47].

System Soluplus® - Ibuprofen

In figure 81 frequency sweep data and the corresponding Carreau-Yasuda fits of pure Soluplus® and the formulation of Soluplus® with 20% ibuprofen at three different temperatures are shown. Both neat polymer and the formulation exhibit decreasing viscosity with increasing temperature and the typical shear-thinning behavior of polymer melts. At $120°C$ the viscosity of the neat polymer would be too high for processing (abobe $10^5\ Pas$), however, ibuprofen has a tremendous plasticizing effect so the processing temperature window is shifted to lower temperatures. Thus, no comparison data of neat Soluplus® at $120°C$ is available. The zero-shear viscosity is reduced due to addition of the API by a factor between 37 at $160°C$ and almost 50 at $140°C$. At $160°C$ the formulation almost exhibits Newtonian behavior. The zero-shear plateau is relatively wide and the slope of the terminal region at high frequencies is relatively flat. Generally, the parameter n describing the slope of the power-law region, declines with higher temperature, as the behavior in the measured frequency range becomes increasingly Newtonian. The API/polymer formulation at $120°C$ has almost the same zero shear viscosity as the neat polymer at $160°C$, but the shear-thinning behavior is much more pronounced for the former. Thus, it is not sufficient to describe the plasticizing effect of APIs on pharmaceutical polymers using a single viscosity value, like the often used melt-flow index (MFI), as the processing behavior of both will be significantly different. That the processing temperature window is lowered by addition of API is especially beneficial if thermally sensitive APIs are used. Thus, rheological testing of API/polymer formulations can help to rationally select the optimal HME processing temperature for each formulation [95].

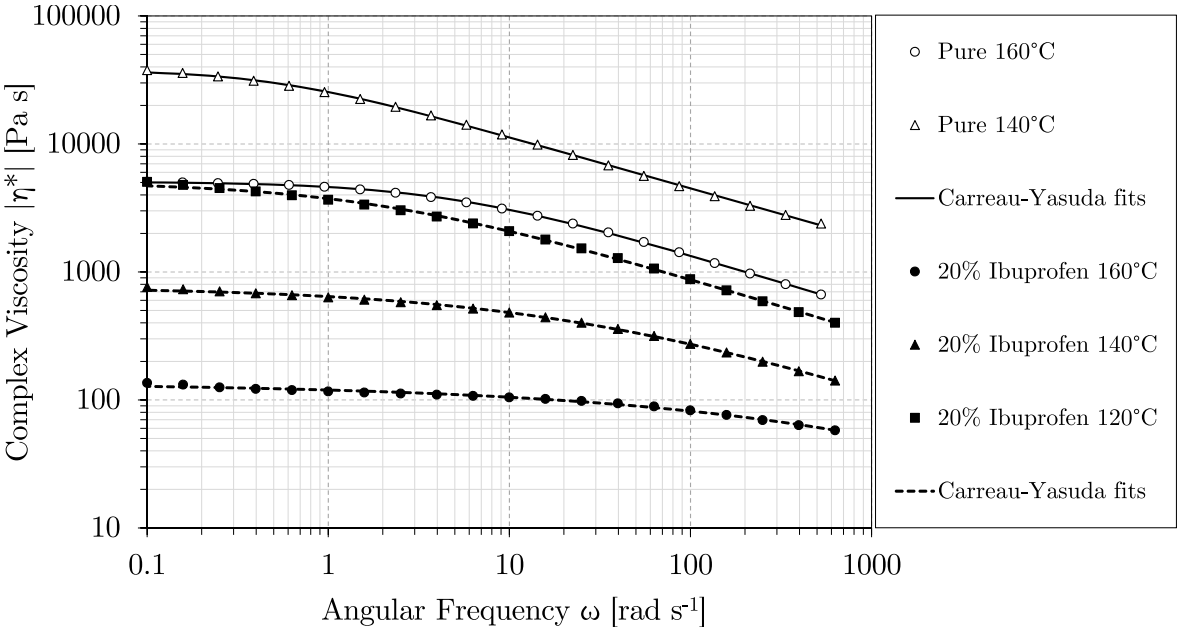

Figure 81 : Comparison of flow curves of pure Soluplus® and the formulation of Soluplus® with 20% ibuprofen

System Kollidon® VA64-Itraconazole

In figure 82 frequency sweep data and the corresponding Carreau-Yasuda fits of pure Kollidon® VA64 and the formulation of Kollidon® VA64 with 15% itraconazole at three different temperatures are shown. Also in this case, decreasing viscosity with increasing temperature and the typical shear-thinning behavior of polymer melts. The Carreau-Yasuda fits represent the measured data very well. The plasticizing effect of the API itraconazole on Kollidon® VA64 is pronounced. At the same temperature, the zero-shear viscosity decreases approximately by a factor of four due to addition of the API. Also all other rheological parameters are affected. The slope of the power law region, characterized by the power-law exponent n is noticeably higher for the API-loaded formulation than for the neat polymer at $160°C$ and $150°C$. However, at $170°C$ the power law-region of the API-loaded formulation is flatter compared to the neat polymer. The terminal relaxation times (obtained using Carreau-Yasuda) are reduced by approximately a factor of four. Therefore, not only the viscosity, but also the relaxation times are significantly reduced, meaning that the influence of viscoelastic effects on flow behavior becomes significant at much lower temperatures compared to the neat polymer.

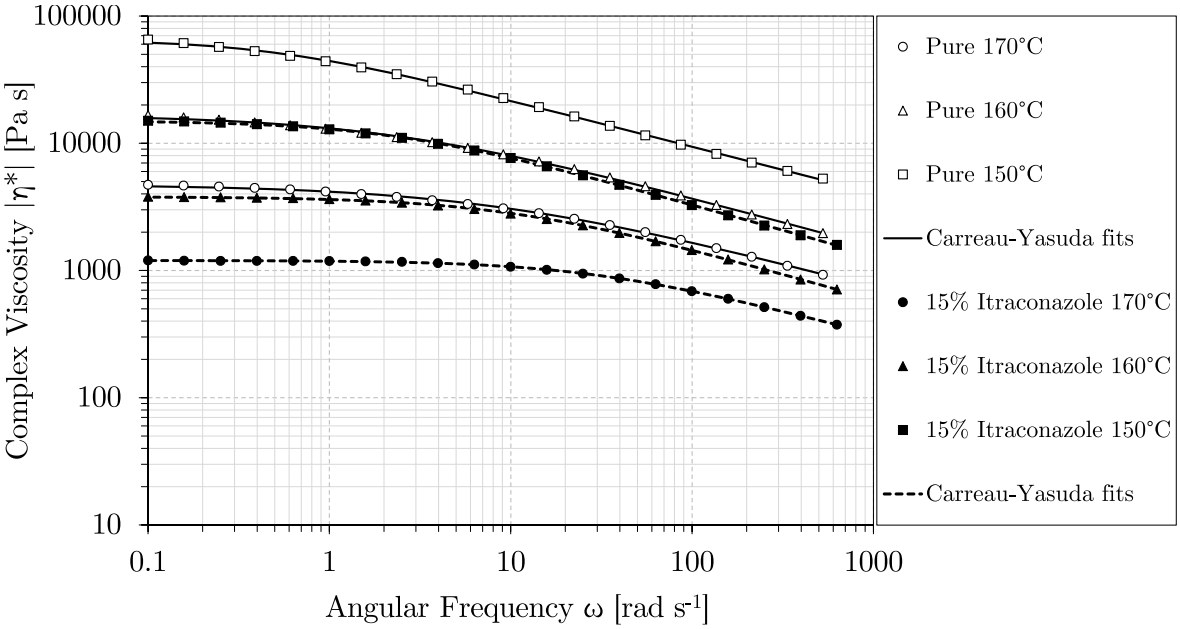

Figure 82 : Comparison of flow curves of pure Kollidon® VA64 and the formulation of Kollidon® VA64 with 15% itraconazole

Summary and Conclusion

The melt rheological characterization of two polymeric formulations could be carried out with a high degree of reproduciblity. The Carreau-Yasuda model was found to represent the data of all runs well. Equally to neat polymers, also the API loaded samples exhibit strongly shear-thinning behavior. The calculated Carreau-Yasuda fit parameters of all measured data and the corresponding mean relative standard deviations (MRSD) are summarized in table 5. The data of the neat polymers was, as already mentioned, taken from previous work [47]. The measurement reproducibility of the API-loaded systems (characterized by the MRSD values given in the table) is comparable to the neat polymers. The reason that Soluplus®/ibuprofen has a higher standard deviation is probably due to the very low viscosity, which causes the polymer to slightly flow out of the gap during measurement. The addition of API plasticizes the polymers and influences the shear rheological behavior in a complex manner. The relationship between viscosity and shear rate changes, e.g. the slope in the power-law region is influenced by addition of API. The relaxation time is significantly lower for API loaded polymers, which means that viscoelastic effects have less influence on the flow.

Table 5 : Carreau-Yasuda Fit Parameters of the rheological measurements

Material	η_0 [Pa s]	λ [s]	n [-]	a [-]	MRSD [%]
Soluplus® 160°C	5070	0.209	0.569	0.938	2.8
Soluplus® 140°C	37766	1.992	0.598	1.218	2.3
Soluplus® 120°C	n/a	n/a	n/a	n/a	n/a
Soluplus® - 20%IBU 160°C	136	3.509e-5	0.003	0.312	6.4
Soluplus® - 20%IBU 140°C	764	0.035	0.518	0.491	6.2
Soluplus® - 20%IBU 120°C	5053	0.542	0.567	0.715	6.6
Kollidon® VA64 170°C	4723	0.119	0.610	0.664	1.5
Kollidon® VA64 160°C	16650	0.443	0.617	0.721	1.7
Kollidon® VA64 150°C	65275	2.024	0.635	1.079	1.4
Kollidon® VA64 - 15%ITRA 170°C	1200	0.034	0.627	0.985	2.6
Kollidon® VA64 - 15%ITRA 160°C	3800	0.095	0.592	0.909	1.7
Kollidon® VA64 - 15%ITRA 150°C	15033	0.432	0.598	0.974	0.8

4.3.2 Extensional Rheology

Soluplus®

All extensional rheology measurements were performed at 140°C. In figure 83 shows two films of a Soluplus® melt after the extension experiment. The homogeneous appearance of the melt is remarkable. No inclusions or air bubbles can be observed. Thus, the sample preparation using the VCM Bar Tool seems to be well suited for this extensional-rheological technique as well. In the left picture, a extensional strain rate $\dot{\epsilon_H}$ of 0.1 s^{-1} was applied, while it were 25 s^{-1}in the right case. When slowly deformed, the polymer chains have time to relax, and exhibit viscous flow and no rupture occurs. If deformed rapidly, like in the right case, the chains do not manage to relax during deformation, and the material exhibits a rubber-like failure.

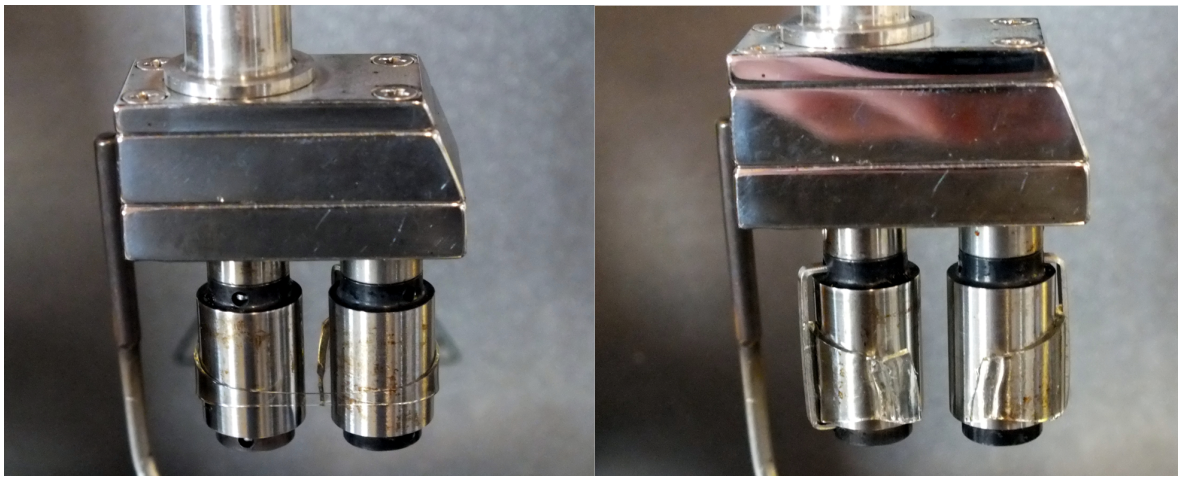

Figure 83 : Melt films of Soluplus® after being stretched using the SER fixture at an extensional strain rate of $0.1s^{-1}$ (left) and $25s^{-1}$ (right)

The shear-rheological data of Soluplus® at this temperature was used to calculate the so-called linear envelope curve. The envelope is called linear, because the experiment to determine it is carried out within the linear viscoelastic (LVE) range. The linear envelope represents is the extensional viscosity the material would exhibit in this experiment if it would satisfy the roule of Trouton, that the extensional viscosity η_E is equal to three times the shear viscosity η_S, in uniaxial extension. The linear envelope in this case can be obtained via plotting $3\eta_S$ versus $1/\omega$. Non-branched polymers like *linear* low density polyethylene (LLDPE) usually satisfy the Trouton rule, independent on the strain rate, thus at any rate the extensional viscosity coincides with the linear envelope. In contrast, branched polymers, e.g. low density polyethylene, exhibit a strongly increasing extensional viscosity at higher strain rates. This effect is called *strain hardening* and is a nonlinear viscoelastic effect.

The results of a multitude of runs at different extensional strain rates and the linear envelope of Soluplus® at a constant temperature of $140°C$ are depicted in 84. Repeated measurements at the individual strain rates yielded overlapping curves, thus the measurement was repeatable (not shown). At low strain rates, the measured extensional viscosity curve coincides with the linear envelope. This means that the Trouton rule is satisfied at low strain rates, and the measurement yields the correct viscosity values. At an extensional strain rate of $0.5s^{-1}$ strain hardening begins to occur and the curves start deviate from the linear envelope. The behavior is therefore similar to branched polymers like LDPE. Soluplus® exhibits the mentioned strain hardening effect, because it has a branched structure due to its grafted side chains. This non-linear rheological behavior of Soluplus® in extension could fill the missing link to understand possible unknown phenomena in processing operations involving extensional flow components, e.g. injection molding, extrusion or melt electrospinning of Soluplus® or even lead to new techniques which exploit this behavior.

According to the shear-rheological data the relaxation time parameter λ at $140°C$ for Soluplus® has a value of approximately $2s$. Therefore, the Deborah number becomes equal to one if the deformation timescale is of the same order. The nonlinear strain hardening effect interestingly starts becoming pronounced at an extensional strain rate of $0.5s^{-1}$, thus coincides with $De \cong 1$ obtained using the Carreau-Yasuda relaxation

time parameter.

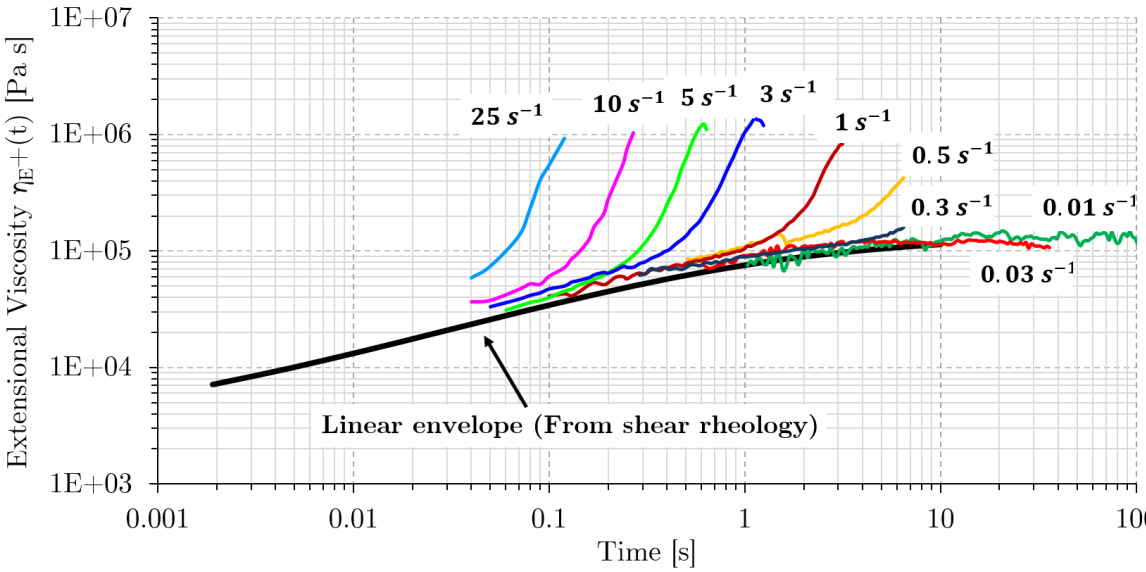

Figure 84 : Tensile stress growth curves of Soluplus® at 140°C , revealing its strain-hardening behavior

Summary and Conclusion

It was found that Soluplus® exhibits strain-hardening behavior in uniaxial extensional flow experiments, similarly to branched polymers, possibly due to its grafted side chains. This could fill the missing link to understand possible unknown phenomena in processing operations involving extensional flow components, e.g. injection molding, extrusion or melt electrospinning of Soluplus® or even lead to new techniques which exploit this behavior.

5 Summary and Conclusion

The preparation of appropriate specimens of pharmaceutical polymers starting from powders can proof to be a challenge for certain material characterization methods. State of the art methods are often tedious, time and material consuming and not suitable for sensitive pharmaceutical materials. To improve specimen preparation for differential scanning calorimetry (DSC) and dynamic mechanical analysis (DMTA), two novel VCM tools were designed and successfully manufactured, which allowed to produce homogeneously fused specimens in a very short time as well as with minimal material consumption. Thus, by using these specimens, better results in subsequent analyses are to be expected. This presumption was evaluated with a series of DSC and DMTA tests using a variety of polymers relevant for pharmaceutical applications.

The DSC measurements showed that the sensitivity of the measurement is in many cases improved by using specimens which were prepared utilizing the newly developed VCM DSC Tool, compared to the traditional approach of heating the powder in the DSC pans before the measurement. This is due to a more effective heat transfer between the sample and the pan. For many of the investigated pharmaceutical polymers, a lower glass transition temperature (T_g) is detected for samples prepared using the VCM approach. Furthermore, no disturbances (due to incomplete particle fusion or gas inclusions) influenced the measurements, which allowed for better detection of weak thermal events (e.g. glass transitions).

The ability to prepare VCM specimens with variable thickness, allowed the direct determination of the thermal conductivity of pharmaceutical polymers and formulations using a special modulated DSC method. Thus, the thermal conductivity of a variety of relevant pharmaceutical polymers was determined by using this method as a function of temperature. The measured values of thermal conductivity (at $50°C$) varied between 0.217 W/mK for HPMC Affinisol®100 LV, and 0.130 W/mK for the Soluplus®/Ibuprofen system. For most polymers the thermal conductivity did not considerably change with temperature; however for Eudragit®E, Soluplus®, Kollidon®VA64 and HPMCAS-LF, a slight drop of thermal conductivity was observed near the T_g of the polymers. HPMC Affinisol®100 LV is the only polymer which clearly exhibited a higher thermal conductivity than the other investigated polymers. The thermal conductivity of the investigated formulations Kollidon®VA64 and Itraconazole (85:15) as well as Soluplus®and Ibuprofen (85:15) did not differ significantly from the values of the neat polymers. Thus, it seems that an addition of API only has a low influence on thermal conductivity in this case. A previously developed MATLAB routine enabled the quick and unambiguous evaluation of the raw data, in order to obtain the thermal conductivity.

The acquired knowledge about thermal conductivity contributes to a better understanding of the heat transfer behavior of pharmaceutical polymers. This is especially important for polymer processing operations, which involve transient heat transfer, e.g. injection molding, extrusion and many others. The developed method for measuring

the thermal conductivity using a combination of a modulated DSC and VCM DSC tool is unprecedented, because it allows, as it was demonstrated, to screen the thermal conductivity of many different materials in a very short time with minimum material requirements (¡100mg). The VCM DSC tool significantly shortens the time ordinarily needed to prepare appropriate specimens using conventional methods, e.g. injection molding. Furthermore, the method is universally applicable and is carried out using a commonly available instrument. In the future the data about thermal conductivity obtained by this method could fill the missing link for unsolved problems in polymer processing, as well as other fields of research.

The ability to produce high-quality rectangular specimens (10x40x1mm) using the newly developed VCM Bar Tool has enabled to realize repeatable DMTA measurements of pharmaceutical polymers. It was possible to obtain accurate information about the viscoelastic moduli (G' and G") and the loss factors of pharmaceutical polymers, which helps to bridge the gap from shear rheology of polymer melts to glassy and rubbery materials. The glass transition temperatures (T_g) of Soluplus®and Eudragit®E could successfully be determined using DMTA. Compared to the values obtained by DSC, the T_g measured by DMTA is slightly lower for both mentioned polymers. The investigated EVA types differed in terms of their viscoelastic behavior. Ateva 1820, with a vinyl-acetate fraction of 18%, exhibited a higher storage modulus and a lower loss factor (tan δ) as Greenflex ML60 and Evathene UE654-04, due to its higher degree of crystallinity. Greenflex ML60 and Evathene UE654-04 showed very similar viscoelastic behavior, despite their differing vinyl acetate content. Using the information obtained from DMTA tests, could allow for a correlation to be found between the viscoelastic moduli and the wearing comfort properties of intravaginal rings (e.g. NuvaRing). The ability of rapid production of rectangular bar specimens of polymeric formulations for DMTA testing will yield valuable information for formulation- and process development in the future. Thus, the development of the VCM-bar-tool presents a significant research potential.

A shear rheological characterization of molten API/Polymer mixtures could be carried out with a similarly high degree of reproducibility, as was demonstrated in earlier work for neat polymers. The addition of API plasticizes the polymers and influences the shear rheological behavior in a complex manner. The relationship between viscosity and shear rate changes, e.g. the slope in the power-law region is influenced by addition of API. The relaxation times are significantly lowered, after an addition of API, as compared to pure polymers. Thus, the flow during processing is less influenced by viscoelastic effects. The obtained data represents an accurate data basis for simulation tasks. Furthermore, a better understanding of the effect of API on flow behavior was achieved.

The VCM Bar Tool also enabled a preparation of high quality specimens for extensional rheology using the Sentmanat Extensional Rheometer (SER) system. Using this technique, it was found that Soluplus®exhibits pronounced strain-hardening behavior in uniaxial extension. This is a typical effect, commonly observed for branched polymers like low-density polyethylene (LDPE). Soluplus®likely exhibits this behavior due to its structure, which comprises grafted side chains. This finding could fill the missing link to understand possible unknown phenomena in processing operations involving extensional flow components, e.g. injection molding, extrusion or melt electrospinning of Soluplus®; furthermore it could even lead to new techniques exploiting this effect.

In this work, the VCM method for specimen preparation was transferred to new fields of application. In particular, it was shown that the samples prepared using this approach can successfully be utilized for DSC, DMTA and extensional rheometry measurements. The bottleneck in pharmaceutical material characterization, which arises from the necessity to utilize tedious and time consuming conventional preparation methods, can effectively be overcome by these new VCM tools, which in turn lead to a streamlined workflow. Moreover, the comparatively very low material expense of the VCM preparation makes it especially suitable for the screening of formulations comprising expensive APIs.

List of Figures

List of Tables

Appendix

MATLAB Script for Thermal Conductivity Data Analysis

```
clear all
clc

%Evaluation MDSC Thermal Conductivity (ASTM Method)
%(C) 2016 - Alexander Troiss
%alex.troiss@gmail.com

%Load Data

duennmat=xlsread('thin.csv');
dickmat=xlsread('thick.csv');
saphirmat=xlsread('sapphire.csv');
blankmat=xlsread('blank.csv');

%DSC cell asymmetry correction using a blank sample


prompt = 'Please enter specimen name:  ';
name=input(prompt,'s');


%Netzsch Sapphire Standard Data Fit(CP [j/kgK] vs Temperature [C])
%Attention: Determined between 20C and 220C


cp_std=inline('0.000000000000035136657987452600.*x
    .^6-0.000000000018318165587909500000.*x.^5-0.000000006934926914355710000000.*x
    .^4+0.000011428268144681800000000000.*x.^3-0.006591829319096620000000000000.*x
    .^2+2.439461052693350000000000000000.*x+ 717.906861479233000000000000000000');


%Thermal Conductivity Calibration Factor(Version 28.1.2017)

D=inline('0.022229419');

%Define Experimental Parameters
%Specimen Thickness (thick sample)[mm]
prompt1 = 'Please enter thickness of thick specimen in mm:  ';
L=input(prompt1);
%Specimen diameter [mm]
prompt2 = 'Please enter diameter of thick specimen in mm:  ';
dia=input(prompt2);
%Oscillation Period (s) (ASTM = 80s)
period=80;

%Sampling Rate of Netzsch Modulated DSC: 2 Hz
samplingrate=2;
%Automatic Determination of further Parameters

%Thickness (thick sample)[mm]
mduenn=duennmat(1,2);
%Specimen mass (thin sample) [mg]
mdick=dickmat(1,2);
%Specimen mass (sapphire standard) [mg]
msaphir=saphirmat(1,2);
%angular frequency
omega=2*pi*(1/period);


%Define Data Range for Analysis
%(Last 10 min of modulated temperatur interval, according to ASTM)

anfang=1200;
ende=2400;
num=ende-anfang;
bereich=linspace(anfang,ende,num);


```

```
66
67
68  i=1;
69  n=1;
70  dim=length(duennmat);
71
72  while i<=dim
73
74      if isnan(duennmat(i,1))== 0
75
76        temp1(n,1)=duennmat(i,1);
77
78        n=n+1;
79
80      else
81
82     n=n;
83
84      end
85
86      i=i+1;
87
88
89  end
90
91  i=1;
92  n=1;
93  dim=length(dickmat);
94
95  while i<=dim
96
97      if (isnan(dickmat(i,1))== 0  && (dickmat(i,2)>=0))
98
99        temp2(n,1)=dickmat(i,1);
100
101       n=n+1;
102
103     else
104
105    n=n;
106
107     end
108
109     i=i+1;
110
111
112 end
113
114 i=12; %12 (twelve) is correct!
115 n=1;
116 dim=length(duennmat);
117
118 while i<=dim
119
120     if (isnan(duennmat(i,2))== 0) && (duennmat(i,2)>=0)
121
122       time1(n,1)=duennmat(i,2);
123
124       n=n+1;
125
126     else
127
128    n=n;
129
130     end
131
132     i=i+1;
133
134
135 end
136
137
138 i=12; %12 ist gewollt
```

```
139 n=1;
140 dim=length(dickmat);
141
142 while i<=dim
143
144     if isnan(dickmat(i,2))== 0
145
146       time2(n,1)=dickmat(i,2);
147
148       n=n+1;
149
150     else
151
152    n=n;
153
154     end
155
156     i=i+1;
157
158
159 end
160
161 dim1=length(duennmat);
162 dim2=length(dickmat);
163 dim3=length(saphirmat);
164 dim4=length(blankmat);
165
166 %Determine Number of DSC Segments
167
168 seg=duennmat(:,5);
169 segsap=saphirmat(:,5);
170 segblank=blankmat(:,5);
171 anz=max(seg);
172 anzsap=max(segsap);
173 anzblank=max(segblank);
174 anzseg=ceil((anz)/2);
175 sapind=(anzsap-1)/2+1;
176 blankind=(anzblank-1)/2+1;
177
178
179 %Split up Segments
180 j=0;
181 i=1;
182 n=1;
183
184 %Temperature_Blank
185 temp_blank=zeros(dim4,anz);
186 while j<=anzblank
187
188     while(i<dim4)
189
190         if (blankmat(i,5)==j)
191         temp_blank(n,j)=blankmat(i,1);
192          if(temp_blank(i,j)==0)
193              n=n+1;
194          else
195              n=n;
196          end
197         end
198         i=i+1;
199
200     end
201
202        j=j+1;
203          i=1;
204          n=1;
205
206     end
207 j=0;
208 i=1;
209 n=1;
210
211 %Temperature_Saphir
```

```
212 temp_saphir=zeros(dim3,anz);
213 while j<=anzsap
214
215     while(i<dim3)
216
217         if (saphirmat(i,5)==j)
218         temp_saphir(n,j)=saphirmat(i,1);
219          if(temp_saphir(i,j)==0)
220              n=n+1;
221          else
222              n=n;
223          end
224         end
225         i=i+1;
226
227     end
228
229        j=j+1;
230          i=1;
231          n=1;
232
233     end
234 j=0;
235 i=1;
236 n=1;
237
238 %Temperature_thin specimen
239 temp_duenn=zeros(dim1,anz);
240 while j<=anz
241
242     while(i<dim1)
243
244         if (duennmat(i,5)==j)
245         temp_duenn(n,j)=duennmat(i,1);
246          if(temp_duenn(i,j)==0)
247              n=n+1;
248          else
249              n=n;
250          end
251         end
252         i=i+1;
253
254     end
255
256        j=j+1;
257          i=1;
258          n=1;
259
260 end
261
262 j=0;
263 i=1;
264 n=1;
265
266 %Temperature thick specimen
267 temp_dick=zeros(dim2,anz);
268 while j<=anz
269
270     while(i<dim2)
271
272         if (dickmat(i,5)==j)
273         temp_dick(n,j)=dickmat(i,1);
274          if(temp_dick(i,j)==0)
275              n=n+1;
276          else
277              n=n;
278          end
279         end
280         i=i+1;
281
282     end
283
284        j=j+1;
```

```
285             i=1;
286             n=1;
287
288         end
289
290     %Write Segments into Matrix
291
292     dsc_blank=zeros(dim4,anzblank);
293
294     j=0;
295     i=1;
296     n=1;
297
298     while j<=anzblank
299
300         while(i<dim4)
301
302             if (blankmat(i,5)==j)
303             dsc_blank(n,j)=blankmat(i,3);
304              if(dsc_blank(i,j)==0)
305                  n=n+1;
306              else
307                  n=n;
308              end
309             end
310             i=i+1;
311
312         end
313
314            j=j+1;
315              i=1;
316              n=1;
317
318     end
319
320     dsc_saphir=zeros(dim3,anzsap);
321
322     j=0;
323     i=1;
324     n=1;
325
326     while j<=anzsap
327
328         while(i<dim3)
329
330             if (saphirmat(i,5)==j)
331             dsc_saphir(n,j)=saphirmat(i,3).*msaphir;
332              if(dsc_saphir(i,j)==0)
333                  n=n+1;
334              else
335                  n=n;
336              end
337             end
338             i=i+1;
339
340         end
341
342            j=j+1;
343              i=1;
344              n=1;
345
346     end
347
348     j=0;
349     i=1;
350     n=1;
351
352     %Temperature_sapphire standard
353     temp_saphir=zeros(dim3,anzsap);
354     while j<=anzsap
355
356         while(i<dim3)
357
```

```
358           if (saphirmat(i,5)==j)
359           temp_saphir(n,j)=saphirmat(i,1);
360            if(temp_saphir(i,j)==0)
361                 n=n+1;
362            else
363                 n=n;
364            end
365           end
366           i=i+1;
367
368       end
369
370          j=j+1;
371            i=1;
372            n=1;
373
374       end
375
376   dsc_duenn=zeros(dim1,anz);
377
378   j=0;
379   i=1;
380   n=1;
381
382   while j<=anz
383
384       while(i<dim1)
385
386           if (duennmat(i,5)==j)
387           dsc_duenn(n,j)=duennmat(i,3).*mduenn;
388            if(dsc_duenn(i,j)==0)
389                 n=n+1;
390            else
391                 n=n;
392            end
393           end
394           i=i+1;
395
396       end
397
398          j=j+1;
399            i=1;
400            n=1;
401
402       end
403
404   dsc_dick=zeros(dim2,anz);
405   j=0;
406   i=1;
407   n=1;
408
409   while j<=anz
410
411       while(i<dim2)
412
413           if (dickmat(i,5)==j)
414           dsc_dick(n,j)=dickmat(i,3).*mdick;
415            if(dsc_dick(i,j)==0)
416                 n=n+1;
417            else
418                 n=n;
419            end
420           end
421           i=i+1;
422
423       end
424
425          j=j+1;
426            i=1;
427            n=1;
428   end
429
430   %Calculate Mean Heat Flow of Segments
```

```
431
432 j=1;
433 %Start Calculating Mean Heat Flow After 3 Full Periods (Exclude Transients)
434 anfang1=period*samplingrate*3;
435
436 while j<=anz
437
438  mean_hf_thick(j,1)=mean(dsc_dick(anfang1:ende,j));
439  mean_hf_thin(j,1)=mean(dsc_duenn(anfang1:ende,j));
440
441  j=j+1;
442
443 end
444
445 j=1;
446 n=1;
447
448 while j<=anzsap
449
450 mean_hf_sapphire(j,1)=mean(dsc_saphir(anfang1:ende,j));
451
452  j=j+1;
453
454 end
455
456 j=1;
457 n=1;
458
459 while j<=anzblank
460
461  mean_hf_blank(j,1)=mean(dsc_blank(anfang1:ende,j));
462
463  j=j+1;
464
465 end
466
467 %Mean Temperatures of Segments
468
469 j=1;
470
471 while j<=anz
472
473  mean_temps_dick(j,1)=mean(temp_dick(anfang:ende,j));
474  mean_temps_duenn(j,1)=mean(temp_duenn(anfang:ende,j));
475
476  j=j+1;
477
478 end
479
480 j=1;
481 n=1;
482
483
484 while j<=anzblank
485
486     if mean(temp_blank(anfang:ende,j))==0
487
488     else
489
490     mean_temps_blank(n,1)=mean(temp_blank(anfang:ende,j));
491
492           n=n+1;
493
494     end
495
496     j=j+1;
497 end
498
499 j=1;
500 n=1;
501
502 while j<=anzsap
503
```

```
504       if mean(temp_saphir(anfang:ende,j))==0
505
506       else
507
508       mean_temps_saphir(n,1)=mean(temp_saphir(anfang:ende,j));
509
510             n=n+1;
511
512       end
513
514       j=j+1;
515   end
516
517    %Rearrangement of Temperature Values of Specimen
518   j=1;
519   n=1;
520   while j<=anz
521
522       if(mean_temps_duenn(j,1)>0)
523
524             temperature(n,1)=mean_temps_duenn(j,1);
525
526             n=n+1;
527
528       else
529
530           n=n;
531
532       end
533
534       j=j+1;
535   end
536
537   j=0;
538   i=1;
539   n=1;
540
541   temp_ampli_dick=[];
542
543           j=j+1;
544             i=1;
545             n=1;
546
547   %Calculation of Temperature Amplitudes
548
549   while j<=anz
550
551
552       while i<=ende
553
554
555            if(mean_temps_duenn(j,1)<=0)
556           break
557            else
558
559           temp_ampli_duenn(i,j)=temp_duenn(i,j)-mean_temps_duenn(j,1);
560
561
562           i=i+1;
563
564            end
565       end
566
567       i=1;
568
569
570           while i<=ende
571
572                if(mean_temps_dick(j,1)<=0)
573
574                     break
575            else
576
```

```
577         temp_ampli_dick(i,j)=temp_dick(i,j)-mean_temps_dick(j,1);
578
579               end
580
581                i=i+1;
582         end
583
584           j=j+1;
585           i=1;
586           n=1;
587 end
588
589  i=1;
590  n=1;
591  j=1;
592
593     while j<=anzsap
594
595
596          while(i<=ende)
597
598     temp_ampli_saphir(i,n)=temp_saphir(i,j)-mean_temps_saphir(n,1);
599
600     i=i+1;
601
602          end
603
604          i=1;
605
606           if mean(temp_saphir(anfang:ende,j))==0
607
608    else  n=n+1;
609
610           end
611
612           j=j+1;
613
614     end
615
616       i=1;
617  n=1;
618  j=1;
619
620     while j<=anzblank
621
622          while(i<=ende)
623
624     temp_ampli_blank(i,n)=temp_blank(i,j)-mean_temps_blank(n,1);
625
626     i=i+1;
627
628          end
629
630          i=1;
631
632           if mean(temp_blank(anfang:ende,j))==0
633
634    else  n=n+1;
635
636           end
637
638           j=j+1;
639
640     end
641
642  j=1     ;
643  i=1;
644
645 %Subtract Mean Values of Heat Flow from DSC Signals
646 %Variables with German names e.g. "Dick" -> Mean Heat Flow not subtracted
647 % Variables with English names e.g. "Thick" -> Mean Heat Flow subtracted
648
649 while j<=anz
```

```
650
651         while i<=ende
652     dsc_thick(i,j)=dsc_dick(i,j)-mean_hf_thick(j);
653     dsc_thin(i,j)=dsc_duenn(i,j)-mean_hf_thin(j);
654     i=i+1;
655         end
656         j=j+1;
657         i=1;
658
659     end
660
661     j=1;
662     i=1;
663
664     while j<=anzsap
665
666         while i<=ende
667     dsc_sapphire(i,j)=dsc_saphir(i,j)-mean_hf_sapphire(j);
668     i=i+1;
669         end
670         j=j+1;
671         i=1;
672
673     end
674
675     j=1;
676     i=1;
677
678     while j<=anzblank
679
680         while i<=ende
681     dsc_blank_norm(i,j)=dsc_blank(i,j)-mean_hf_blank(j);
682     i=i+1;
683         end
684         j=j+1;
685         i=1;
686
687     end
688
689     %Number of local maxima during evaluation interval
690     numpoints=ende/(period*samplingrate);
691
692     %Calculate average peaks of temperature modulation (very important for
693     %apparent thermal conductivity!)
694      j=1;
695
696     while j<=anz
697
698
699     l1=length(findpeaks(abs(temp_ampli_dick(anfang:ende,j)),'MINPEAKHEIGHT',0.1,'
            MINPEAKDISTANCE',10));
700     [t_peaks_dick(1:l1,j),locstdick(1:l1,j)]=findpeaks(abs(temp_ampli_dick(anfang:ende,j))
            ,'MINPEAKHEIGHT',0.1,'MINPEAKDISTANCE',10);
701
702     l2=length(findpeaks(abs(temp_ampli_duenn(anfang:ende,j)),'MINPEAKHEIGHT',0.1,'
            MINPEAKDISTANCE',10));
703     [t_peaks_duenn(1:l2,j),locstduenn(1:l1,j)]=findpeaks(abs(temp_ampli_duenn(anfang:ende,
            j)),'MINPEAKHEIGHT',0.1,'MINPEAKDISTANCE',10);
704
705
706     t_peaks_mean_dick(1,j)=mean(t_peaks_dick(1:l1,j));
707     t_peaks_mean_duenn(1,j)=mean(t_peaks_duenn(1:l2,j));
708
709
710     j=j+1;
711
712     end
713
714
715     j=1;
716
717     while j<=sapind
718
```

```
719 l3=length(findpeaks(abs(temp_ampli_saphir(anfang:ende,j)),'MINPEAKHEIGHT',0.1,'
        MINPEAKDISTANCE',10));
720 t_peaks_saphir(1:l3,j)=findpeaks(abs(temp_ampli_saphir(anfang:ende,j)),'MINPEAKHEIGHT'
        ,0.1,'MINPEAKDISTANCE',10);
721
722 t_peaks_mean_saphir(1,j)=mean(t_peaks_saphir(1:l3,j));
723
724 j=j+1;
725 end
726
727 j=1;
728
729 while j<=blankind
730
731 l4=length(findpeaks(abs(temp_ampli_blank(anfang:ende,j)),'MINPEAKHEIGHT',0.1,'
        MINPEAKDISTANCE',10));
732 t_peaks_blank(1:l4,j)=findpeaks(abs(temp_ampli_blank(anfang:ende,j)),'MINPEAKHEIGHT'
        ,0.1,'MINPEAKDISTANCE',10);
733
734 t_peaks_mean_blank(1,j)=mean(t_peaks_blank(1:l4,j));
735
736 j=j+1;
737 end
738
739 %Calculate average DSC peaks per segment
740
741 j=1;
742
743 while j<=anz
744
745
746 l1=length(findpeaks(abs(dsc_thick(anfang:ende,j)),'MINPEAKHEIGHT',0.1,'MINPEAKDISTANCE
        ',10));
747 [dsc_peaks_dick(1:l1,j),locsdscdick(1:l1,j)]=findpeaks(abs(dsc_thick(anfang:ende,j)),'
        MINPEAKHEIGHT',0.1,'MINPEAKDISTANCE',10);
748
749 l2=length(findpeaks(abs(dsc_thin(anfang:ende,j)),'MINPEAKHEIGHT',0.1,'MINPEAKDISTANCE'
        ,10));
750 [dsc_peaks_duenn(1:l2,j),locsdscduenn(1:l1,j)]=findpeaks(abs(dsc_thin(anfang:ende,j)),
        'MINPEAKHEIGHT',0.1,'MINPEAKDISTANCE',10);
751
752 dsc_peaks_mean_dick(1,j)=mean(dsc_peaks_dick(1:l1,j));
753
754 dsc_peaks_mean_duenn(1,j)=mean(dsc_peaks_duenn(1:l2,j));
755
756 j=j+1;
757
758 end
759
760 j=1;
761
762 while j<=anzsap
763
764     l3=length(findpeaks(abs(dsc_sapphire(anfang:ende,j)),'MINPEAKHEIGHT',0.1,'
            MINPEAKDISTANCE',50));
765 dsc_peaks_saphir(1:l3,j)=findpeaks(abs(dsc_sapphire(anfang:ende,j)),'MINPEAKHEIGHT'
        ,0.1,'MINPEAKDISTANCE',50);
766
767
768     dsc_peaks_mean_saphir(1,j)=mean(dsc_peaks_saphir(1:l3,j));
769     j=j+1;
770 end
771
772 j=1;
773
774 while j<=anzblank
775
776     l4=length(findpeaks(abs(dsc_blank_norm(anfang:ende,j)),'MINPEAKHEIGHT',0.1,'
            MINPEAKDISTANCE',50));
777 dsc_peaks_blank(1:l4,j)=findpeaks(abs(dsc_blank_norm(anfang:ende,j)),'MINPEAKHEIGHT'
        ,0.1,'MINPEAKDISTANCE',50);
778
779
```

```
780         dsc_peaks_mean_blank(1,j)=mean(dsc_peaks_blank(1:l4,j));
781         j=j+1;
782     end
783
784     %Rerrange Values
785
786     j=1;
787     n=1;
788
789     while j<=anzblank
790
791
792         if isnan(dsc_peaks_mean_blank(1,j))==1
793
794         else
795
796             dsc_peaks_mean_blank(1,n)=dsc_peaks_mean_blank(1,j);
797
798              n=n+1;
799
800         end
801
802         j=j+1;
803
804     end
805      dsc_peaks_mean_blank(blankind+1:anzblank)=[];
806     j=1;
807     n=1;
808
809     while j<=anz
810
811
812         if isnan(dsc_peaks_mean_dick(1,j))==1
813
814         else
815
816             dsc_peaks_mean_dick(1,n)=dsc_peaks_mean_dick(1,j);
817
818              n=n+1;
819
820         end
821
822         j=j+1;
823
824     end
825
826     dsc_peaks_mean_dick(anzseg+1:anz)=[];
827     j=1;
828     n=1;
829
830     while j<=anz
831
832      if isnan(dsc_peaks_mean_duenn(1,j))==1
833
834         else
835
836             dsc_peaks_mean_duenn(1,n)=dsc_peaks_mean_duenn(1,j);
837
838              n=n+1;
839
840         end
841
842         j=j+1;
843
844     end
845
846      dsc_peaks_mean_duenn(anzseg+1:anz)=[];
847
848     j=1;
849     n=1;
850
851     while j<=anz
852
```

```
853       if isnan(t_peaks_mean_dick(1,j))==1
854
855       else
856
857           t_peaks_mean_dick(1,n)=t_peaks_mean_dick(1,j);
858
859            n=n+1;
860
861       end
862
863       j=j+1;
864
865   end
866   t_peaks_mean_dick(anzseg+1:anz)=[];
867
868   j=1;
869   n=1;
870
871   while j<=anz
872
873       if isnan(t_peaks_mean_duenn(1,j))==1
874
875       else
876
877           t_peaks_mean_duenn(1,n)=t_peaks_mean_duenn(1,j);
878
879
880            n=n+1;
881
882       end
883
884       j=j+1;
885
886
887   end
888
889   t_peaks_mean_duenn(anzseg+1:anz)=[];
890
891   j=1;
892   n=1;
893
894   while j<=anzsap
895
896       if isnan(dsc_peaks_mean_saphir(1,j))==1
897
898       else
899
900
901           dsc_peaks_mean_saphir(1,n)=dsc_peaks_mean_saphir(1,j);
902
903
904            n=n+1;
905
906       end
907
908       j=j+1;
909
910   end
911
912   dsc_peaks_mean_saphir(sapind+1:anzsap)=[];
913
914   j=1;
915
916
917   %Calculate Apparent CP due to DSC Cell Asymmety (using Blank) [J/K]
918   j=1;
919
920   while j<=blankind
921
922   app_cp_blank(j,1)=(dsc_peaks_mean_blank(1,j).*0.001)/((omega*t_peaks_mean_blank(1,j)))
          ;
923   j=j+1;
924   end
```

```
925
926 %Baseline Correction of thin and thick sample with Reversing CP of Blank
927
928 j=1;
929 n=1
930
931 while n<=anzseg
932
933 if abs(temperature(n)-mean_temps_blank(j))<0.5
934
935 app_cp_dick_raw(n,1)=(dsc_peaks_mean_dick(1,n).*0.001)/((omega*t_peaks_mean_dick(1,n))
      );
936 app_cp_dick(n,1)=(app_cp_dick_raw(n,1)+app_cp_blank(n,1));
937
938 app_cp_duenn_raw(n,1)=(dsc_peaks_mean_duenn(1,n).*0.001)/((omega*t_peaks_mean_duenn(1,
      n)));
939 app_cp_duenn(n,1)=(app_cp_duenn_raw(n,1)+app_cp_blank(n,1))./(mduenn.*10.^(-6));
940
941 n=n+1;
942
943
944 %
945 else
946
947 end
948
949 j=j+1;
950
951
952 end
953
954
955 %
956
957 %Calculation of the true heat capacity of the thin sample
958 %Assignment of correct calibration temperature value from sapphire
959 %Add Baseline to Sapphire Apparent CP (Modulated Heat Flow and Modulated
960 %Temperature are in Phase)
961 j=1;
962 n=1;
963
964 while n<=anzseg
965
966 if abs(temperature(n)-mean_temps_saphir(j))<1
967
968 app_cp_saphir_raw(n,1)=(dsc_peaks_mean_saphir(1,n).*0.001)/((omega*t_peaks_mean_saphir
      (1,n)));
969
970 %Apply Baseline Correction
971
972 app_cp_saphir(n,1)=(app_cp_saphir_raw(n,1)+app_cp_blank(n,1))./(msaphir.*10.^(-6));
973
974 n=n+1;
975
976 else
977
978 end
979
980 j=j+1;
981
982 end
983
984 %Calculation of the correction factor (KCp) of the heat capacity (comparison with
985 %sapphire standard
986 j=1;
987 n=1;
988
989 while j<=anzseg
990
991 KCp(j,1)=cp_std(mean_temps_saphir(j,1))./app_cp_saphir(j,1);
992
993 j=j+1;
994
```

```
995 end
996
997 %Calculate mean value of CP Calibration Constant (suggested by ASTM)
998 kcp_mean=mean(KCp);
999
1000
1001 %
1002
1003 %Calculation of the true heat capacity of the thin sample
1004 %Assignment of correct calibration temperature value from sapphire
1005 j=1;
1006 n=1;
1007 anzseg1=anzseg;
1008
1009 while n<=anzseg
1010
1011
1012 if abs(temperature(n)-mean_temps_saphir(j))<1
1013
1014 Cp(n,1)=app_cp_duenn(n,1).*kcp_mean;
1015
1016 Cp_calibration_constant(n,1)=kcp_mean;
1017
1018 n=n+1;
1019
1020 end
1021
1022 j=j+1;
1023
1024 end
1025
1026
1027 % Correction of apparent CP (thick specimen) with Sapphire
1028
1029 n=1;
1030 j=1;
1031
1032 while n<=anzseg
1033
1034
1035 if abs(temperature(n)-mean_temps_saphir(j))<1
1036
1037 Cp_thick(n,1)=app_cp_dick(n,1).*kcp_mean;
1038
1039 n=n+1;
1040
1041
1042 end
1043
1044 j=j+1;
1045
1046 end
1047
1048
1049 %Calculation of apparent thermal conductivity
1050 j=1;
1051
1052 while j<=anzseg
1053
1054 lambda0(j,1)=(8.*L.*10.^(-3).*Cp_thick(j,1).^2)/(Cp(j,1).*mdick.*10.^(-6).*(dia
      .*10.^(-3)).^2.*period);
1055
1056
1057 j=j+1;
1058
1059 end
1060
1061 %Write Results Vector
1062
1063 j=1;
1064 n=1;
1065
1066 while j<=anzseg
```

```
1067
1068        if(lambda0(j,1)>0)
1069
1070             apparent_thermal_conductivity(n,1)=lambda0(j,1);
1071
1072             n=n+1;
1073
1074        else
1075
1076            n=n;
1077
1078
1079        end
1080
1081        j=j+1;
1082   end
1083
1084
1085
1086
1087   %Apply Purge Gas Correction
1088   j=1;
1089   while j<=anzseg
1090   D_val(j,1)=D(temperature(j,1));
1091   j=j+1;
1092   end
1093
1094   j=1;
1095   while j<=anzseg
1096   thermal_conductivity(j,1)=(apparent_thermal_conductivity(j,1)-2.*D(temperature(j,1))+(
          apparent_thermal_conductivity(j,1).^2-4.*D(temperature(j,1)).*
          apparent_thermal_conductivity(j,1)).^(0.5))./2;
1097   j=j+1;
1098   end
1099
1100
1101
1102
1103   %Write Results to File
1104
1105
1106
1107   i=1;
1108   n=1;
1109
1110   while i<=anzseg
1111
1112        if(Cp(i)>0)
1113
1114       heat_capacity(n,1)=Cp(i);
1115
1116        n=n+1;
1117
1118        else
1119
1120   n=n;
1121
1122        end
1123
1124        i=i+1;
1125
1126   end
1127
1128   i=1;
1129   n=1;
1130   while i<=anzseg
1131
1132        if(Cp(i)>0)
1133
1134       apparent_heat_capacity(n,1)=app_cp_dick(i);
1135
1136        n=n+1;
1137
```

```
1138        else
1139
1140    n=n;
1141
1142        end
1143
1144        i=i+1;
1145
1146    end
1147
1148
1149    %Write Results to XLS File
1150
1151    %Date of Evaluation
1152
1153    filename='results.csv';
1154
1155    xlswrite(filename, {'Sample'}, 'Sheet1', 'A1')
1156    xlswrite(filename, {name}, 'Sheet1', 'B1')
1157
1158    xlswrite(filename, {'Date and Time of Evaluation'}, 'Sheet1', 'A2')
1159    xlswrite(filename, {datestr(now)}, 'Sheet1', 'B2')
1160    xlswrite(filename, {'Specimen Thickness [mm]'}, 'Sheet1', 'A3')
1161    xlswrite(filename, {L}, 'Sheet1', 'B3')
1162    xlswrite(filename, {'Specimen Diameter [mm]'}, 'Sheet1', 'A4')
1163    xlswrite(filename, {dia}, 'Sheet1', 'B4')
1164
1165    xlswrite(filename, {'Temperature [C]'}, 'Sheet1', 'A7')
1166    xlswrite(filename, {'Heat Capacity [J/kgK]'}, 'Sheet1', 'B7')
1167    xlswrite(filename, {'Apparent Heat Capacity (thick) [J/K]'}, 'Sheet1', 'C7')
1168    xlswrite(filename, {'CP Calibration Constant [-]'}, 'Sheet1', 'D7')
1169    xlswrite(filename, {'Apparent Thermal Conductivity [W/mK]'}, 'Sheet1', 'E7')
1170    xlswrite(filename, {'Purge Gas Correction Factor [?]'}, 'Sheet1', 'F7')
1171    xlswrite(filename, {'Thermal Conductivity [W/mK]'}, 'Sheet1', 'G7')
1172
1173
1174    xlswrite(filename, temperature, 'Sheet1', 'A8')
1175    xlswrite(filename, heat_capacity, 'Sheet1', 'B8')
1176    xlswrite(filename, apparent_heat_capacity, 'Sheet1', 'C8')
1177    xlswrite(filename, Cp_calibration_constant, 'Sheet1', 'D8')
1178    xlswrite(filename, apparent_thermal_conductivity, 'Sheet1', 'E8')
1179    xlswrite(filename, D_val, 'Sheet1', 'F8')
1180    xlswrite(filename, thermal_conductivity, 'Sheet1', 'G8')
1181
1182
1183    %Segments to be plotted
1184
1185    if temp_dick(ende,1)==0
1186
1187    begin=2;
1188
1189    else
1190
1191    begin=1;
1192
1193    end
1194
1195    %Specimens
1196    seg1=[begin:2:anz];
1197    %Sapphire
1198    seg2=[1:2:anzsap];
1199    %Blank
1200    seg3=[1:2:anzblank];
1201
1202    %Write Time Vector
1203
1204    time(:,1)=linspace(0,20,length(dsc_duenn(1:ende,seg1)));
1205
1206    %Define Interval Time
1207    inttime=linspace(0,10,1201);
1208
1209
1210    figure
```

```
1211 hold on;
1212 plot(temperature,apparent_thermal_conductivity,'g-o');
1213 plot(temperature,thermal_conductivity,'b-o');
1214 xlabel('Temperature [C]')
1215 ylabel('Thermal Conductivity [W/mK])')
1216 legend('Apparent Thermal Conductivity','Thermal Conductivity')
1217 grid on;
1218
1219
1220 figure
1221 plot(temperature,Cp,'Marker','*')
1222 title('Thin Specimen')
1223 xlabel('Temperature [C]')
1224 ylabel('Heat Capacity [J/kgK])');
1225 grid on;
1226
1227
1228 figure
1229 plot(temperature,Cp_thick,'Marker','*')
1230 title('Thick Specimen')
1231 xlabel('Temperature [C]')
1232 ylabel('Apparent Heat Capacity [J/K])');
1233 grid on;
1234
1235
1236 figure
1237 plot(temperature,app_cp_saphir_raw./(msaphir.*10.^(-6)),'-r*')
1238 hold on;
1239 plot(temperature,app_cp_saphir,'-b*')
1240 plot(temperature,cp_std(temperature),'-g*')
1241 title('Sapphire')
1242 xlabel('Temperature [C]')
1243 ylabel('Apparent Heat Capacity [J/kgK])')
1244 legend('Sapphire - uncorrected','Sapphire with Baseline correction','Literature Values
     ')
1245 grid on;
1246 saveas(gcf,'graphs.png')
1247
1248
1249 %Plot Lissajous Figures, to identify possible signal drift due to melting
1250 %or other events of the sample
1251
1252 % Plot Lissajous Figure of DSC Measurement
1253
1254
1255 figure
1256 plot(temp_duenn(anfang:ende,seg1),dsc_duenn(anfang:ende,seg1))
1257 title('Lissajous Thin')
1258 xlabel('Modulated Temperature [C]')
1259 ylabel('Heat Flow [mW]')
1260 grid on;
1261
1262
1263 figure
1264 plot(temp_dick(anfang:ende,seg1),dsc_dick(anfang:ende,seg1))
1265 title('Lissajous Thick')
1266 xlabel('Modulated Temperature [C]')
1267 ylabel('Heat Flow [mW]')
1268 grid on;
1269
1270
1271 figure
1272 plot(temp_saphir(anfang:ende,seg2),dsc_saphir(anfang:ende,seg2))
1273 title('Lissajous Sapphire]')
1274 xlabel('Modulated Temperature [C]')
1275 ylabel('Heat Flow [mW]')
1276 grid on;
1277
1278
1279 figure
1280 plot(temp_blank(anfang:ende,seg3),dsc_blank(anfang:ende,seg3))
1281 title('Lissajous Blank')
1282 xlabel('Modulated Temperature [C]')
```

```
1283 ylabel('Heat Flow [mW]')
1284 grid on;
1285
1286
1287
1288
1289 % Plot DSC and Temperature Waves in Evaluation Time Range (last 10 min of
1290 % 20 min Interval)
1291 figure
1292 plot(inttime,temp_ampli_dick(anfang:ende,seg1))
1293 hold on
1294 plot(locstdick(:,seg1)./120,t_peaks_dick(:,seg1),'LineStyle','none','Marker','x','
     MarkerEdgeColor','black','MarkerSize',8)
1295 title('Peak Evaluation Temperature Modulation (Thick Specimen)')
1296 xlabel('Time [min]')
1297 ylabel('Temperature Amplitude')
1298 hold on;
1299 grid on;
1300
1301
1302
1303 figure
1304 plot(inttime,dsc_thick(anfang:ende,seg1))
1305 hold on
1306 plot(locsdscdick(:,seg1)./120,dsc_peaks_dick(:,seg1),'LineStyle','none','Marker','x','
     MarkerEdgeColor','black','MarkerSize',8)
1307 title('Peak Evaluation Thick Specimen')
1308 xlabel('Time [min]')
1309 ylabel('Modulated Heat Flow [mW]')
1310 grid on;
1311
1312
1313 figure
1314 plot(inttime,temp_ampli_duenn(anfang:ende,seg1))
1315 hold on
1316 plot(locstduenn(:,seg1)./120,t_peaks_duenn(:,seg1),'LineStyle','none','Marker','x','
     MarkerEdgeColor','black','MarkerSize',8)
1317 title('Peak Evaluation Temperature Modulation (Thin Specimen)')
1318 xlabel('Time [min]')
1319 ylabel('Temperature Amplitude')
1320 grid on;
1321
1322
1323 figure
1324 plot(inttime,dsc_thin(anfang:ende,seg1))
1325 hold on
1326 plot(locsdscduenn(:,seg1)./120,dsc_peaks_duenn(:,seg1),'LineStyle','none','Marker','x'
     ,'MarkerEdgeColor','black','MarkerSize',8)
1327 title('Peak Evaluation Thin Specimen')
1328 xlabel('Time [min]')
1329 ylabel('Modulated Heat Flow[mW]')
1330 grid on;
1331
1332 saveas(gcf,'waveseval.png')
```

Bibliography

[1] D. Treffer, A. Troiss, and J. Khinast, "A novel tool to standardize rheology testing of molten polymers for pharmaceutical applications," *International Journal of Pharmaceutics*, vol. 495, no. 1, pp. 474–481, 2015.

[2] M. Bonnet, "Kunststoffe in der Ingenieuranwendung," *Vieweg+ Teubner, Wiesbaden, Germany*, 2009.

[3] I. M. Hodge, "Enthalpy relaxation and recovery in amorphous materials," *Journal of Non-Crystalline Solids*, vol. 169, no. 3, pp. 211–266, 1994.

[4] R. Surana, A. Pyne, M. Rani, and R. Suryanarayanan, "Measurement of enthalpic relaxation by differential scanning calorimetry - Effect of experimental conditions," *Thermochimica Acta*, vol. 433, no. 1-2, pp. 173–182, 2005.

[5] S. R. Elliott, *Physics of amorphous materials*. Longman London; New York, 1983.

[6] M. Keating and C. McLaren, "Thermal conductivity of polymer melts," *Thermochimica Acta*, vol. 166, pp. 69–76, 1990.

[7] D. V. Rosato and M. G. Rosato, *Injection molding handbook*. 2000.

[8] D. David and A. Misra, "Relating materials properties to structure," *Technomic: Lancaster, PA*, 1999.

[9] C. Leuner and J. Dressman, "Improving drug solubility for oral delivery using solid dispersions," *European journal of Pharmaceutics and Biopharmaceutics*, vol. 50, no. 1, pp. 47–60, 2000.

[10] "Solid solutions and dispersions, technical brief: 2012: Volume 3," tech. rep., Particle Sciences Inc., Bethlehem, PA, 2012.

[11] J. Djuris, I. Nikolakakis, S. Ibric, Z. Djuric, and K. Kachrimanis, "Preparation of carbamazepine–soluplus® solid dispersions by hot-melt extrusion, and prediction of drug–polymer miscibility by thermodynamic model fitting," *European Journal of Pharmaceutics and Biopharmaceutics*, vol. 84, no. 1, pp. 228–237, 2013.

[12] K. Kolter, M. Karl, and A. Gryczke, *Introduction to Solid Dispersions*. 2012.

[13] K. Eggenreich, S. Windhab, S. Schrank, D. Treffer, H. Juster, G. Steinbichler, S. Laske, G. Koscher, E. Roblegg, and J. G. Khinast, "Injection molding as a one-step process for the direct production of pharmaceutical dosage forms from primary powders," *International Journal of Pharmaceutics*, vol. 505, no. 1-2, pp. 341–351, 2016.

[14] D. Treffer, P. Wahl, D. Markl, G. Koscher, E. Roblegg, and J. Khinast, *Hot Melt Extrusion as a Continuous Pharmaceutical Manufacturing Process*. 2013.

[15] L. Tung, "Melt viscosity of polyethylene at zero shear," *Journal of Polymer Science*, vol. 46, no. 148, pp. 409–422, 1960.

[16] C. Rogers, W. Vroom, and R. Westover, "Getting most from a polymer by vacuum-compression molding," *Modern Plastics*, vol. 45, no. 13, p. 200, 1968.

[17] M. A. Rao and J. L. Throne, "Principles of rotational molding," *Polymer Engineering & Science*, vol. 12, no. 4, pp. 237–264, 1972.

[18] Y. H. Kim and R. P. Wool, "A theory of healing at a polymer-polymer interface," *Macromolecules*, vol. 16, no. 7, pp. 1115–1120, 1983.

[19] A. Greco and A. Maffezzoli, "Polymer melting and polymer powder sintering by thermal analysis," *Journal of Thermal Analysis and Calorimetry*, vol. 72, no. 3, pp. 1167–1174, 2003.

[20] M. Narkis, "Sintering behavior of poly(methyl methacrylate) particles," *Polymer Engineering & Science*, vol. 19, no. 13, pp. 889–892, 1979.

[21] C. T. Bellehumeur, M. Kontopoulou, and J. Vlachopoulos, "The role of viscoelasticity in polymer sintering," *Rheologica Acta*, vol. 37, no. 3, pp. 270–278, 1998.

[22] M. Kontopoulou and J. Vlachopoulos, "Bubble dissolution in molten polymers and its role in rotational molding," *Polymer Engineering and Science*, vol. 39, no. 7, pp. 1189–1198, 1999.

[23] F. Wolff and H. Münstedt, "Artefacts of the storage modulus due to bubbles in polymeric fluids," *Rheologica Acta*, vol. 52, no. 4, pp. 287–289, 2013.

[24] P. Kelly, "A microscopic examination of rotomoulded polyethylene," *Du pont, Toronto, Canada*, 1981.

[25] L. Blyler and T. Kwei, "Flow behavior of polyethylene melts containing dissolved gases," in *Journal of Polymer Science: Polymer Symposia*, vol. 35, pp. 165–176, Wiley Online Library, 1971.

[26] F. Winslow, W. Matreyek, and S. Stills, "Division of polymer science: Oxidative embrittlement of polyethylene," *Transactions of the New York Academy of Sciences*, vol. 28, no. 2 Series II, pp. 304–315, 1965.

[27] B. Fayolle, L. Audouin, and J. Verdu, "Oxidation induced embrittlement in polypropylene—a tensile testing study," *Polymer Degradation and Stability*, vol. 70, no. 3, pp. 333–340, 2000.

[28] B. Fayolle, L. Audouin, and J. Verdu, "Initial steps and embrittlement in the thermal oxidation of stabilised polypropylene films," *Polymer Degradation and Stability*, vol. 75, no. 1, pp. 123–129, 2002.

[29] C. Kwag, C. W. Manke, and E. Gulari, "Effects of dissolved gas on viscoelastic scaling and glass transition temperature of polystyrene melts," *Industrial & engineering chemistry research*, vol. 40, no. 14, pp. 3048–3052, 2001.

[30] H. Li, L. J. Lee, and D. L. Tomasko, "Effect of carbon dioxide on the interfacial tension of polymer melts," *Industrial & engineering chemistry research*, vol. 43, no. 2, pp. 509–514, 2004.

[31] G. Kasaliwal, A. Göldel, and P. Pötschke, "Influence of processing conditions in small-scale melt mixing and compression molding on the resistivity and morphology of polycarbonate–mwnt composites," *Journal of Applied Polymer Science*, vol. 112, no. 6, pp. 3494–3509, 2009.

[32] M. T. Shaw, *Introduction to polymer rheology*. John Wiley & Sons, 2012.

[33] J.-W. Rhim, A. K. Mohanty, S. P. Singh, and P. K. Ng, "Effect of the processing methods on the performance of polylactide films: thermocompression versus solvent casting," *Journal of Applied Polymer Science*, vol. 101, no. 6, pp. 3736–3742, 2006.

[34] J. M. Saldanha and T. Kyu, "Influence of solvent casting on evolution of phase morphology of PC/PMMA blends," *Macromolecules*, vol. 20, no. 11, pp. 2840–2847, 1987.

[35] H. Lim and S. W. Hoag, "Plasticizer Effects on Physical – Mechanical Properties of Solvent Cast Soluplus ® Films," pp. 13–16, 2013.

[36] Z. Li, Y. Shi, H. Liu, F. Chen, Q. Zhang, K. Wang, and Q. Fu, "Effect of melting temperature on interfacial interaction and mechanical properties of polypropylene (PP) fiber reinforced olefin block copolymers (OBCs)," *RSC Adv.*, vol. 4, no. 85, pp. 45234–45243, 2014.

[37] A. Guevara-Morales and U. Figueroa-López, "Residual stresses in injection molded products," *Journal of Materials Science*, vol. 49, no. 13, pp. 4399–4415, 2014.

[38] N. J. Coleman and D. Q. Craig, "Modulated temperature differential scanning calorimetry: a novel approach to pharmaceutical thermal analysis," *International Journal of Pharmaceutics*, vol. 135, no. 1, pp. 13–29, 1996.

[39] S.-D. Clas, C. R. Dalton, and B. C. Hancock, "Differential scanning calorimetry: applications in drug development," *Pharmaceutical Science & Technology Today*, vol. 2, no. 8, pp. 311–320, 1999.

[40] K. Jones, I. Kinshott, M. Reading, A. Lacey, C. Nikolopoulos, and H. Pollock, "The origin and interpretation of the signals of mtdsc," *Thermochimica Acta*, vol. 304, pp. 187–199, 1997.

[41] D. Q. Craig and M. Reading, *Thermal analysis of pharmaceuticals*. CRC press, 2006.

[42] K. J. Jones, I. Kinshott, M. Reading, A. A. Lacey, C. Nikolopoulos, and H. M. Pollock, "The origin and interpretation of the signals of MTDSC," *Thermochimica Acta*, vol. 305, pp. 187–199, 1997.

[43] A. Frick and C. Stern, *DSC-Prüfung in der Anwendung*. Hanser, 2006.

[44] J. Rieger, "The glass transition temperature of polystyrene: results of a round robin test," *Journal of Thermal Analysis and Calorimetry*, vol. 46, no. 3-4, pp. 965–972, 1996.

[45] J. Aho, J. P. Boetker, S. Baldursdottir, and J. Rantanen, "Rheology as a tool for evaluation of melt processability of innovative dosage forms," *International Journal of Pharmaceutics*, vol. 494, no. 2, pp. 623–642, 2015.

[46] D. Binding, M. Couch, and K. Walters, "The pressure dependence of the shear and elongational properties of polymer melts," *Journal of Non-Newtonian Fluid Mechanics*, vol. 79, no. 2, pp. 137–155, 1998.

[47] A. Troiss, "Melt-rheological characterization of selected pharmaceutical polymers." Bachelor Thesis, Graz University of Technology, 2014.

[48] H. Wilson, "Polymeric fluids - lecture notes," *University College of London*, vol. 1, 2006.

[49] W. Cox and E. Merz, "Rheology of polymer melts—a correlation of dynamic and steady flow measurements," in *International Symposium on Plastics Testing and Standardization*, ASTM International, 1959.

[50] P. J. Carreau, "Rheological equations from molecular network theories," *Transactions of the Society of Rheology*, vol. 16, no. 1, pp. 99–127, 1972.

[51] K. Yasuda, R. Armstrong, and R. Cohen, "Shear flow properties of concentrated solutions of linear and star branched polystyrenes," *Rheologica Acta*, vol. 20, no. 2, pp. 163–178, 1981.

[52] T. G. Mezger, *The rheology handbook: for users of rotational and oscillatory rheometers*. Vincentz Network GmbH & Co KG, 2006.

[53] A. Paradkar, A. Kelly, P. Coates, and P. York, "Shear and extensional rheology of hydroxypropyl cellulose melt using capillary rheometry," *Journal of Pharmaceutical and Biomedical analysis*, vol. 49, no. 2, pp. 304–310, 2009.

[54] J. Wisniak, "Frederick thomas trouton: the man, the rule, and the ratio," *The Chemical Educator*, vol. 6, no. 1, pp. 55–61, 2001.

[55] Z. K. Nagy, A. Balogh, B. Vajna, A. Farkas, G. Patyi, Á. Kramarics, and G. Marosi, "Comparison of electrospun and extruded soluplus®-based solid dosage forms of improved dissolution," *Journal of Pharmaceutical Sciences*, vol. 101, no. 1, pp. 322–332, 2012.

[56] U. Paaver, I. Tamm, I. Laidmäe, A. Lust, K. Kirsimäe, P. Veski, K. Kogermann, and J. Heinämäki, "Soluplus graft copolymer: potential novel carrier polymer in electrospinning of nanofibrous drug delivery systems for wound therapy," *BioMed research international*, vol. 2014, 2014.

[57] D.-G. Yu, X.-X. Shen, C. Branford-White, K. White, L.-M. Zhu, and S. A. Bligh, "Oral fast-dissolving drug delivery membranes prepared from electrospun polyvinylpyrrolidone ultrafine fibers," *Nanotechnology*, vol. 20, no. 5, p. 055104, 2009.

[58] G. Bruni, L. Maggi, L. Tammaro, R. Di Lorenzo, V. Friuli, M. Maietta, V. Berbenni, C. Milanese, A. Girella, A. Marini, *et al.*, "Electrospun fibers as potential carrier systems for enhanced drug release of perphenazine," *International Journal of Pharmaceutics*, vol. 511, no. 1, pp. 190–197, 2016.

[59] Z. K. Nagy, A. Balogh, G. Drávavölgyi, J. Ferguson, H. Pataki, B. Vajna, and G. Marosi, "Solvent-free melt electrospinning for preparation of fast dissolving drug delivery system and comparison with solvent-based electrospun and melt extruded systems," *Journal of Pharmaceutical Sciences*, vol. 102, no. 2, pp. 508–517, 2013.

[60] Z. K. Nagy, A. Balogh, B. Démuth, H. Pataki, T. Vigh, B. Szabó, K. Molnár, B. T. Schmidt, P. Horák, G. Marosi, *et al.*, "High speed electrospinning for scaled-up production of amorphous solid dispersion of itraconazole," *International Journal of Pharmaceutics*, vol. 480, no. 1, pp. 137–142, 2015.

[61] A. Balogh, G. Drávavölgyi, K. Faragó, A. Farkas, T. Vigh, P. L. Sóti, I. Wagner, J. Madarász, H. Pataki, G. Marosi, *et al.*, "Plasticized drug-loaded melt electrospun polymer mats: Characterization, thermal degradation, and release kinetics," *Journal of Pharmaceutical Sciences*, vol. 103, no. 4, pp. 1278–1287, 2014.

[62] M. Wang, A. Hsieh, and G. Rutledge, "Electrospinning of poly (mma-co-maa) copolymers and their layered silicate nanocomposites for improved thermal properties," *Polymer*, vol. 46, no. 10, pp. 3407–3418, 2005.

[63] C. Clasen, *15th European School on Rheology - Courseware*, ch. Extensional Rheology. KU Leuven, 2015.

[64] A. Müllertz, Y. Perrie, and T. Rades, "Analytical techniques in the pharmaceutical sciences," *Advances in Delivery Science and Technology*, 2016.

[65] M. L. Sentmanat, "Miniature universal testing platform: from extensional melt rheology to solid-state deformation behavior," *Rheologica Acta*, vol. 43, no. 6, pp. 657–669, 2004.

[66] J. Aho, V. H. Rolón-Garrido, S. Syrjälä, and M. H. Wagner, "Measurement technique and data analysis of extensional viscosity for polymer melts by Sentmanat extensional rheometer (SER)," *Rheologica Acta*, vol. 49, no. 4, pp. 359–370, 2010.

[67] G. W. Ehrenstein, G. Riedel, and P. Trawiel, *Thermal analysis of plastics: theory and practice*. Carl Hanser Verlag GmbH Co KG, 2012.

[68] D. ASTM, "4065 (2001)," *Standard Practice for Plastics-Dynamic Mechanical Properties-Determining and Reporting of Procedures*.

[69] R. Kazakevičiūtė-Makovska, A. Özlem Özarmut, and H. Steeb, "Characterization of shape memory polymer estane by means of dynamic mechanical thermal analysis technique," *Smart Materials Research*, vol. 2014, 2014.

[70] K. P. Menard, "Dynamic mechanical analysis basics: Part 2 thermoplastic transitions and properties," *Perkin Elmer: Application Note*, 1999.

[71] R. Chartoff and E. Turi, "Thermal characterization of polymeric materials," *Academic Press: New York*, vol. 1, p. 513, 1997.

[72] A. Paudel, J. Meeus, and G. Van den Mooter, "Structural characterization of amorphous solid dispersions," in *Amorphous Solid Dispersions*, pp. 421–485, Springer, 2014.

[73] N. Soutari, A. B. M. Buanz, M. Orlu, C. Tuleu, and S. Gaisford, "Quantifying crystallisation rates of amorphous pharmaceuticals with dynamic mechanical analysis (DMA)," *International Journal of Pharmaceutics*, vol. 423, no. 2, pp. 335–340, 2012.

[74] D. Q. Craig and F. A. Johnson, "Pharmaceutical applications of dynamic mechanical thermal analysis," *Thermochimica Acta*, vol. 248, pp. 97–115, 1995.

[75] M. G. Abiad, O. H. Campanella, and M. T. Carvajal, "Assessment of thermal transitions by dynamic mechanical analysis (dma) using a novel disposable powder holder," *Pharmaceutics*, vol. 2, no. 2, pp. 78–90, 2010.

[76] S. Kar, *A viscoelastic analysis of particle-particle deformation in pharmaceutical powder compaction*. PhD thesis, University of Toronto, 1999.

[77] D. A. Pai, A. A. Hayes, and M. R. Okos, "Modeling pharmaceutical compacts tensile strength based on viscoelastic properties," *Powder Technology*, vol. 239, pp. 441–450, 2013.

[78] V. M. Ndesendo, V. Pillay, Y. E. Choonara, E. Buchmann, D. N. Bayever, and L. C. Meyer, "A review of current intravaginal drug delivery approaches employed for the prophylaxis of hiv/aids and prevention of sexually transmitted infections," *AAPS Pharmscitech*, vol. 9, no. 2, pp. 505–520, 2008.

[79] A. Loxley, M. Mitchnick, O. Okoh, J. McConnell, L. Goldman, C. Morgan, M. Clark, and D. R. Friend, "Ethylene vinyl acetate intravaginal rings for the simultaneous delivery of the antiretroviral uc781 and contraceptive levonorgestrel," *Drug Delivery and Translational Research*, vol. 1, no. 3, pp. 247–255, 2011.

[80] R. Malcolm, S. McCullagh, A. D. Woolfson, M. Catney, and P. Tallon, "A dynamic mechanical method for determining the silicone elastomer solubility of drugs and pharmaceutical excipients in silicone intravaginal drug delivery rings," *Biomaterials*, vol. 23, no. 17, pp. 3589 – 3594, 2002.

[81] J. T. Clark, T. J. Johnson, M. R. Clark, J. S. Nebeker, J. Fabian, A. L. Tuitupou, S. Ponnapalli, E. M. Smith, D. R. Friend, and P. F. Kiser, "Quantitative evaluation of a hydrophilic matrix intravaginal ring for the sustained delivery of tenofovir," *Journal of Controlled Release*, vol. 163, no. 2, pp. 240–248, 2012.

[82] M. R. Clark, T. J. Johnson, R. T. Mccabe, J. T. Clark, A. Tuitupou, H. Elgendy, D. R. Friend, and P. F. Kiser, "A hot-melt extruded intravaginal ring for the sustained delivery of the antiretroviral microbicide uc781," *Journal of Pharmaceutical Sciences*, vol. 101, no. 2, pp. 576–587, 2012.

[83] D. A. Quinteros, V. R. Rigo, A. F. J. Kairuz, M. E. Olivera, R. H. Manzo, and D. A. Allemandi, "Interaction between a cationic polymethacrylate (eudragit e100) and anionic drugs," *European Journal of Pharmaceutical Sciences*, vol. 33, no. 1, pp. 72–79, 2008.

[84] R. N. Shamma and M. Basha, "Soluplus®: A novel polymeric solubilizer for optimization of carvedilol solid dispersions: Formulation design and effect of method of preparation," *Powder Technology*, vol. 237, pp. 406–414, 2013.

[85] S. Huang, K. P. O'Donnell, J. M. Keen, M. A. Rickard, J. W. McGinity, and R. O. Williams, "A New Extrudable Form of Hypromellose: AFFINISOL™ HPMC HME," *AAPS PharmSciTech*, vol. 17, no. 1, pp. 106–119, 2016.

[86] K. N. Sarfaraz and K. Niazi, "Handbook of pharmaceutical manufacturing formulations," *Compressed Solid Products*, vol. 1, 2009.

[87] N. Hoshi, H. Kokubo, T. Nagai, and S. Obara, "Application of hpmc and hpmcas to film coating of pharmaceutical dosage forms, in aqueous polymeric coatings for pharmaceutical dosage forms," *McGinity JW, Marcel Decker, Inc., New York and Basel*, pp. 177–225, 1997.

[88] K. Nakamichi, T. Nakano, S. Izumi, H. Yasuura, and Y. Kawashima, "The preparation of enteric solid dispersions with hydroxypropylmethylcellulose acetate succinate using a twin-screw extruder," *Journal of Drug Delivery Science and Technology*, vol. 14, no. 3, pp. 193–198, 2004.

[89] Y. Huang and W.-G. Dai, "Fundamental aspects of solid dispersion technology for poorly soluble drugs," *Acta Pharmaceutica Sinica B*, vol. 4, no. 1, pp. 18 – 25, 2014. SI: Drug Delivery System and Pharmaceutical Technology.

[90] B. Lang, J. W. McGinity, and R. O. Williams, "Hot-melt extrusion - basic principles and pharmaceutical applications.," *Drug Development and Industrial Pharmacy*, vol. 9045, no. 9, pp. 1–23, 2014.

[91] K. Mattes, "Methoden zur Charakterisierung des nichtlinear viskoelastischen Verhaltens von Polymerschmelzen," 2007.

[92] J. Boon, G. Challa, and D. Van Krevelen, "Crystallization kinetics of isotactic polystyrene. ii. influence of thermal history on number of nuclei," *Journal of Polymer Science Part A-2: Polymer Physics*, vol. 6, no. 11, pp. 1835–1851, 1968.

[93] C. Migliaresi, A. De Lollis, L. Fambri, and D. Cohn, "The effect of thermal history on the crystallinity of different molecular weight plla biodegradable polymers," *Clinical Materials*, vol. 8, no. 1-2, pp. 111–118, 1991.

[94] H. Bauer, D. Study, and P. Engineering, "Transient thermal analysis of a vacuum compression molding cycle for the production of thermoplastic specimens," no. August, 2015.

[95] F. Yang, Y. Su, J. Zhang, J. DiNunzio, A. Leone, C. Huang, and C. D. Brown, "Rheology guided rational selection of processing temperature to prepare copovidone–nifedipine amorphous solid dispersions via hot melt extrusion (hme)," *Molecular Pharmaceutics*, vol. 13, no. 10, pp. 3494–3505, 2016.

[96] D. Fiedler, "Vakuumkompressionsformen als screening methode für pharmazeutische spritzgussformulierungen," BSc Thesis, Graz University of Technology, 2015.

[97] S. Radl, "Lecture Script "Mehrphasenprozesstechnik"." Graz University of Technology, 2015.

[98] K. J. Crowley and G. Zografi, "Cryogenic grinding of indomethacin polymorphs and solvates: assessment of amorphous phase formation and amorphous phase physical stability," *Journal of Pharmaceutical Sciences*, vol. 91, no. 2, pp. 492–507, 2002.

[99] S. Baghel, H. Cathcart, and N. J. O'Reilly, "Polymeric Amorphous Solid Dispersions: A Review of Amorphization, Crystallization, Stabilization, Solid-State Characterization, and Aqueous Solubilization of Biopharmaceutical Classification System Class II Drugs," *Journal of Pharmaceutical Sciences*, vol. 105, no. 9, pp. 2527–2544, 2016.

[100] S. Rustige, "Herstellung homogener ausgangsmaterialien für das vakuumkompressionsformen," Bachelor Thesis, Graz University of Technology, 2015.

[101] T. Nguyen, "Drilling Engineering - PE 311 Laminar Flow in Pipes and Annuli Newtonian Fluids - Lecture Notes," 2011.

[102] A. Boller, Y. Jin, and B. Wunderlich, "Heat Capacity Measurement by Modulated DSC at Constant Temperature "," vol. 42, pp. 307–330, 1994.

[103] S. O. Otun, E. Meehan, S. Qi, and D. Q. Craig, "The use of quasi-isothermal modulated temperature differential scanning calorimetry for the characterization of slow crystallization processes in lipid-based solid self-emulsifying systems," *Pharmaceutical Research*, vol. 32, no. 4, pp. 1316–1324, 2015.

[104] "ASTM E1952 - 11," Standard Test Method for Thermal Conductivity and Thermal Diffusivity by Modulated Temperature Differential Scanning Calorimetry, ASTM International, West Conshohocken, PA, 2011.

[105] S. M. Marcus and R. L. Blaine, "Thermal conductivity of polymers, glasses and ceramics by modulated dsc," *Thermochimica Acta*, vol. 243, no. 2, pp. 231–239, 1994.

[106] R. L. Blaine and S. M. Marcus, "Derivation of Temperature-Modulated DSC Thermal Conductivity Equations," 1998.

[107] C. M. Lopes and M. I. Felisberti, "Thermal conductivity of pet/(ldpe/ai) composites determined by mdsc," *Polymer Testing*, vol. 23, no. 6, pp. 637–643, 2004.

[108] Y. Lin, Z. Shi, and P. L. D. Wildfong, "Journal of Pharmaceutical and Biomedical Analysis Thermal conductivity measurements for small molecule organic solid materials using modulated differential scanning calorimetry (MDSC) and data corrections for sample porosity," vol. 51, pp. 979–984, 2010.

[109] S. L. Simon, "Measurements of thermal conductivity using TMDSC: Solution to the heat flow problem," *Journal of reinforced plastics and composites*, vol. 18, pp. 559–571, 1995.

[110] N. Nyamweya and S. W. Hoag, "Assessment of polymer-polymer interactions in blends of hpmc and film forming polymers by modulated temperature differential scanning calorimetry," *Pharmaceutical Research*, vol. 17, no. 5, pp. 625–631, 2000.

[111] I. Özgüney, D. Shuwisitkul, and R. Bodmeier, "Development and characterization of extended release Kollidon SR mini-matrices prepared by hot-melt extrusion," *European Journal of Pharmaceutics and Biopharmaceutics*, vol. 73, no. 1, pp. 140–145, 2009.

[112] U. Gaur and B. Wunderlich, "Heat capacity and other thermodynamic properties of linear macromolecules. v. polystyrene," *Journal of Physical and Chemical Reference Data*, vol. 11, no. 2, pp. 313–325, 1982.

[113] Y. Sakakibaba, I. Yamada, S. Hirako, and T. Aragaki, "Thermal conductivity of polystyrene above and below the glass transition temperature," 1990.

[114] P. Dashora and G. Gupta, "On the temperature dependence of the thermal conductivity of linear amorphous polymers," *Polymer*, vol. 37, no. 2, pp. 231–234, 1996.

[115] W. N. Dos Santos, J. A. De Sousa, and R. Gregorio, "Thermal conductivity behaviour of polymers around glass transition and crystalline melting temperatures," *Polymer Testing*, vol. 32, no. 5, pp. 987–994, 2013.

[116] M. Brogly, M. Nardin, and J. Schultz, "Effect of vinylacetate content on crystallinity and second-order transitions in ethylene—vinylacetate copolymers," *Journal of Applied Polymer Science*, vol. 64, no. 10, pp. 1903–1912, 1997.